Department of Chemical Engineering

Identification of Clinker Formation in Power Station Boilers – CFD Based Approach

Nilesh Chandulal Kotadiya

This thesis is presented for the Degree of
Master of Engineering
of
Curtin University of Technology

March 2010

Declaration

To the best of my knowledge and belief this thesis contains no material previously published by any other person except where due acknowledgment has been made.

This thesis contains no material which has been accepted for the award of any other degree or diploma in any university.

Signature: ……

Date: ……..

Abstract

Pulverised coal combustion continues to be one of the main conventional methods of producing electricity over the last several decades. Mineral matter present in coal is usually present as free ions, salts, organically bound inorganic and hard minerals. During coal combustion these minerals partly vaporized, coalesce or fragment. The mineral matter in coal transforms into ash during combustion and deposition on wall surfaces causing problems such as fouling and slagging. The deposited lumps called clinkers, mainly in radiation zone directly exposed to flame radiation resulting to slagging, while sintered deposit in convection zone not directly exposed by flame radiation called fouling. The scope of this work encompasses identification of slagging and clinker formation areas in a typical 330 MW boiler using commercial code FLUENT and several available empirical indices. The propensity of the slagging with the used coal is calculated by several thermal indices. Temperature distributions, velocity profiles and particle trajectories were analysed and utilised to predict the most probable zones likely to experience clinker formation. Most probable spots for slagging were found in the radiation zone near to the nose of furnace and left-top side of superheater tube sections which agrees closely with the plant observations. However, the propensity of deposited ash obtained from the plant is seemed low to medium using several indices. Results from the current investigation demonstrate the usefulness of modelling approach in identifying the probable zones of clinker formation which can prove to be valuable for power utilities to adopt corrective measures for soot blowing to clean the ash deposits before it grows bigger in size.

Acknowledgements

I would like to thank a number of people who have provided me with a great deal of help to complete this project. I am grateful to project supervisors A/Professor Hari Vuthaluru and Dr Rupa Vuthaluru for giving me an opportunity to pursue Master Degree in the “Energy” field and their incredible support during this study. Their valuable guidance and motivation have helped me lot for versatile development and to complete the work in time. I would like to thank Dr Hon Lye (Pacific West) for providing technical assistance in this project. I express my sincere gratitude to the Chairman of Thesis Committee Professor Moses Tadé and Head of the Chemical Engineering Department Professor Ming H. Ang for their constant support and advice. I would like to thank all members of the administrations at Chemical Engineering Department as well as library staff for their help during this course. I am also thankful to my colleagues, Kalpit Shah, Pradip Shukla, Tejas Bhatelia, Milin Shah, Deepak Jagannatha, Nadeem Chaudhary and Mikil Gandhi at Curtin University of Technology for their outstanding assistance in technical and non-technical matters during this project. I am also thankful to my friends in Perth; Shreyas, Chirag, Milan, Kishan, Paras, Dhaval, Hiren, Dipak and Mrugraj, who have provided me best support during the stay in Australia. Last but not least, I would like to thank Gostellow Family, for providing accommodation and great family environment during the study tenure.

Finally, all the credentials of this degree go to my beloved parents. This course would not have been possible without the financial support given by my father Mr Chandulal Kotadiya. I am deeply indebted to my parents, my younger brother and entire Kotadiya Family, who have been with me at every step before and during this project completion. I would like to thank every hand that helped me directly or indirectly in completion of this project work.

Brief Biography of Author

Author of this thesis Mr Nilesh Kotadiya has completed Bachelor of Chemical Engineering in year 2006 from V.V.P. Engineering College, Rajkot, India, standing with First Class Distinction. He has joined Curtin University of Technology, Perth, Australia, in February 2007 with the enrolment in Master of Chemical Engineering by coursework. After completion of First semester in the coursework author has transferred to Master by Research program in Chemical Engineering.

He has written the following paper in the support of this thesis:

- "**Identification of Clinker Formation Regions in Large Scale Utility Boiler Using Fluent"**, Conference Paper submitted for Chemeca2009, Perth, Australia.
- **"CFD Based model for the Identification of Clinker Formation in wall-fired Boiler**", A paper to be submitted to Fuel Processing Technology, 2009.

Thesis Contents

Abstract……I

Acknowledgments……..II

Brief Biography of Author……..III

List of Figures……VIII

List of Tables……...XII

Nomenclature…….XIV

Chapter 1

Introduction and Objectives…….....1

1.1 Objectives……...2

1.2 Thesis Outline.....4

Chapter 2

Literature Review……...5

2.1 Coal Combustion and Mineral Matter Transformations…….5

2.1.1 Coal combustion……..5

2.1.2 Mineral matter in coal……..7

2.2 Ash Formation during Combustion……8

2.3 Ash Deposition Mechanism……....9

2.4 Slagging, Fouling and Clinker Formation……11

2.5 Predictive Indices, Ash Deposition Codes and Modelling of Combustors

…….16

2.6 Summary of Literature Review…….21

Chapter 3

CFD in Pulverised Coal Combustion……..22

3.1 Introduction to CFD……..22

3.1.1 Elements of CFD code …….23

3.1.2 Background of the selected CFD package…….26

3.2 Mathematical Models……27

3.2.1 Basic conservation equations…….28

3.2.2 General transport equation…….30

3.3 Solution Methods in Computational Fluid Dynamics……..30

3.4 Turbulence Models……...32

3.4.1 Time-averaged transport equations……32

3.4.2 The standard $k-\varepsilon$ model…….33

3.4.3 RNG $k-\varepsilon$ model……..35

3.4.4 The $k-\varepsilon$ model via convective heat and mass transfer……37

3.5 Radiation Models……..39

3.5.1 P-1 radiation model……....40

3.6 Gaseous Turbulent Combustion Models……...43

3.6.1 Mixture fraction approach……..44

3.6.2 PDF approach…….46

3.7 Discrete Phase Modelling…….47

3.8 Particle Reaction Sub Models……...48

Chapter 4

Modelling Approach…….49

4.1 Simulation Object and Problem Definition……...49

4.2 Calculated Cases……...53

4.3 Solution Procedure……56

Chapter 5

Results and Discussion……..58

5.1 Different Operational Cases……..58

5.2 Temperature Distribution……..59

5.3 Species Distribution……..64

5.4 Comparison with Literature and other Resource……..65

5.5 Flow Fields, Particle Tracks and Areas of Clinker Formation…….70

5.5.1 Flow fields…….70

5.5.2 Particle tracks and areas of clinker formation……71

Chapter 6

Conclusions and Recommendation…….84

6.1 Conclusions……...84

6.2 Recommendation……..86

Appendices…….88

References…….....117

List of Figures

Figure 2. 1: Coal combustion processes (Wu, 2003)……6

Figure 2. 2: Schematic illustrations of ash formation paths (adapted from (Kær et al., 2006)…….....10

Figure 2. 3: Slagging and fouling in pulverised coal combustion boiler……13

Figure 2. 4: View of real plant deposits (a) clinkers on furnace wall (b) burner throat (c) hanging clinkers on superheater (as received)…….....15

Figure 2. 5: Schematic of ash deposition model (adopted from (Lee and Lockwood, 1998)……...……20

Figure 3. 1: Representations of different meshing schemes (a) structured grid, (b) unstructured grid…….25

Figure 4. 1: Schematic of modelled furnace……...50

Figure 4. 2: Schematic arrangements of 25 burners on front and rear boiler walls (as received)…….....55

Figure 4. 3: Fuel consumption for actual plant values and calculated values for present model……..55

Figure 4. 4: Distribution of primary air (PA), secondary air (SA) and coal for different operational cases……..56

Figure 5. 1: Temperature distribution along cross-section A, for cases A to E (Y-Y planes)…….60

Figure 5. 2: Temperature distribution across various cross-sections B, C and D for all cases (Z-Z planes)……..61

Figure 5. 3: Iso-surfaces for different cases representing average burner zone temperature…….62

Figure 5. 4: Temperature comparison with reference across cross-section A (Std.Abs.Dev. < 2.5%)……65

Figure 5. 5: Temperature comparison with literature values near burner region (Std.Abs.Dev. < 8%)……...66

Figure 5. 6: Temperature for case of over fire air according to literature (present study, excess air) (Std.Abs.Dev. = 3.425%)……...67

Figure 5. 7: Comparison of O_2 concentration through cross-section A (Std.Abs.Dev. = 0.001%)……67

Figure 5. 8: Comparison of CO_2 concentration through line A-A* (Std.Abs.Dev. = 2.31%)……68

Figure 5. 9: Radiation heat flux (w/m2) to the walls……..69

Figure 5. 10: Flow fields on different cross-sections for case A……..70

Figure 5. 11: Particle trajectories for selected burners for case A……73

Figure 5. 12: Particle trajectories for selected burners for case B……74

Figure 5. 13: Particle trajectories for selected burners for case C……75

Figure 5. 14: Particle trajectories for selected burners for case D……76

Figure 5. 15: Particle trajectories for selected burners for case E……77

Figure A. 1: Major dimensions (all in meter) reported for created boiler model…88

Figure D. 1: Geometry showing different cross-sections for result representations (CS – Cross-section, specifications of locations are given in Table D. 1)……..94

Figure D. 2: Geometry showing different lines for result representations (Specifications are given in Table D. 2)……95

Figure E. 1: Temperature distribution for case A on line A-A*……97

Figure E. 2: Temperature distribution for case B on line A-A*…….97

Figure E. 3: Temperature distribution for case C on line A-A*…….98

Figure E. 4: Temperature distribution for case D on line A-A*…….98

Figure E. 5: Temperature distribution for case E on line A-A*…….99

Figure E. 6: Temperature distribution for case A on three lines near burner…….99

Figure E. 7: Temperature distribution for case B on three lines near burner……100

Figure E. 8: Temperature distribution for case C on three lines near burner……100

Figure E. 9: Temperature distribution for case D on three lines near burner…...101

Figure E. 10: Temperature distribution for case E on three lines near burner……101

Figure E. 11: Temperature distribution for case A on CS-H……..102

Figure E. 12: Temperature distribution for case B on CS-H……..102

Figure E. 13: Temperature distribution for case C on CS-H……..103

Figure E. 14: Temperature distribution for case D on CS-H……..103

Figure E. 15: Temperature distribution for case E on CS-H……...104

Figure F. 1: % O_2 on line B-B* for cases A, B, C and D…….105

Figure F. 2: % CO_2 on line B-B* for cases A, B, C and D……...105

Figure F. 3: % O_2 on line C-C* for cases A, B, C and D…….106

Figure F. 4: % CO_2 on line C-C* for cases A, B, C and D……...106

Figure F. 5: % O_2 on line D-D* for cases A, B, C and D…….107

Figure F. 6: % CO_2 on line D-D* for cases A, B, C and D……..107

Figure F. 7: % O_2 on line B-B*, line C-C* and line D-D* for case E……..108

Figure F. 8: % CO_2 on line B-B*, line C-C* and line D-D* for case E……...108

Figure F. 9: % O_2 on line A-A* for cases A, B, C and D…….109

Figure F. 10: % O_2 on line A-A* for case E……...109

Figure F. 11: % CO_2 on line A-A* for cases A, B, C and D……..110

Figure F. 12: % CO_2 on line A-A* for case E……110

Figure F. 13: % O_2 on line E-E* for cases A, B, C and D……..111

Figure F. 14: % O_2 on line E-E* for case E……111

Figure F. 15: % CO_2 on line E-E* for cases A, B, C and D……...112

Figure F. 16: % CO_2 on line E-E* for case E…….112

Figure H. 1: Flow fields on different cross-sections for case B……114

Figure H. 2: Flow fields on different cross-sections for case C……114

Figure H. 3: Flow fields on different cross-sections for case D……115

Figure H. 4: Flow fields on different cross-sections for case E……115

Figure H. 5: Flow fields for all cases on cross-section B……..116

Figure H. 6: Flow fields for all cases on cross-section H……..116

List of Tables

Table 2. 1: Distribution of mineral elements and their potential to cause fireside problems (Bryers, 1995)……...8

Table 2. 2: Major causes of wall slag……13

Table 3. 1: List of available meshing schemes in GAMBIT (user's guide)…….24

Table 3. 2: Energy and mass transport equations for turbulence models…….38

Table 4. 1: Proximate and ultimate analysis of coal…….52

Table 4. 2: Different operating cases based on active burners……..54

Table 4. 3: Slagging indices results (Couch, 1994)……..57

Table 5. 1: Summary of mean temperature in burner zone, peak temperature and FEGT……...63

Table 5. 2: Species concentration (%)……...68

Table 5. 3: Furnace exit gas temperature (K)……68

Table 5. 4: Heat transfer to walls (W)……...69

Table 5. 5: Predicted average residence time and relevant burner numbers for different cases…….72

Table 5. 6: Information on probable spots of clinker formation on the furnace walls……80

Table 5. 7: Governing parameters for clinker accumulation on probable surface of furnace walls……...83

Table C. 1: Boundary conditions for case A……..91

Table C. 2: Boundary conditions for case B……..91

Table C. 3: Boundary conditions for case C……..91

Table C. 4: Boundary conditions for case D……..91

Table C. 5: Boundary conditions for case E……..91

Table C. 6: Model inputs for all cases…….....92

Table C. 7: Calculated air and coal flow rates for 330MW power plant using coal type A (case A)……...92

Table C. 8: Calculated air and coal flow rates for 330MW power plant using coal type B (case E)……93

Table D. 1: Specifications for different cross-sections and lines in geometry…..96

Table D. 2: Specifications for different cross-sections and lines in geometry…..96

Table G. 1: Summary of literatures taken as a reference for comparison of present model…….113

Nomenclature

A	pre-exponential factor(-)
A	area (m^2)
a	absorption coefficient(-)
C_p	specific heat at constant pressure (kJ/kg)
C_v	specific heat at constant volume (kJ/kg)
D	diffusion coefficient (m^2/s)
D	diameter of particle (m)
$\overline{D}$	mean diameter of particle (m)
d	diameter of particle (m)
E	activation energy (kJ/kmol.K)
F	force (N)
f	mixture fraction
G	incident radiation
H	heat of reaction (kJ)
h	enthalpy (kJ/kg)
I	radiation intensity (W/m^2)
J	diffusion flux ($mol/m^2.s$)
k	turbulence kinetic energy (m^2/s^2)
M	molecular weight (kg/kmol)
m	mixing factor
m_i	mass of species i
n	size (spread) distribution parameter (-)
N	total number of chemical species (-)
p	pressure (kg/m^2)
P_r	Prandtl number ($P_r = C_p \mu / k$)
Q	energy flux (kJ/s)
q	radiation heat flux
R	universal gas constant (kJ/kmol.K)
R_i	reaction rate of ith reaction

R_e	Reynolds number $(R_e = \rho u d / \mu)$
S	Source term
S_c	Schmidt number ($(S_c = \mu / \rho D)$
T	temperature (K)
t	time (s)
V	volume (m^3)
V	turbulent velocity (m/s)
u	velocity (m/s)
α	absorptivity or degree of non-mixing
ε	emissivity (-)
ε	turbulence dissipation rate (m^2/s^3)
Φ	phase function
δ_{ij}	kronecker delta function (-)
ϕ, ψ	general physical variable
Γ	diffusion coefficient
γ	the ratio of specific heats (C_p / C_v)
μ	fluid viscosity (kg/ms)
Π	product(-)
v	kinematic viscosity (m^2/s)
v_i	exponent on the concentration of species i
ρ	density (kg/m^3)
σ	Stefan-Boltzman constant
σ	scattering coefficient (-)
ρ	density (kg/m^3)
τ_{ij}	stress tensor
ω	solid angle
Ω	hemispherical solid angle

Abbreviation

CFD	computational fluid dynamics
CS	cross-section of area
DNS	direct numerical simulation
DPM	discrete phase model
FEGT	furnace exit gas temperature
FVM	finite volume method
LES	large eddy simulation
RANS	Reynolds averaged Navier-Stokes equation
RNG	renormalized group
RSM	Reynolds stress model
RTE	radiation transport equation
PDE	partial differential equation
PDF	probability density function
PISO	pressure implicit with splitting of operators
RTE	radiation transfer equation
SIMPLE	semi-implicit method for pressure-linked equation
SIMPLEC	SIMPLE-consistent
UDF	user defined function
WSGGM	Weighted Sum-of-Gray gases model

Chapter 1

Introduction and Objectives

Pulverised coal combustion is the most widely used technology for power production across the world due to its wide availability. According to various surveys, it is speculated that world coal consumption will be nearly doubled in coming decades. Despite its wide usage for electricity production, there are several paradigms to look for; which are mineral matter in coal, slagging/fouling, clinker formation on refractory walls, and last but not least, emission of pollutants, all of these cost to several billion dollars maintenance in global utilities. Raising issues of global warming and dwindling coal reserves along with government's stringent environment legislation, called for reanalysing the production of electricity towards a cleaner environment and better efficiency. Technological advances and efforts by various researchers, have explored the understanding of the fundamental factors leading to slagging, fouling and clinkering phenomena. Ash is the key derivative from coal combustion which causes slagging, fouling and clinker formation in a boiler. The ash from coal combustion has been a long-standing problem for the utility boilers, causing a reduction in thermal efficiency and unit availability and increases in operating and maintenance budget. Ash deposition is related to both the nature of mineral matter in coal and the boiler operating conditions. Ash release from the coal combustion can behave randomly due to the harsh environment in a furnace, which lead to problems in slagging and fouling at various locations in power plant combustors. When these deposits fuse to the refractory walls of a boiler it makes a strong bonded deposit called a clinker. These clinkers make sootblowing ineffective and, when they detach and fall down from the walls, they damage boiler tubes resulting in power disruptions or outages of plants, and ash hopper explosions. To reduce these issues in a boiler, one such route is to use biomass and coal co-firing technology, but supply problems for the physical quantities of biomass and other maintenance issues limit its feasibility at this stage. Nevertheless, ongoing research will strive towards efficient improvement in the pulverised coal combustion furnace as to meet the stringent policies and demands set by global countries.

Significant number of research and development has been done in last two decades for efficient operation of coal combustion in utility boiler. In spite of wide, on going research activities, there is still much to be explored in terms of fuel characterisation, ash chemistry, slagging/fouling, corrosion, intelligent sootblowing, fundamental deposition, modelling of combustors and cost in utilities firing coal. However, the main objective of this work is the identification of zones with higher propensity of clinker formation in utility boilers with computational fluid dynamics (CFD) modelling.

1.1 Objectives

As mentioned above, there are several issues which exist in a pulverised coal-fired boiler. Therefore, this study is aimed at developing a 3D model of a large scale opposite wall-fired utility boiler in CFD code. In a real boiler operation, temperature distribution and particle trajectories at various fuel loads are the key parameters, which govern the clinker accumulation on the furnace walls. Hence, to identify high propensity areas of clinker formation, it has been decided to investigate pulverised coal combustion inside a 330MW power plant with opposite wall-fired pattern. The driving reason for this objective the limited information provided on opposite wall-fired furnace in open literature and power plant issues with the clinker formation. The modelling of coal combustion is mentioned in the literature from last three decades, but all reported various boiler configurations, loads as well as assumptions. This project will provide the different configuration results with several fuel loads. Fuel load, boiler configuration, coal quality and stoichiometric air requirements are the key parameters for the boiler performance calculations and modelling study. These variables impact significantly on particle behaviour inside a boiler, which in turn reflects the effect of clinker formation on furnace walls.

This thesis articulates the identification of probable faces of clinker formation in pulverised coal-fired utility boiler. Modelling has been done with commercial code FLUENT, which is an unparalleled CFD package with comprehensive combustion models, sought considerably by combustor engineers and researchers for the past decade due to its easy application as well as prediction reliability.

The objectives of this work include:

- the development of a computational domain with actual boiler configuration and mesh generation;
- the use of the comprehensive combustion models available in code;
- investigating the influence of various cases according to fuel load changes for different feed coal in conjunction with real plant data;
- brief discussion and evaluation of temperature distribution, particle trajectories and other parameters for calculated cases;
- validation of the model results using available plant data and literature, as well as identification of furnace walls with a high propensity for clinker formation;
- analysis of probable areas in a furnace to visualise its consequences and governing parameters of those issues in actual utility boiler.

1.2 Thesis Outline

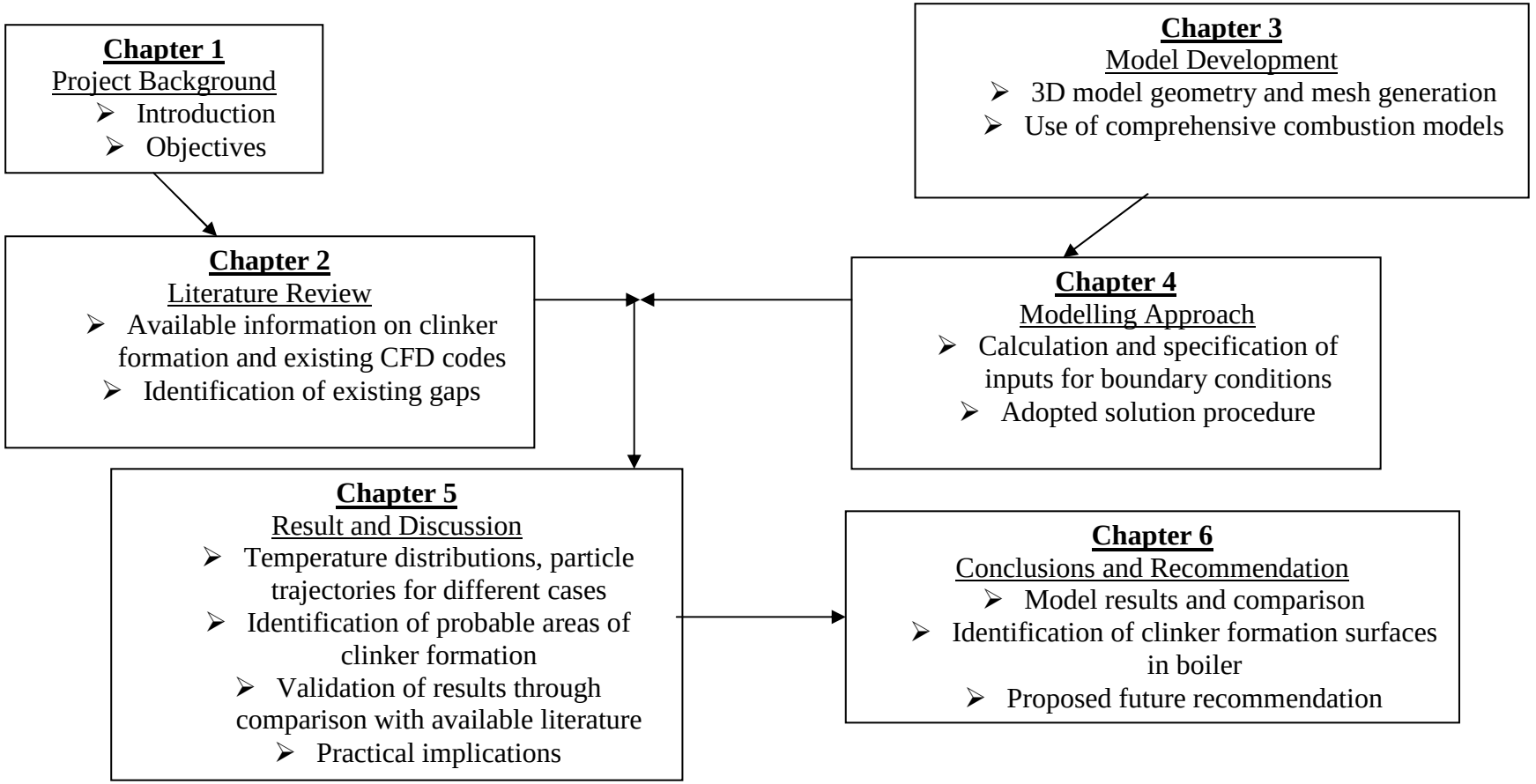

Chapter 2

Literature Review

The brief literature review for this project provides an itinerary of research progress that has been carried out from past to date, stating pulverised coal combustion, modelling, and ash deposition problem or clinkering of coal and its prediction models.

The first section will address pulverised coal combustion and the mineral matter transformation in it. The second section involves review of literature on the ash deposition mechanism, definition of slagging and fouling, predictive indices for slagging and fouling, clinker formation and the effect of ash deposition on furnace operating conditions. This part also provides insight into responsible parameters for ash deposition in a pulverised coal furnace, by addressing some mechanistic studies on mineral size and composition distribution and its analysis techniques. The third section is introduced here, which gives a review on industrial pulverised coal combustors modelling at a glance and also incorporates the work done by various researchers on ash deposition modelling. The final section of this chapter will summarise the available literature review and provide additional research to show the probability to identifying effective areas of clinker formation (big lump deposition) in industrial coal combustors.

2.1 Coal Combustion and Mineral Matter Transformations

2.1.1 Coal combustion

Pulverised coal combustion continues to be one of the main conventional methods of producing electricity over the last several decades, with continuous enhancements in design and performance. To date, it accounts for 40% of total electricity production across the globe. For smooth and efficient operation in an industrial pulverised coal combustor, understanding the coal combustion process to a fundamental stage is necessary. This understanding provides a good platform for the design improvements and modelling of all industrial combustor systems. Combustion is simply referred to

as spontaneous oxidation of coal accompanied by the evolution of heat. To achieve complete combustion of coal in an industrial combustor, the first and foremost parameter is an adequate supply of oxygen. In addition to the supply of oxygen, other parameters like temperature, turbulence and time need to be controlled appropriately to get good combustion. The combustion process of a coal particle can be defined in following steps below, as well as shown in Figure 2.1:

- coal particle drying and then heating-up to the pyrolysis reaction temperature;
- pyrolysis of coal particle to produce non-condensable volatiles (gases), condensable;
- volatiles (tars) and a carbonaceous char;
- Oxidation of the combustible volatiles;
- Char oxidation.

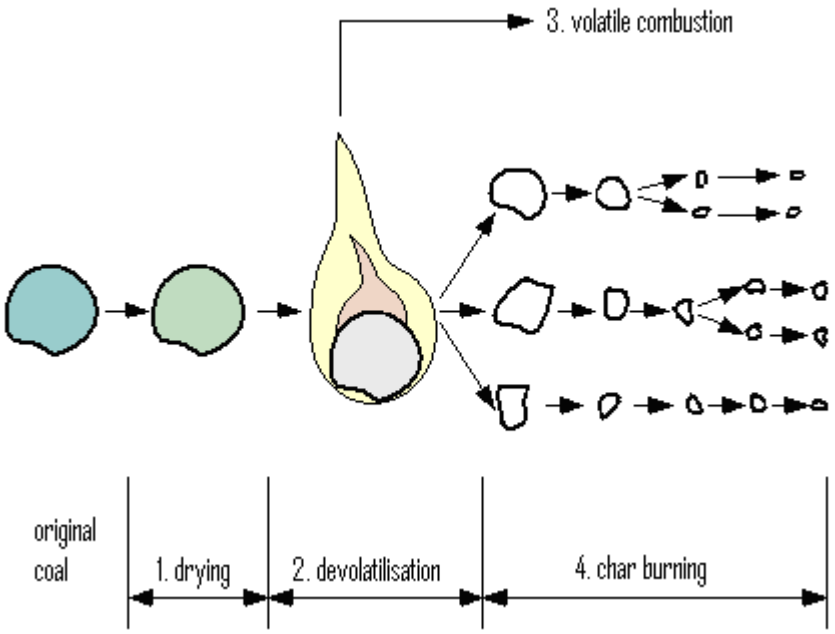

Figure 2. 1: Coal combustion processes (Wu, 2003)

Combustion of coal starts from the burner and appears in the whole combustor. It appears that drying and heating, devolatilisation, and char ignition occur in the region of the burner quarl, whist, final char oxidation and burnout tend to occur in the furnace section (Tillman, 1991). Coal combustion is a very complex process; here it is not the intent to describe all the physicochemical processes and underlying mechanisms involved in it. There are lot of reports and books available stating

the basis of the coal combustion process. The next section will focus on mineral matter in coal, which is the main source of difficulties arising in the coal combustion process.

2.1.2 Mineral matter in coal

Coal is very heterogeneous material composed of both organic and inorganic material. Most commonly, 10-25% of mineral matter presents in feed coal, and it has a major impact on the combustor. Many evaluation techniques are available for mineral matter, though it is still a source of slagging, fouling or corrosion in combustors. Coal contains both organically-bound inorganic elements and mineral matter such as mineraloids and crystalline phases, which result in ash formation during combustion (Couch, 1994). Despite vital design improvements in boiler and prediction methods developed to eradicate mineral matter impact, output is very little.

The mineral matter found in coal includes most of the known elements; only 14 of them are in significant concentrations to contribute to fireside problems. The distribution of these elements and their potential to cause fireside problems for different coal is represented in Table 2.1

Coal is a heterogeneous substance composed of an array of mineral and coal components and exhibits different behaviours during combustion due to its geological origin across the globe. Mineral matter occurs in coal in two general forms: (1) as elements required for the growth of the original plant life from which the coal was formed and (2) as inorganic material, typically sand or silt, or clay, deposited in the accumulating plant debris as discrete particles of foreign material. Association of these minerals affect the true melting and solidifying temperature of each fly ash species entering the steam generator (Bryers, 1995). The major groupings of mineral matter in coals include silicates, oxides, carbonates, sulphides, sulphates and phosphates. The brief study on genesis of coal, distribution of minerals in coal, inorganic characterisation in coal and ash, thermal behaviour of mineral matter is given in literatures (Baxter, 1990, Bryers, 1995, Charon et al., 1990, Couch, 1994, Huffman et al., 1990, Liu et al., 2005, Reid, 1984, Srinivasachar et al., 1990, Thiessen et al., 1936, Walsh et al., 1990).

Table 2. 1: Distribution of mineral elements and their potential to cause fireside problems (Bryers, 1995)

	Element	Bituminous	Sub-Bituminous
Mineral Elements	Si	S	
	Al	S	
	Fe	S	
	Mg	S	
	Ca	S	S,F
	Na	F,C	F
	K	S	
	Pb	-	-
	Zn	-	-
	Ni	-	-
	V	-	-
	Cl	C	
	S	C	S,F

C = corrosion – by Cl or s of metal surfaces in excess of 600^{o}F under reducing conditions and 830^{o}F under oxidising conditions by v above 950^{o}F.

S = slagging – by partial or fully formed melts due to fluxing of quartz by heavy metals at flue gas temperature > 1065^{o}F.

F = fouling – fused or sintered ash due to condensation of volatile species, solid-gas reactions with SO_3 or Cl, solid state reaction at flue gas temperatures from 648 - 1037^{o}C between sulphates and oxides, and molten sulphates.

2.2 Ash Formation during Combustion

Ash is another major pollutant produced from the coal combustion process, only when handled incorrectly. Right use of ash would deliver valuable commercial product. Coal contains both organically-bounded inorganic elements and inorganic mineral matter, which undergo various transformations to form ash. Ash formation involves various processes including coalescence, fragmentation, fusion, vaporisation and condensation that can occur sequentially or simultaneously (Wu,

2005). The mechanisms involved in ash formation (Couch, 1994), the variety of intermediates and products are well addressed in literatures (Hurley and Schobert, 1992, Wall, 1992, Yan et al., 2001, Yan et al., 2002). The type of reaction undergone by a coal mineral during combustion depends on both its chemical composition and its physical morphology. Mainly fragmentation and coalescence occur during the coal combustion. The main ash formation for coal occurs from the included and excluded mineral particles. As included minerals are close to each other in a char particle, during char combustion, they often appear as molten on the char surface and enable coalescence and agglomeration to occur. Excluded minerals behave quite differently from included minerals; it releases several fragments of ash particles from one char particle and cause deviation in the particle size distribution (PSD). Considerable efforts have been made in the last two decades for the development of prediction schemes for coal slagging and fouling propensity, mostly emphasising on ash composition and mechanistic approaches. Those approaches describe the evolution of size and composition distribution in detail, which is summarised in Figure 2.2.

A number of approaches have been proposed to predict ash formation and deposition of various types of coal during combustion. A mathematical model developed for ash formation during pulverised coal combustion (Yan et al., 2002) uses computer controlled scanning electron microscope (CCSEM) analysis as the input data. CCSEM technique also provides information on mineral size, mineral chemical composition and the association with coal particles. Extensive literature review is available for coal quality assessment (Carpenter, 1995).

2.3 Ash Deposition Mechanism

This topic discusses the theory behind important factors related to ash deposition and the research which has been done for modelling of deposition-related processes. The deposition process depends directly on the nature of the mineral matter in coal. It also depends on the conditions inside the boiler of temperature, residence time, fluid dynamics and of the locally oxidising or reducing environment. For ash or volatiles to cause problems they have to be transported to and held on the heat transfer surface, where transport mechanisms within the gas include (Couch, 1994):

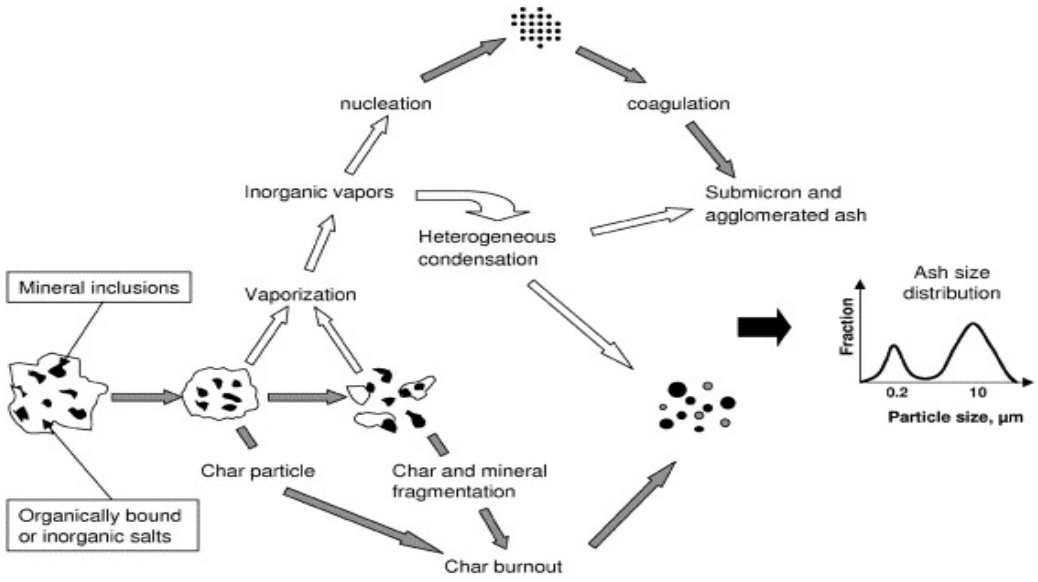

Figure 2. 2: Schematic illustrations of ash formation paths (adapted from (Kær et al., 2006))

- Molecular and Brownian diffusion;
- Thermal diffusion;
- Eddy diffusion;
- Gravity effects;
- Electrostatic effects.

The ash deposition process mainly includes four principle mechanisms according to recent analysis(Baxter and DeSollar, 1993):

- Inertial impaction;
- Condensation;
- Thermophoresis;
- Chemical reaction.

Inertial impaction is believed to be the dominant deposition mechanisms on superheater tubes or at any location where entrained ash particles are required to turn sharp corners at high velocity. Inertial impaction occurs when a particle has sufficient momentum to impact on the surface by penetrating the flow-field surrounding the obstruction; it is more common for larger particles. The sticking propensity of a particle to the surface or tube depends on the particle properties at the moment of impact as well as those of impacted surface.

Condensation occurs when mass from the gas phase pass over cool heat transfer surfaces and various components collect over the boundary layer. Thermophoresis is only significant for very fine particles which transports and deposits on cooled surfaces like superheater tubes, where temperature is lower. As the insulating layer of ash accumulates and the temperature difference between the gas and the deposit surface temperature decreases, thermophoretic deposition also decreases (Kær et al., 2006).

Once the particle comes to the tube or deposit surface, some bonding will be driven by chemical reactions. These reactions may also affect the properties of ash deposit by changing the temperatures of the deposit. Some of the leading chemical reactions in respect to ash deposition process are(Couch, 1994):

- The formation of low temperature eutectics from the interaction of iron, sodium or calcium, and the alumina and silica;
- Sulphation;
- Alkali absorption;
- Oxidation.

Chemical reactions are strongly temperature dependent and on the contrary its effect on deposition will come up according to different temperatures of boiler. With these four mechanisms there are several other mechanisms prevailing for the deposition process. These other mechanisms include electrostatic forces, photophoresis, and brownian motion. According to the literature, these mechanisms are not significant for ash deposition.

2.4 Slagging, Fouling and Clinker Formation

Slagging refers to the deposition taking place in the parts of boiler, which are highly exposed by flame radiation. These areas include burners, the main boiler's water walls, the bottom hopper and the bottom of the heat exchange tubes. On the contrary, fouling takes place in the parts of boiler which are cooler; say the convection section where flue gas cools. Sections of the boilers where slagging and fouling takes place are shown in Figure 2.3. In case of high temperature fouling, deposits takes place in the superheater and reheater regions of the boiler.

Slagging and fouling deposits in a boiler occur via many different mechanisms; many slagging deposits have pyrites as the main mineral matter and as it forms clinkers on furnace walls, some have calcium and/or sodium rather than iron. On contrary presence of iron in the slagging deposit tends to react with the alumino-silicates (clays) to form low melting point (creates low melting point eutectics) or low viscosity particles which stick to the walls or tubes.

The deposit may consist of one or more types of forms like metallic, amorphous, vesicular and sintered. According to the Figure 2.3, deposits in utility boilers occur on the wall, superheater, convection pass, air heater blockages and stack. There are some major causes mentioned in Table 2.2 for wall slag. In dry bottom boilers, wall slag changes from sintered to vesicular or amorphous and can run down the wall plugging the opening at the bottom of the furnace. Wall slag acts as an insulator, impedes heat transfer to the water wall, which results in an increase of furnace exit gas temperature (FEGT) and allows molten particles to escape the furnace where they can cause slagging of the screen tubes and convection passes. Slag build up around burners (called ‘eyebrows’) can occur, blocking the coal flow into the furnace and will result in damage to the burner, windbox, and coal pipe.

Wall slag exacerbates other deposition problems and the most common is raising the FEGT, which leads to superheater slagging. When slag build up between superheater tube spacing, the flue gas velocity increases, which results in slag formation in the next section of the convection pass. As mentioned in the Table 2.2, several boiler modifications and coal quality changes can solve slagging problems.

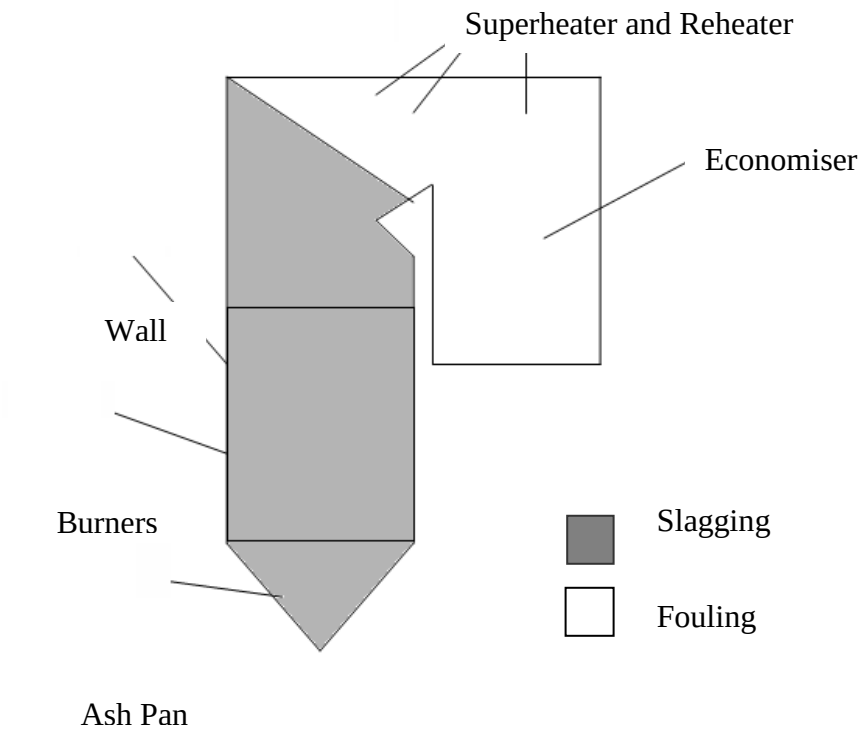

Figure 2. 3: Slagging and fouling in pulverised coal combustion boiler

Table 2. 2: Major causes of wall slag

Coal Related	➢ Large excluded pyrite particles that could impact the inner wall before they complete combustion ➢ Illites-clay minerals that contain impurities such as iron, potassium, or sodium that flux aluminosilicates glasses ➢ Interaction of included pyrites, quartz and clays to form viscous glassy phases
Equipment Related	➢ Soot blowers not effective or not used ➢ Coal size from pulveriser too large ➢ Improper fuel/air ratio ➢ Burners damaged or not adjusted properly ➢ Furnace size too small to handle coal properties of coal being burned

The boiler modifications generally try to decrease the FEGT by adding additional surface area, or by adding additional soot blowers to improve heat transfer; in the same way, modifications in boiler capacity to reduce FEGT, coal quality change and addition of copper oxychloride to eliminate ash deposition in utility boilers. Fouling deposits occur when sulphur oxides from the flue gas reacts with alkali ash components and form alkali sulphates. After a period of time, a deposit which formed in the radiation zone fuses to the surface and forms a permanent, strongly-bonded deposit which is hard to remove with a soot blower, called clinkers. Clinkers mainly formed due to low fusion temperature of ash present in coal. The build up of clinkers mostly occurs on the refractory surfaces surrounding the burners, where considerable presence of CaO, MgO, Feo, Fe_2O_3 and Fe_3O_4 as well as alumina and silica can be found. Clinker has tendency to grow on hot surfaces rather than cold surfaces. Because it is very dangerous if those clinkers fall inside the furnace, they should be removed before performing the inspection work. An investigation into the clinker formation problem has been carried out which suggests that the problem is related to burner aerodynamics and, in particular, the degree of swirl on the burners (Boyd and Lowe, 1990). A clinker around the burner causes the problem of flame distortion and subsequent burner trips due to flame scanners being unable to detect the flame. This deposit leads to reduced heat transfer in the boiler and corrosion of boiler tubes, which may result in reduced generating capacity and unscheduled outages. Here, build up of deposits on burner throat, furnace wall and superheater is shown in Figure 2.4. Fouling deposits mainly form due to the presence of silicate liquids in deposits and according to their concentration on surface the deposit becomes strong or weak bonded. Power utilities had little success in solving fouling problems in boilers not designed for high fouling coals. Most solutions have been to increase the number of soot blowers in the affected region with an increase in soot blowing intensity. After the flue gas leaves the convection passage of the furnace it still contains a considerable amount of energy. To recover the energy from flue gas, utilities have two primary types of heat exchangers (or air heaters). Sulphuric acid condensing from the flue gas and mixing with fly ash forms acid smut, which cause blockages in air heaters. The major causes of ash deposits are widely cited in literatures and referred to by various combustor designers (Hatt, 1990).

While designing the combustors there are many factors to consider in preventing slagging and fouling during operation, which are heat transfer/boiler size, global and local thermal level, combustion conditions, and soot blowing frequency in boiler. There are many reasons due to which boiler operation, according to one specific coal, is not possible; usually power plant operators are forced to switch the fuel due to fuel cost, supply from the mine and demands to meet emission restriction due to global-warming.

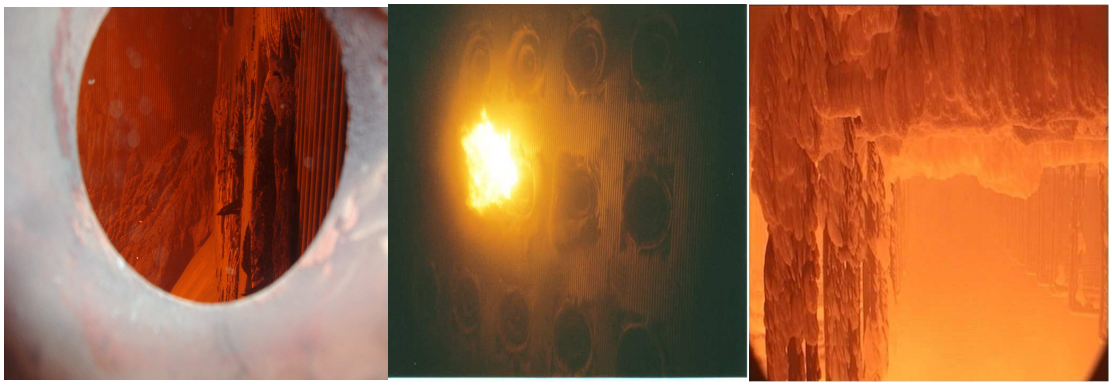

(a) (b) (c)

Figure 2. 4: View of real plant deposits (a) clinkers on furnace wall (b) burner throat (c) hanging clinkers on superheater (as received)

During the past decade, considerable advances have been made in developing models to predict ash deposition behaviour, especially in the prediction of fly ash size and composition distributions, the development of improved slagging and fouling indices, and the prediction of the relative slagging and fouling potential of different coals or coal blends (Wang and Harb, 1997). Predictive indices and deposition models help plant operators and designers to diagnose and rectify operational problems which arise due to this unwanted deposit. Literature review on predictive indices and different deposition models with computational modelling of combustors, developed in recent years by various researchers across the globe, is mentioned in next section.

2.5 Predictive Indices, Ash Deposition Codes and Modelling of Combustors

The growing interest in global warming due to carbon dioxide emissions and the price hike in fuel has drawn attention to all pulverised coal combustion operators for switching fuel and efficient operation. In the last two decades, numerous works have been done to combat pulverised coal combustion issues like ash deposition, slagging/fouling, corrosion and erosion in utility boilers. Boiler design and the choice of coal for an existing unit have always been, and still are, largely based on empirical indices derived from past experience. Traditional approaches to the prediction of the deposition behaviour of coal usually involve the use of empirical indices and ASTM ash fusion temperatures. During the last decade, a number of techniques have been tested and developed which can help in boiler troubleshooting and to check where the unwanted ash deposits formed.

Mainly, these techniques include measurements and samples taken from inside a boiler, experimental tests on drop tube furnaces and pilot scale combustors, ash analysis via CCSEM and indices, direct metering of heat flux and modelling of combustors to see the flow patterns and combustion behaviour inside the furnace. This topic is too vast to include in one chapter, although an effort has been made to incorporate major topics related to this project. The main purpose of these predictive indices, modelling and laboratory test work are so that an operator can assess the alternative coal supply in an existing unit, to help an operator with particular deposition like slagging and fouling, and to help provide a base for a new boiler design.

Traditionally, empirical indices have been used to predict coal deposition tendencies and they are still widely used due to their easy application in spite of their misleading results. There is abundant information about definition and practical use of many of these indices reported in published literatures (Couch, 1994, DeSollar, 1995). To overcome the restriction of traditional indices, researchers across the globe have come across new deposition models developed over the year. Ash transformation models have been developed with the better understanding of coal inorganic matter. Inputs of these models have incorporated advanced coal analysis method CCSEM,

which is already described earlier in the chapter. The detailed discussion on literature review on ash transformation models is provided in the given reference (Wang and Harb, 1997). Development of these models paved the way for deposition models.

These models are based on issues which include: (Wang and Harb, 1997):

- ash formation;
- fluid dynamics and particle transport;
- particle impaction and sticking;
- deposit growth as a function of location in the combustion chamber;
- deposit properties and strength development;
- heat transfer through the deposit;
- the effect of deposition on operating conditions (e.g. temperature and heat fluxes); in the combustor;
- deposit structure and its effect on flow patterns in the combustor.

Recent developments in these models for particle impaction rates in the near-burner region, particle boundary layer transport model, prediction of fouling tendencies, sticking propensity models incorporating variables like particle velocity, viscosity, surface tension, temperature, size and impact angle have been formulated for the prediction of ash deposition. In order to develop a comprehensive mathematical model that can simulate ash deposition and its impact on power plant overall efficiency, a mechanistic modelling approach should be followed. Information of coal samples using the advanced techniques gives data feed into mineral-to-ash transformation model followed by generation of ash particles and their properties. Integration of this data with combustion code will predict the ash deposit behaviour in the utility boiler and the effect of ash deposition on the boiler operating conditions. Some of these ash deposition codes (Wang and Harb, 1997, Srinivasachar et al., 1992) are not incorporated into the comprehensive combustion code. Models for slagging and fouling addressed by two separate sub modules introduced (Erickson et al., 1995) on the basis of coal mineralogy data obtained from CCSEM particle size distribution data, boiler design details, and boiler operating conditions with the validation of laboratory, pilot, and field test data. As the research goes on and researchers compiled with the computational fluid dynamics code to predict the behaviour inside industrial combustors. Before describing the ash deposition code with combustion

code, here is some discussion provided for the earliest research on modelling of combustors. Some of the earliest work was done at imperial college (U.K.),(Patankar and Spalding, 1973). A review on the approaches, equations and solution methods employed by using CFD to model practical combustors including industrial furnaces is given by (Lilley, 1979). Three-dimensional analytical model of a large tangentially-fired furnace is presented by (Robinson, 1985); alternatively, prediction of three-dimensional flows in utility boiler furnaces and its comparison with experiments (Gorner and Zinśer, 1988, Boyd and Kent, 1988) and transfer of fundamental results to the modelling is achieved (Lockwood et al., 1988, Lockwood et al., 1980). After a decade, commercial software programs like PHOENICS, FLUENT, FLOW-3D, TEACH and PCGC-3 emerged as a new era in modelling of combustors. PCGC-3 combustion model developed to simulate large-scale, steady-state, gaseous and particle-laden, reacting and non-reacting systems. Recent combustion modelling in front-wall fired furnace (Vuthaluru and Vuthaluru, 2006, Xu et al., 2001) and tangential-fired furnace (Belosevic et al., 2006, Belosevic et al., 2008, Choi and Kim, 2009, Fan et al., 2001a, Filkoski et al., 2007, Korytnyi et al., 2009, Vuthaluru et al., 2008, Yin et al., 2002, Yin et al., 2003, Zheng et al., 2002) using other computational codes are developed and contains the best insight into combustion behaviour in different utility boilers across the globe . On the other side of modelling ash deposition with predictive scheme based on CCSEM fly ash data and computational fluid dynamics was developed to study the slagging propensity of coals it was applied to predict the deposition potential of three UK coals in a pilot scale single burner ash deposition test facility. This study reveals fundamental aspects of slagging in pulverised coal-fired boiler by predicting the relative slagging propensity (Lee and Lockwood, 1998). The overview of this model is given in Figure 2.5, which represents the schematic of the model input and output.

An advanced model to assess fouling and slagging was given with the strategy to investigate this influence by introducing heat resistance to represent fouling and slagging on furnace walls using plant heat flux reading data together with computational fluid dynamics code (Xu et al., 2002). Another model has been developed (Fan et al., 2001b) to simulate deposit growth under slagging conditions coupled with comprehensive combustion code to predict the flow-field, the temperature field and the deposit growth behaviour in a pulverised coal-fired boiler.

The result shows that deposits in a boiler grow rapidly where particle impaction probability and the temperature of wall surface are too high. Another mechanistic model is developed to simulate the ash deposition behaviour of Australian high-rank coals in the radiant section (slagging) of a test furnace at the Australian Coal Industry Research Laboratories Limited (ACIRL) (Rushdi et al., 2005).

This approach starts with the analysis of coal samples, which generates detailed information of coal particles and mineral grains, which is eventually used for the calculation of mineral-to-ash transformations. To simulate the deposition process, a CFD code called 'teach' was used in the study. This approach was used successfully in ranking the ash deposition behaviour for Australian high-rank coals in the radiant section (slagging) of a pilot-scale furnace An integrated tool predicting ash formation, transport and deposition, as well as deposit growth and strength development has been developed by RMT, inc., a subsidiary company of Alliant Energy Corporation and the university of North Dakota Energy And Environmental research Center (EERC) called AshPro^{sm}. This model was applied to a 512MW tangentially-fired boiler at Wisconsin power & light's Columbia Energy Center to evaluate the localised slagging on furnace walls and fouling in convective pass (Ma et al., 2007). Overall, step-by-step improvement occurs as various researchers gain an understanding of pulverised coal combustion.

Via a CCD (charge coupled device) camera, visualisation of ash deposition is possible; observation of clinker formation behaviour, and determining the location and extent of clinker formation has been achieved. A model that predicts deposit growth and the exfoliation process was developed to simulate a probable clinker formation zone (Yamashita et al., 2008).

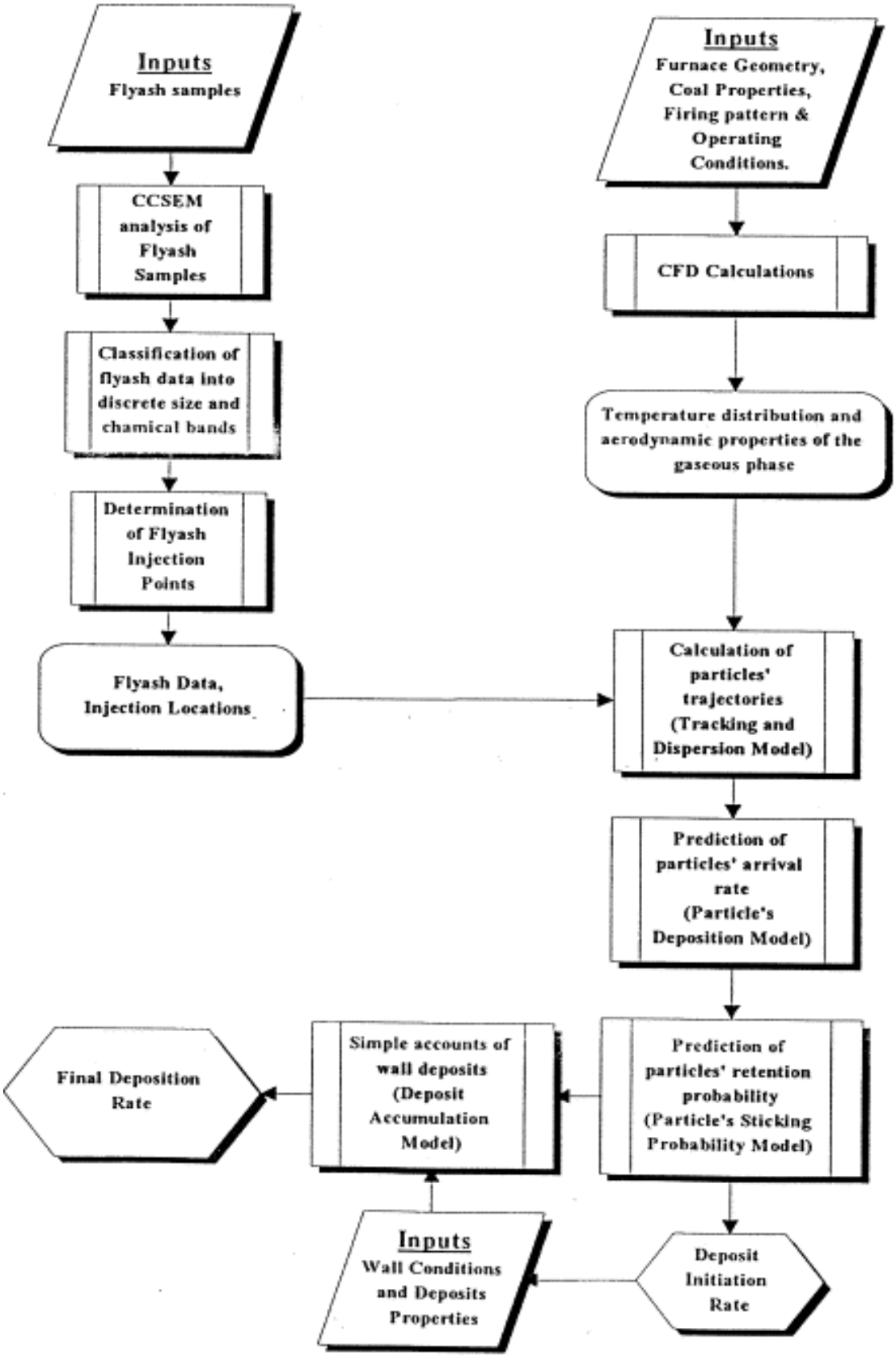

Figure 2. 5: Schematic of ash deposition model (adopted from (Lee and Lockwood, 1998)

2.6 Summary of Literature Review

Although many studies of ash deposition in pulverised coal combustion have been conducted, there still remains much to be learned in terms of slagging, fouling and clinker formation. Advanced research has emerged in coal combustion, where particle size distribution and fly ash generation can be determined by extravagant analytical techniques such as CCSEM. These analysis and calculations are necessary for the development of ash deposition model. It is known from the available literature review that in order to predict clinker formation or the probable zone for deposition in utility boilers, which postulates wide range of information from basic coal properties to up-to-date modelling softwares to model the power plant boiler.

The vital and foremost step to tackle this problem is to have more detailed knowledge of coal combustion and modelling of coal combustion in commercial CFD code. Second step would be identification of governing parameters which regulates accumulation of clinker on furnace walls. To date, there are many models developed for predicting ash deposition with combustion code, which yields good results, but only specified to one particular condition or based on laboratory test data or different plant circumstances. There is no generalised model for the identification of clinker formation zones in boilers, exist to date. Hence, this study will suggest wall surfaces in particular designed boiler, where there are extreme chances of ash deposition. Identification of these wall surfaces could be beneficial for power plant engineers to identify ash deposition mechanism as well as low temperature eutectics from interaction of mineral matter present in flow gases. This study can provide the strong platform to study the series of mechanism for clinker formation.

In view of the above necessity, a study has been undertaken to develop a 3D model for front wall-fired utility boiler of 330MW capacity with commercial code FLUENT. The study incorporates analytical observations of temperature zones at different level, particle trajectories and velocity profiles. A particle tracking within the boiler provides residence time and their appropriate temperature range. Analysing temperatures of particles provides probable location of clinker formation on the furnace walls. This will enable the process operator to opt for intelligent sootblowing and take informed decisions to control and/or reduce clinker formation in boilers.

Chapter 3

CFD in Pulverised Coal Combustion

Computational fluid dynamics is a numerical tool for simulating the complicated fluid flow, heat transfer, and chemical reactions in a combustor (Baukal et al.,2000). The role of CFD in engineering prediction has become so strong that, today, it has taken a permanent place in all aspects of fluid dynamics from basic pipe flow to complex engineering design. In past times, to simulate any unit operations or unit processes, industry people used to set up workstation. Today, we have superpower computers and even personal computers are fast compared to workstation. Today we have superpower computers. Another reason for wide use of CFD codes is that they are easily available at moderate cost. There are many important factors, which lead to modelling a combustion system. The simplest and foremost thing is to optimise a system. To study 330MW power plant parameters, CFD commercial code FLUENT and pre-processor GAMBIT are adapted to model and create the geometry of the furnace. Operational data were used to model the furnace and install burners. For several possible configurations of the burners and fuel load, the flue gas path in the boiler was analysed. Before describing modelling theory for non-premixed combustion, basic concept of CFD codes, which reveals its working path, essential components and numerical solution techniques described in following sections. This study entails use of non-premixed combustion modelling but, prior to that, modelling of basic fluid flow, turbulence, heat transfer and finite rate chemistry are described in this chapter. Before using CFD code, one must understand that it is not a panacea. The user must understand the problem definition thoroughly and set up pre-analysis to make assumptions for a given problem without affecting the result accuracy for the given problem. All the models available in CFD code have their certain limitations that the user must take care of (Baukal et al.,2000).

3.1 Introduction to CFD

It was in early 19^{th} century that Navier (1827), Poisson (1831) and Stokes (1845) derived the fluid flow equation commonly known as Navier-Stokes equation, which

forms the basis for CFD calculations. In CFD, physical systems involving fluid flow within definite boundaries can be represented in terms of mathematical equations, usually in the form of partial differential equation (Bashir et al., 2004). as "Computational fluid dynamics is a discipline that encompasses the numerical solution of the equations of motion (mass, momentum and energy) in a flow geometry of interest, together with subsidiary sets of equations reflecting the problem at hand" (Harris et al., 1996).

The physical aspects of any computational fluid dynamics are governed by the following three basic principles:

(1) Mass is conserved (or Equation of Continuity)
(2) F = ma (Newton's Second Law)
(3) Energy is conserved (First Law of Thermodynamics)

Description for basic equations is provided followed by elements of CFD code in this chapter.

3.1.1 Elements of CFD Code

CFD codes are equipped with numerical algorithms to solve any fluid flow problems. There are three main elements (Versteeg and Malalasekera, 2007):

(I) a pre–processor (in this project GAMBIT is used)
(II) a solver
(III) a post–processor

(I) Pre–processing

Once problem specifications and assumptions are made, the user will be in the pre–processing stage to define the geometry of the problem of interest in computational domain. For this project, the author used GAMBIT pre–processor to develop furnace geometry. Development of a grid (or mesh) of cells (or control volumes or elements) in the computational domain by sub–division in smaller number. Once mesh is generated in the domain, define the appropriate boundary condition to represent different parameters of flow problem. Meshing task is an important factor for

accuracy, as large numbers of mesh volume improve the solution. There are some factors having influence in mesh generation, like appropriate spacing, skewness, computational time on domain and so forth. After taking care of all these factors, two kinds of mesh generation are possible

To specify meshing scheme, there are two parameters which come into the picture, namely

- Element
- Type

The elements parameter defines the shape(s) of the elements that are used to mesh the volume. The type parameter defines the meshing algorithm and, therefore, the overall pattern of mesh elements in the volume. A list of meshing scheme elements is shown in Table 3.1

Table 3. 1: List of available meshing schemes in GAMBIT (user's guide)

Element Option	**Description**
Hex	The mesh includes hexahedral mesh elements only
Hex/wedge	The mesh composed primarily of hexahedral mesh elements but includes wedge elements where appropriate
Tet/hybrid	The mesh composed primarily of tetrahedral mesh elements but may include hexahedral, pyramidal, and wedge elements where appropriate

In the same way, type parameter includes Map, Submap, Tet Primitive, Cooper, Tet/Hybrid and Stairstep. As noted above, each of the elements options are associated with a specific set of one or more of the type options. The structured grid, for the furnace created with the use of hex scheme, is represented above in figure 3.1(a). This structured mesh represents 296756 hexahedral cells, which requires large

construction time, but gives solution accurate and with less computer time on an ordinary computer system.

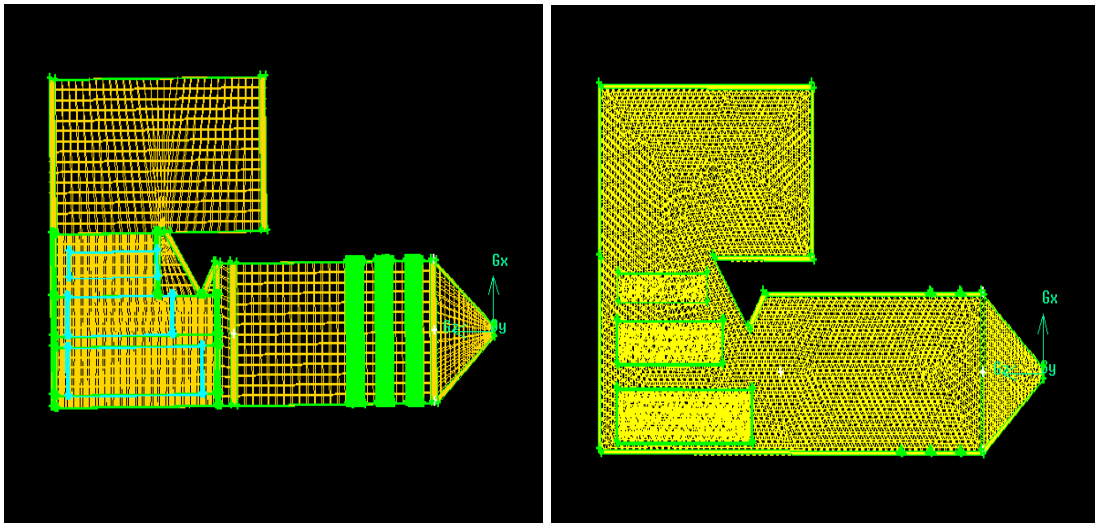

(a) (b)

Figure 3. 1: Representations of different meshing schemes (a) structured grid, (b) unstructured grid

To achieve result quickly with appropriate accuracy, user can adopt tetrahedral grid elements scheme via constructing an unstructured grid, as schematically represented in figure 3.1(b). Over half of the project period spent on this project is devoted to the definition of the domain geometry, grid generation and grid dependency study.

(II) Solver

There are three kinds of numerical solution techniques available in CFD codes.

- finite difference method;
- finite element method;
- finite volume method.

in general, these described methods create the base for solver to perform the following steps (Versteeg and Malalasekera, 2007);

- approximation of the unknown variables by means of simple functions;
- discretisation by substitution of the approximations into the governing flow equations and subsequent mathematical manipulations;
- solution of the algebraic equations.

The main difference between the three methods is the way the approximation and discretisation processes are done for flow variables. Solver used in this project is fluent commercial code, which is solely based on finite volume method. Finite volume method and numerical method for solving combustion task is described in later sections.

(III) Post–processor

Once the solution for a given problem is converged, the post–processing step comes into the picture. In recent years, there has been a tremendous work done in this area to increase graphics capabilities. There are many data visualisation tools available in software packages, which are:

- domain geometry and grid display;
- vector plots for different process parameters;
- probability density function display;
- contour plots stating various parameters;
- particle tracking;
- species fraction;
- flux reports.

Likewise, there are many more post-processing steps to assess problem solution. The graphics output in today's available CFD codes have given new era to visualise the problem in any problem.

3.1.2 Background of the selected CFD package

FLUENT was originally developed by Swithenbank, et al. (Boysan, et al., 1981) and extended by FLUENT Inc., headquartered in Lebanon, New Hampshire. As mentioned integration of two individual programs to carry out research are: Gambit and FLUENT. Gambit is used for geometry creation and meshing, and FLUENT

performs the remainder of the model selection, calculations, and post-processing. FLUENT is a state of the art program which has hundreds of options for materials (gas, liquid, and solid), material properties, flow (laminar and turbulent), heat transfer (conduction, convection, and radiation), reacting flow, boundary conditions, and solution techniques. Models adopted for coal combustion in this project, which are referred in later on sections of this chapter. This software is fairly easy to learn, and has helpful guides (Fluent, 2007) that explain most of its options. This package emerges the most robust among all other CFD codes like PHOENICS, STAR-CD, GLACIER, FLOW-3D and many more. One limitation of this package is the pre-processing tool is not able to create complex domain generation. Another complexity of this software is too creating and hooking up user defined functions in the defied problem.

Nevertheless, it has gained lot of attraction from CFD users across the globe and proven best in a past decade.

3.2 Mathematical Models

A pulverised coal combustion simulation involves modelling a continuous gas phase flow regime and its interaction with a discrete phase of coal particles. Here, reaction is modelled using non-premixed combustion model, which includes PDF (probability density function)/mixture fraction approach. However, you can model by species transport model as well. This modelling approach considers all physical processes as turbulence ($k-\varepsilon$ model), radiation (P1), and discrete phase model incorporating rosin – rammler size distribution correlation. Stochastic tracking is employed to include the effects of turbulent dispersion. Coal devolatilisation is modelled with a single rate kinetic model and char combustion is modelled with weighted kinetics/diffusion model.

Basically, mathematical modelling is based on a set of coupled conservation equations of mass, momentum and energy and chemical species transport and reactions, and the state equations of the fluid system. Most practical flows are turbulent, thus determining all the conservation equations as a function of space and time. Differential relationships, in the form of partial differential equations, are the

form most often employed in developing CFD numerical procedures and are mentioned in this study as well.

3.2.1 Basic conservation equations

The governing equations of fluid flow represent mathematical representations of the conservation laws of physics. The fluid will be regarded as a continuum. Equation of continuity is derived from the law of conservation of mass. A mass balance for a fluid element can be written as rate of change of mass in fluid element is equal to net rate of flow of mass into element.

$$\frac{\partial \rho}{\partial t} + \frac{\partial (\rho u_i)}{\partial x_i} = S^m \tag{3.1}$$

where ρ is the fluid density, u_i are the velocity components in each directions x_i, and S^m is the mass source in the system.

The mass balance for multi–component system, can be delivered as,

$$\frac{\partial (\rho m_i)}{\partial t} + \frac{\partial (\rho u_i m_{i'})}{\partial x_i} = -\frac{\partial}{\partial x_i} J_{i',i} + R_i + S^m \tag{3.2}$$

where parameters,

$J_{i',i}$, is the diffusion flux of species i' due to concentration gradients and can be represented by fick's law of diffusion.

$m_{i'}$ is the local mass fraction of each species in the system.

R_i is the mass rate of formation and S^m represents a source of mass generated.

The momentum equation for the system is derived from the Newton's second law of motion also called Navier-Stokes equations:

$$\frac{\partial (\rho u_i)}{\partial t} + \frac{\partial}{\partial x_i}(\rho u_i u_j) = -\frac{\partial p}{\partial x_i} + \frac{\partial \tau_{ij}}{\partial x_j} + S^{mi} \tag{3.3}$$

where p is the local (static) pressure, τ_{ij} is the stress tensor, S^{mi} are the momentum in each of the coordinate directions. The stress tensor τ_{ij} can be given by this equation,

$$\tau_{\mathrm{ij}} = \mu\left(\frac{\partial u_i}{\partial x_j} + \frac{\partial u_j}{\partial x_i}\right) - \frac{2}{3}\mu\frac{\partial u_k}{\partial x_k}\delta_{ij} \tag{3.4}$$

where μ is the viscosity of fluid. In this equation, the first term on the left side represents the rate change of momentum per unit volume with time and second term represents the change of momentum generated from convective motion.

The conservation equation of energy can be derived from the first law of thermodynamics and can be described in following way, “rate of increase of energy in system is equal to sum of net work done on system and total heat addition to the system”.

Hence the equation can be written as,

$$\frac{\partial(\rho h)}{\partial t} + \frac{\partial(\rho h u_i)}{\partial x_i} = \frac{\partial p}{\partial t} + \mu_i\frac{\partial p}{\partial x_i} - \frac{\partial}{\partial x_i}\left(k\frac{\partial T}{\partial x_i}\right) - \frac{\partial}{\partial x_i}\sum_{j'} h_j J_{j'} + \tau_{ik}\frac{\partial u_i}{\partial x_k} + S^h \tag{3.5}$$

where specific enthalpy calculated as,

$$h = \sum_{j'} m_{j'} h_{j'} \tag{3.6}$$

$$h_{j'} = \int_{T_{ref}}^{T} c_{p,j'}\,dT \tag{3.7}$$

In the equation energy source S^h due to chemical reactions can be expressed as

$$S^{h}{}_{reaction} = \sum_{j'}\left|\frac{h_{j'}^{o}}{M_{j'}} + \int_{T_{ref_{j'}}}^{T_{ref}} c_{p,j'}\,dT\right| R_{j'} \tag{3.8}$$

As in the eq. (3.5), the first term on the left hand side of the equation represents the rate of change of enthalpy per unit volume with time and the second term represents

the change of enthalpy resulting from convective motion. Similarly, on the right hand side is molecular diffusion of enthalpy based on Fourier's law of heat conduction. Energy transfer due to radiation is described in radiation models.

3.2.2 General transport equation

For a general variable ψ of the fluid, mass, species, momentum and energy equations can be summarized into a general transport equation of ψ as

$$\frac{\partial(\rho\psi)}{\partial t}+\frac{\partial\left(\rho\psi u_j\right)}{\partial x_j}=\frac{\partial}{\partial x_j}\left(\Gamma_\psi\frac{\partial\psi}{\partial x_j}\right)+S_\psi \tag{3.9}$$

where, Γ_ψ and S_ψ are diffusivity and corresponding source term for scalar quantity ψ respectively. The solution for these conservation equations is a very complex task. There are various numerical techniques available to solve, which are described in following section.

3.3 Solution Methods in Computational Fluid Dynamics

There are various methods available to solve the equation of motion. The Navier-Stokes equations provide an "exact" model for turbulence in general cases of fluid flow systems (Baukal et al., 2000). The solutions to these equations are too complicated to solve exactly either analytically or numerically. Therefore, different types of approximations are taken into consideration to solve these equations.

There are four types of approximations available in various literatures, namely moment averaging, vortex methods, spectral and direct numerical simulations (DNS). The direct numerical simulation (DNS) is a fundamental solution technique. In this technique, exact Navier-Stokes equations are solved for the largest and smallest turbulent length and time scales. To solve these Navier-Stokes equations requires huge computing power; hence, it is not a viable method to solve industrial combustion problems. The second type of numerical approaches closely related to DNS is known as vortex methods. Two different schemes are available; one is fine discretisation with Eulerian scheme, whereas the second is coarser discretisation with

Lagrangian formulation. As with the DNS simulations, these techniques have been applicable to limited study of flow characteristic.

To simulate large scale of combustion systems, moment averaging is a famous solution technique because it is widely available in commercial software programmes like PHOENICS, FLUENT, FLOW-3D, TEACH, PCGC-3 and many others (Launder and Spalding, 1974). This method utilizes averaging of turbulent velocity components by solving $k-\varepsilon$ turbulence model as closure equations. In these methods, the derivatives in PDE's are approximated by algebraic expressions representing the discrete distances in the flow field. Either of the finite difference, finite element and finite volume based methods are used for discretisation (Eaton et al., 1999). Where,

- finite difference method - based on Taylor's series, polynomial expansions;
- finite element method - based on calculus of variations and the method of weighted residuals;
- finite volume method - based on integral form of the conservation equations instead of differential form.

Among all of these methods, the finite-volume approach has been adopted by many users for many computational fluid dynamics applications, including most comprehensive combustion codes because it is applicable to a variety of grid structures. The end-result of the discretisation method is a set of algebraic equations that can be solved to calculate mass, momentum and energy transport on discrete points in the flow field. These calculated points are generated as a grid. The grid structure, as described in earlier meshing section, holds simple and complex construction made of rectangular and tetrahedral elements. To solve these grid discretisation equations, they must be divided into main two categories based on whether the compressible or incompressible forms for the equations of motion are being solved; mainly for compressible flow regimes, referred to as density-based solver because of the relation between the pressure and density established in equation of state. The solution techniques for incompressible form of equations of motion are solely based on pressure variation. An additional relationship for pressure called Poisson equation can be derived via mathematical manipulations of continuity and momentum equations. To solve this additional relationship for pressure, there are

many approaches like SIMPLE (Semi-Implicit Method for Pressure-Linked Equations), SIMPLER (Simple Revised), SIMPLEC (Simple Consistent) and PISO (Pressure Implicit with Splitting of Operators) (Versteeg and Malalasekera, 2007).

In most practical combustion problems, the incompressible form of the equations of motion using a FV form of the discretisation equations are solved with the simple-based approaches, assuming steady-state flow field in many utility furnace problems.

3.4 Turbulence Models

Above described basic governing equations for a homogeneous fluid flow forms a closed set of partial differential equations (PDE). This situation is only viable to solve laminar flow problems.

The effect of turbulence in real practice can be described as a three dimensional, time–dependent, chaotic, random and dissipative flow. To solve turbulence flow with finite–volume approximation is generally not sufficient due to the wide distance between grid points in calculation of turbulent length scales, which is due to steady state assumption of flow simulation. Auxiliary relationships are required to account for the effects of turbulence on the transport processes (Bird et al., 1960, Warnatz et al., 1993,2001). To mitigate this problem, time-averaged transport equations, such as Reynolds-averaged Navier-Stokes (RANS) equations, are established. On the contrary, RANS equations are not closed and thus require additional closure turbulence models.

3.4.1 Time-averaged transport equations

These relationships are based on Reynolds decomposition approach, by dividing instantaneous flow variable ϕ in the conservation equations into mean and fluctuating variables respectively $\bar{\phi}$, ϕ' in order to model the effect of turbulence (Bird et al., 1960, Warnatz et al., 1993,2001).

$$\phi = \bar{\phi} + \phi' \tag{3.10}$$

When ϕ is averaged, the mean fluctuation is zero. For combustion processes there are typical large density variations to mitigate that situation another method of averaging the flow variables known as Favre-averaging. It eliminates density-velocity calculation terms in the momentum equations and shows an effective way to account for density fluctuation effects formed by turbulence (Warnatz et al., 1993,2001).

Thus, the Reynolds-averaged Navier-Stokes (RANS) equations can be written as

$$\frac{\partial(\rho u_i)}{\partial t}+\frac{\partial(\rho u_i u_j)}{\partial x_j}=\frac{\partial}{\partial x_j}\left(\mu\left(\frac{\partial(\rho u_i)}{\partial x_j}+\frac{\partial(\rho u_j)}{\partial x_i}\right)-\frac{2}{3}\mu\frac{\partial u_k}{\partial x_k}\right)-\frac{\partial p}{\partial x_i}+\frac{\partial\left(-\rho\overline{u_i' u_j'}\right)}{\partial x_j}+S_i \qquad (3.11)$$

The terms $-\rho\overline{u_i' u_j'}$ are designated Reynolds stress terms (turbulent transport) and they are additional six unknowns (Bird et al., 1960, Eaton et al., 1999, Versteeg and Malalasekera, 2007). These Reynolds stresses can be modelled using Boussinesq hypothesis by taking viscosity as turbulent viscosity in the calculation. The time-averaged transport equation can be obtained by inserting mean variable ϕ into rans equation

$$\frac{\partial(\rho\phi)}{\partial t}+\frac{\partial(\rho\phi u_i)}{\partial x_i}=\frac{\partial}{\partial x_i}(\Gamma_\phi\frac{\partial\phi}{\partial x_i})+\frac{\partial}{\partial x_i}(-\rho\overline{u_i'\phi'})+S_\phi \qquad (3.12)$$

Where $-\rho\overline{u_i'\phi'}$ can be taken to be proportional to the gradient of the mean variable ϕ as introducing turbulent transport coefficient Γ_t of mean variable ϕ. Reynolds stress model (RSM) is described, as well as turbulent transport coefficient and turbulent viscosity with RANS, in following sections.

3.4.2 The standard $k-\varepsilon$ model

To close the time-averaged PDEs, two parameters equation called the $k-\varepsilon$ model was developed (Jones and Whitelaw, 1982, Jones and Wille, 1996, Launder and Spalding, 1974). It is derived from RANS equations and various model constants mostly used for recirculation flows in a form of the two–equation model. This involves an assumed linear relation between the Reynolds stress and rate of strain,

$$-\rho\overline{u_i'\phi'} = -\Gamma_t \frac{\partial \phi}{\partial x_i}, \quad where, \Gamma_t = \frac{\mu_t}{\sigma_t} \tag{3.13}$$

The turbulent (or eddy) viscosity is given by,

$$\mu_t = C\rho VL \tag{3.14}$$

Where, C = dimension less constant,

V = turbulent velocity scale (m/s),

L = turbulent length scale (m),

as per the dimensionless analysis turbulent velocity and length scale can be represented by considering two parameters, one is turbulent kinetic energy k and second is rate of dissipation ε .

$$V = k^{1/2} \tag{3.15}$$

$$L = k^{3/2} / \varepsilon \tag{3.16}$$

Thus, from equations, turbulent viscosity can be written as

$\mu_t = \rho C_\mu (k^2 / \varepsilon)$, where C_μ is dimensionless constant.

These values of k and ε can be obtained from the solution of the transport equations:

$$\frac{\partial(\rho k)}{\partial t} + \frac{\partial(\rho k u_i)}{\partial x_i} = \frac{\partial}{\partial x_i}\left((\mu + \frac{\mu_t}{\sigma_k})\frac{\partial k}{\partial x_i}\right) + G_k + G_b - \rho\varepsilon \tag{3.17}$$

$$\frac{\partial(\rho \varepsilon)}{\partial t} + \frac{\partial(\rho \varepsilon u_i)}{\partial x_i} = \frac{\partial}{\partial x_i}\left((\mu + \frac{\mu_t}{\sigma_\varepsilon})\frac{\partial \varepsilon}{\partial x_i}\right) + C_{1\varepsilon}\frac{\varepsilon}{k}(G_k + (1 - C_{3\varepsilon})G_b) - C_{2\varepsilon}\rho\varepsilon^2 / k \tag{3.18}$$

Where G_k is the generation of turbulent kinetic energy due to the turbulent stress and it can be determined by Boussinesq hypothesis with the effect of mean strain rate. G_b is the generation of turbulent kinetic energy due to the buoyancy and can be

described by the relationship between turbulent Prandtl number (Pr_t) for temperature or enthalpy (0.85), and β is a coefficient of thermal expansion. These model constants have the following standard value as

$$C_{1\varepsilon} = 1.44, C_{2\varepsilon} = 1.92, C_{\mu} = 0.09, \sigma_k = 1.0, \sigma_{\varepsilon} = 1.3$$

The wall functions (boundary conditions) for solving the equations of standard $k-\varepsilon$ model is available well addressed in the literature (Launder and Spalding, 1974). The accuracy of the near-wall calculations of the flow field is very important for the prediction of wall-bounded turbulent flow. The $k-\varepsilon$ model has become the most widely used approach for the solution of practical fluid dynamics problems because of its general applicability, but in this model turbulence is assumed to be isotropic, i.e. all normal stresses are identical or same in all directions. This disadvantage led development of different approaches for anisotropic effects; one example of this category is the non-linear $k-\varepsilon$ model (Speziale, 1987). This model is a formulation of Reynolds stress tensor as a non-linear expansion of the Boussinesq hypothesis. These non-linear terms allows for more precise prediction compared to standard $k-\varepsilon$ that have been observed experimentally (Speziale, 1987). The $k-\varepsilon$ formulation is adopted for this study because of its general applicability.

3.4.3 RNG $k-\varepsilon$ model

The RNG $k-\varepsilon$ model (renormalisation group) is another example of an "anisotropic" model (Fluent, 2007). It is derived from renormalisation group theory (also called rigorous statistical technique), totally different to the standard $k-\varepsilon$ and carries additional functions in the transport equations for k and ε, effects of swirl on turbulence, analytically-derived differential formula for effective viscosity that accounts for low-Reynolds-number effects and, last but not least, improves the accuracy for rapidly strained flows.

The RNG $k-\varepsilon$ model can be written in the same way as the $k-\varepsilon$ model, except for the additional quantities of the inverse effective Prandtl numbers α_k and α_{ε} and the R term in the equation of dissipation rate

$$\frac{\partial(\rho k)}{\partial t}+\frac{\partial(\rho k u_i)}{\partial x_i}=\frac{\partial}{\partial x_i}(\alpha_k \mu_{eff}\frac{\partial k}{\partial x_i})+G_k+G_b-\rho\varepsilon \tag{3.19}$$

$$\frac{\partial(\rho \varepsilon)}{\partial t}+\frac{\partial(\rho \varepsilon u_i)}{\partial x_i}=\frac{\partial}{\partial x_i}(\alpha_\varepsilon \mu_{eff}\frac{\partial \varepsilon}{\partial x_i})+C_{1\varepsilon}\frac{\varepsilon}{k}(G_k+C_{3\varepsilon}G_b)-C_{2\varepsilon}\rho\varepsilon^2/k-R \tag{3.20}$$

where $\alpha_k=\alpha_\varepsilon=1.393$ at high Reynolds numbers. In these equations G_k and G_b can be calculated same as $k-\varepsilon$ model.

$$R=\frac{C_\mu \rho\eta^3(1-\eta/\eta_o)}{1+\beta\eta^3}\frac{\varepsilon^2}{k} \tag{3.21}$$

where $\eta_o=4.38, \beta=0.012$, $\eta<\eta_o and \eta>\eta_o$ respectively shows positive and negative contribution in logarithmic layer.

the effective viscosity can be modelled by the given equations as

$$d\left(\frac{\rho^2}{\sqrt{\varepsilon\mu}}\right)=1.72\frac{\hat{\nu}}{\sqrt{\hat{\nu}^3-1+C_\nu}}d\hat{\nu}, \hat{\nu}=\frac{\mu_{eff}}{\mu}, C_\nu\approx 100 \tag{3.22}$$

The above equation is formulated to obtain the precise effect of low-Reynolds-number and near-wall flows. When Reynolds numbers are high, this equation becomes the same as turbulent viscosity in the $k-\varepsilon$ model. The RNG $k-\varepsilon$ model can be adopted for the effects of swirl by introducing swirl constant and characteristic swirl number in turbulent viscosity equation. Boundary conditions are the same as the standard $k-\varepsilon$ model.

The RNG $k-\varepsilon$ model constants $C_{1\varepsilon}$ and $C_{2\varepsilon}$ have the following values:

$C_{1\varepsilon}=1.42, C_{2\varepsilon}=1.68$

The model constant $C_{3\varepsilon}$ accounted for the buoyancy effect in transport equations for both models, can be calculated as

$C_{3\varepsilon} = \tanh\left|\frac{v}{u}\right|$, where v and u are velocity components parallel ($C_{3\varepsilon}$ =1) and perpendicular ($C_{3\varepsilon}$ =0) to the gravitational vector.

3.4.4 The $k-\varepsilon$ model via convective heat and mass transfer

The interaction of turbulence model with heat and mass transfer can be modelled using the same concept of Reynolds analogy. Thus, turbulent energy transport equation is given by

$$\frac{\partial}{\partial t}(\rho E) + \frac{\partial}{\partial x_i}(u_i(\rho E + p)) = \frac{\partial}{\partial x_i}(k_{eff}\frac{\partial T}{\partial x_i} + u_j(\tau_{ij})_{eff}) + S^h \tag{3.23}$$

$$where, (\tau_{ij})_{eff} = \mu_{eff}(\frac{\partial u_j}{\partial x_i} + \frac{\partial u_i}{\partial x_i}) - \frac{2}{3}\mu_{eff}\frac{\partial u_i}{\partial x_i}\delta_{ij} \tag{3.24}$$

where k_{eff} is effective conductivity, E is the total energy and $(\tau_{ij})_{eff}$ is effective stress tensor, which represents the viscous heating.

Similarly, the interaction between mass transfer and turbulence can be given by

$$\frac{\partial}{\partial t}(\rho m_{i'}) + \frac{\partial}{\partial x_i}(u_i \rho m_{i'}) = -\frac{\partial}{\partial x_i}(D_{eff}\frac{\partial m_{i'}}{\partial x_i}) + R_{i'} + S^{h'} \tag{3.25}$$

where D_{eff} is the effective diffusivity , $S^{h'}$ is the rate of creation by addition from the any sources, $m_{i'}$ is the local mass fraction of each species in the system and $R_{i'}$ is the chemical reaction rate either by mass formation or depletion in system.

Energy and mass transport equations for both turbulence models are tabulated in Table 3.2.

Table 3. 2: Energy and mass transport equations for turbulence models

Energy Transport Equation	**Mass Transport Equation**
The standard $k-\varepsilon$ model $k_{eff} = k + \frac{c_p \mu_t}{\mathrm{Pr}_t}$ (3.26) where k is thermal conductivity and default value of the turbulent Prandtl number is 0.85. The RNG $k-\varepsilon$ model $k_{eff} = \alpha c_p \mu_{eff}$ (3.27) in this α calculated from inverse effective Prandtl number in the viscosity-dominated, where $\alpha = 1/\mathrm{Pr} = k/\mu c_p$ in the viscosity-dominated region and $\alpha = 1.393$ for fully turbulent region (Kays, 1994).	The standard $k-\varepsilon$ model $D_{eff} = \rho D_{i',m} + \frac{\mu_t}{Sc_t}$ (3.28) Sc_t is the turbulent Schmidt number has value 0.7. The RNG $k-\varepsilon$ model, $D_{eff} = \alpha c_p \mu_{eff}$ (3.29) where $\alpha = 1/Sc$ in the diffusion-dominated region, and $\alpha = 1.393$ in the fully turbulent region.

In spite of the above discussed turbulence model, there are some other models also available in CFD. Models of first moment closure type can be derived using Boussinesq relation and Reynolds stresses with the mean flow velocities. However, due to limitations in predicting the flows with complex strain fields or significant body forces led to the development of a more complex second-moment closure approach, so called Reynolds stress model (RSM), in which the Reynolds stresses are modelled by adopting mean flow velocities and the first-moment closure approach together (Launder, 1989, Launder et al., 1975). Another approach where turbulence model is modified to include terms that account for the transition from fully turbulent to laminar flow behaviour, are called Low-Reynolds number approaches. In the case of $k-\varepsilon$ model, new terms have been incorporated in either one or both variables. To achieve proper transition from fully turbulent flow to the laminar flow, along the

wall, an appropriate number of grid points are included in the near-wall region of the flow. In non-premixed turbulent combustion, the rate of mixing in flow is determined by the motions of the largest eddies, where simulations of domain grid points are not extended to the smallest scale using direct numerical solution method. This concept is under research state and used for general purpose computations at present. Turbulent flow occurs at different length scales and termination of energy cascade into kinetic energy of the many small eddies (at or below Kolmogorov-length scale) is dissipated by viscosity into thermal energy (Warnatz et al., 1993,2001). The energy cascade model has great significance in the development of $k-\varepsilon$ model.

3.5 Radiation Models

Radiation energy transport accounts for a dominant part in heat transfer for many combustion processes. Radiation is directly proportional to the combustor length. Modelling radiative energy transport phenomena is a crucial task in combustion systems and it is complex as well (Eaton et al., 1999). In coal combustion systems, radiation is dominant in superheater region.

The energy source due to radiation in eq. (3.5), $S_{h,radiation}$ can be written as

$$S_{h,radiation} = \int_0^{4\pi} \frac{dI}{ds} d\Omega' \tag{3.30}$$

where *i* is the radiation intensity, s is a function of position and Ω' is a solid angle.

the Radiation Transfer Equation (RTE) (Siegel and Howell, 1992) for an absorbing, emitting and scattering medium can be expressed as

$$\frac{dI(s,\Omega')}{ds} + (a+\sigma_s)I(s,\Omega') = a\frac{\sigma T^4}{\pi} + \frac{\sigma_s}{4\pi}\int_0^{4\pi} I(s,\Omega')\Phi d\Omega' \tag{3.31}$$

where ,

$s =$ Path length

$a =$ Absorption coefficient

σ_s = Scattering coefficient

T = Local temperature

σ = Stefan-Boltzmann constant (5.672×10^{-8}w/M^{2}k^4)

Φ = Phase function

$(a+\sigma_s)$ = Optical thickness or Opacity of the medium

There are vast amount of literature relevant to this subject is present and only a brief overview is given to depict adopted model this project and outline of other available models in CFD code.

There are five models available in CFD codes used according to their suitability for the given process.

- P-1 radiation model
- Rosseland radiation model
- Discrete transfer radiation model
- Discrete ordinates radiation model
- Surface to surface radiation model

All of these models excluding surface to surface model require the absorption coefficient input and it can be a function of local concentration of h_2o and co_2, path length, and total pressure. It carries different values for different radiation model.

3.5.1 P-1 radiation model

The P-1 radiation model is the simplest case of the more general P-N model. It is based on the expansion of the radiation intensity I in an orthogonal series of spherical harmonics (Fluent, 2007, Sazhin et al., 1996, Siegel and Howell, 1992). The P-1 model results obtained in the modelling of coal combustion processes in an industrial furnace shows consistency with experimental observations (Sazhin et al., 1996). This model falls in the category of moment method where the angular dependence is expressed using a Taylor power series expansion. In this method, radiative intensity

is expressed as a series of products of angular and spatial functions, where moment is an integral of intensity multiplied by a power of a direction cosine over a predetermined solid angle division. A short review of solution methods is given after the discussion of radiation models.

Simplified Equation P-N Can Be Expressed As

$$I(s,\theta,\varphi) = \frac{1}{4\pi}(I'^{(0)} + 3I'^{(1)}\cos\theta + 3I'^{(2)}\sin\theta\cos\varphi + 3I'^{(3)}\sin\theta\sin\varphi) \tag{3.32}$$

In eq. (3.32), introducing path length with intensity

$$I'^{(0)}(s) = \int_{\omega=0}^{4\pi} I'(s,\omega)d\omega \tag{3.33}$$

$$I'^{(i)}(s) = \int_{\omega=0}^{4\pi} l_i I'(s,\omega)d\omega \tag{3.34}$$

After some simplification, apply radiation temperature term by analogy with the conventional temperature *t,* the radiation flux $\mathbf{q_r}$ with respect to the components $q_i = I'^{(i)}$ can be reduced to

$$\mathbf{q_r} = -\frac{1}{3(a+\sigma_s) - C\sigma_s}\nabla G \tag{3.35}$$

where *g* is incident radiation, and *c* is the linear-anisotropic phase function. Incident radiation can be further simplified by radiation temperature relationship

$$\theta_R^4 = \frac{I'^{(0)}}{4\sigma} \tag{3.36}$$

The transport equation for G is

$$\nabla \bullet (\Gamma \nabla G) - aG + 4a\sigma T^4 = S_G \tag{3.37}$$

where σ is the Stefan-Boltzmann constant ,s_g is a user-defined radiation source, and *c* phase function coefficient can be given as

$$\Gamma = \frac{1}{(3(a+\sigma_s)-C\sigma_s)} \tag{3.38}$$

from eq. (3.36) and eq. (3.38), radiation flux can be expressed as

$$-\nabla \cdot \mathbf{q_r} = aG - 4a\sigma T^4 \tag{3.39}$$

where $\mathbf{q_r}$ in energy equation accounts for heat sources due to radiation.

P-1 radiation model includes the effect of particles, when dispersed second phase is present in the system and this model assumes that all scattering in the system is due to second phase. Hence, particle radiation can be included in the energy equation to yield heat sources as follows(Fluent, 2007):

$$-\nabla \cdot \mathbf{q_r} = 4\pi(a\frac{\sigma T^4}{\pi} + E_p) + (a+a_p)G \tag{3.40}$$

the boundary conditions for eq. (3.39) can be determined by calculating incident radiation flux equation as follows (Sazhin et al., 1996):

$$\mathbf{q_{inc}} = \sigma T_\omega^4 - \frac{\mathbf{q_r} \cdot \vec{n}}{\varepsilon_\omega} \tag{3.41}$$

Where T_ω is the wall temperature, $\mathbf{q_r} \cdot \vec{n}$ is the normal vector defined by eq. (3.35) and ε_ω is the emissivity of the wall. (Note: $s = 0$ refers boundary).

To eliminate the angular dependence from the incident radiation equation, the Marshak boundary condition (Sazhin et al., 1996) is then used , (for initial condition)

$$\mathbf{q_{inc}} = \varepsilon_\omega \sigma T_\omega^4 + (1-\varepsilon_\omega)\sigma\theta_\mathbf{R}^4(0) + \frac{\varepsilon_\omega - 3}{2} q_n(0) \tag{3.42}$$

where putting $\theta_\mathbf{R}\big|_{\varepsilon_\varpi=1} = \theta\big|_{\mathbf{R}\,\varepsilon_\varpi\to 1}$ by considering continuity requirement in this case, eliminating $\mathbf{q_{inc}}$ from eq. (3.41) and eq. (3.42) the final equation to compute $\mathbf{q}_n(0)$ for the energy equation and for the incident radiation equation boundary conditions written as

$$\mathbf{q}_n(0) = \frac{2\varepsilon_\omega \sigma}{(2-\varepsilon_\omega)}(T_\omega^4 - \theta_R^4) \tag{3.43}$$

The P-1 model has several advantages over the Discrete Transfer Radiation Model, because the general radiation transfer equation in P-1 model is diffusion equation and can be solved easily with little computational power. The effect of scattering can be obtained without additional computer time. For combustion applications, it is in wide use where optical thickness is large, and it works quite well with complex geometries with curvilinear coordinates. The main disadvantage of the P-1 model is that its modelling capacity is based on trial and error rather than rigorous calculations, by scarifying accuracy. Nevertheless, it appears to be of great importance for qualitative predictions without any extra cost and time. Apart from P-1 model, all the other models for radiation and solution methods for radiation heat transfer are addressed well in literature (Siegel and Howell, 1992). For this project, P-1 model is best fit, as it requires very less computational power. In this model, radiative properties of gases can be neglected due to their small concentration of species with negligible scattering. Weighted Sum-of-Gray Gases (WSGGM) is used to predict the radiative properties for gases, but to define radiative properties of entrained particles, absorption coefficients and the scattering phase function are required. To determine these properties, the assumption of spherical particles seems appropriate for pulverized coal combustion systems. These properties mostly depend on particle size distribution, wavelength of the radiation and the complex refractive index, which can be determined by different theories (Eaton et al., 1999).

3.6 Gaseous Turbulent Combustion Models

The simulation of non-premixed turbulent combustion processes requires reaction rate, which can be determined by the mixing of the reacting species and by the reaction kinetics. Both of these factors strongly depend on the reaction temperature of a combustor. However, the combustion process cannot be modelled precisely where thousands of intermediate reactions are happening. To model combustion process at the best level of accuracy, simplifications of the processes and assumptions have been proposed in different methods. The Arrhenius rate expressions, the eddy-dissipation concept (Magnussen and Hjertager, 1977), and the

mixture fraction/PDF approach are the most widely used methods. The Arrhenius rate expression includes conservation equations for species in turbulent reacting systems with forward and backward reaction rate with Arrhenius general correlation. This approach is limiting case scenario, where the reacting species are assumed pre-mixed. In this method, turbulent mixing is ignored, and both the finite-rate chemistry and their reaction rates, which are based on mean flow properties, are not applicable in non-premixed turbulent combustion. To account for the effects of turbulence on the chemical reaction rates, the eddy-dissipation concept (Magnussen and Hjertager, 1977) is similar to the eddy-break-up model (Spalding, 1971) proposed. This model relates the rate of combustion to the rate of dissipation of eddies and expresses the rate of reaction by the mean concentration of a reacting species, the turbulent kinetic energy and the rate of dissipation of this energy. This approach evaluates some proportionality constants in equations of reactions rates, however have not been generalised. One approach that has been used to simplify the chemistry in combustion modelling is probability-density function (PDF) approach (Jones and Kakhi, 1998, Pope, 1985).

3.6.1 Mixture fraction approach

This approach is in contrast to premixed systems, where fuel and oxidiser are initially carried by separate streams, in which reactants are mixed at the molecular level before burning. Here, combustion is simplified to a mixing problem and closure for non-linear rates is avoided. There are mainly two options for simplifying the combustion chemistry, the first option is “mixed is burned,” and the second is “thermodynamic equilibrium assumption”. In the first option, thermochemistry can be reduced to a single parameter called mixture fraction, which originated from the fuel stream. The mixture fraction is a conserved scalar quantity, denoted by f can be defined in terms of elemental mass fractions as (Sivathanu and Faeth, 1990):

$$f = \frac{\mathbf{Z}_k - \mathbf{Z}_{k,O}}{\mathbf{Z}_{k,F} - \mathbf{Z}_{k,O}} \tag{3.44}$$

where $\mathbf{Z}_k$ is the elemental mass fraction of the *k*th element, subscripts *F* and *O* denote fuel and oxidiser inlet stream values respectively. For simple fuel/oxidiser

systems, where two identifiable inlet streams have uniform properties, can be stated simpler in terms of the local fuel mass fraction as

$$f = \frac{m_F}{m_F + m_O} \tag{3.45}$$

The equation for the mixture fraction at each point in the system is computed from the Favre and time-averaged transport equations

$$\frac{\partial(\rho \bar{f})}{\partial t} + \frac{\partial(\rho u_i \bar{f})}{\partial x_i} = \frac{\partial}{\partial x_i}\left(\frac{\mu_t}{\sigma_t}\frac{\partial \bar{f}}{\partial x_i}\right) + S^m \tag{3.46}$$

The source term S^m is the $\bar{f}$ source due to transfer of mass into the gas phase from liquid fuel droplets or combustible particles (i.e. coal).

As a closure of turbulence-chemistry model, the equation for the Favre and time-averaged transport of the mixture fraction variance $\overline{f'^2}$ (Jones and Whitelaw, 1982) can be computed as

$$\frac{\partial(\rho \overline{f'})}{\partial t} + \frac{\partial(\rho u_i \overline{f'^2})}{\partial x_i} = \frac{\partial}{\partial x_i}\left(\frac{\mu_t}{\sigma_t}\frac{\partial \overline{f'^2}}{\partial x_i}\right) + C_g \mu_t \left(\frac{\partial \overline{f'^2}}{\partial x_i}\right) - C_d \rho \frac{\varepsilon}{k}\overline{f'^2} \tag{3.47}$$

where constant values are $\sigma_t = 0.7, C_g = 2.86, C_d = 2.0$.

For adiabatic reacting system, under the assumptions of instantaneous values of mole fractions, density and temperature depend solely on the instantaneous mixture fraction as,

$$\phi_i = \phi_i(f) \tag{3.48}$$

where ϕ_i represents the instantaneous species concentration, density, or temperature.

While, in the case of nonadiabatic systems, flows include systems with radiation, heat transfer through walls, heat transfer to/from discrete phase particles or droplets, and multiple inlets at different temperatures, the effect of heat loss/gain can be given by,

$$\phi_i = \phi_i(f, H) \tag{3.49}$$

The instantaneous enthalpy, can be expresses in following manner,

$$H = \sum_{j_i} m_j \left(\int_{T_{ref}}^{T} c_{p,j'} dT + h_{j'}^{o}(T_{ref_{j'}}) \right) \tag{3.50}$$

3.6.2 PDF approach

PDF approach is used as the closure of turbulence-chemistry interaction. In the non-premixed combustion assumed-shape, PDF approach is taken as its closure model. The probability density function denoted as $p(f)$ is defined as the fraction of time that the fluid spends to come on a value between f and $f + \Delta f$. Plot of time scale in the mixture fraction against probability function, gives value of Δf equal to fraction of time mixture fraction has spent. Its mathematical relation can be written as,

$$p(f)\Delta f = \lim_{t\to\infty} \frac{1}{t} \sum_i \tau_i \tag{3.51}$$

where t is time scale and τ_i is the fraction of time f spend in range of Δf. The shape of $p(f)$ depends on the nature of the turbulent fluctuations in f, so it can be derived from the mean mixture fraction and its variance. There are two mathematical functions available for the calculation of assumed-shape PDF (Fluent, 2007, Jones and Wille, 1996):

- Double delta function
- β function

Both the functions have their own condition for $p(f)$; double delta function is only for two-mixture fraction theory, where β - function can be applied for single and two mixture fraction cases. For adiabatic single mixture fraction system, time-averaged values of species mole fractions, temperature and density can be calculated as,

$$\overline{\phi_i} = \int_0^1 p(f)\phi_i(f) df \tag{3.52}$$

For non-adiabatic system, its relationship can be accounted by means of joint pdf $p(f,H)$. Here, for the ease of computation, it is assumed that the enthalpy fluctuations are independent of the enthalpy level.

$$\bar{\phi}_i = \int_0^1 p(f)\phi_i(f,H)df \tag{3.53}$$

Determination of $\bar{\phi}_i$ requires calculation model transport equation for time averaged enthalpy.

3.7 Discrete Phase Modelling

Several commonly used combustion processes, like fuel oil in an industrial furnace, gasoline in an internal combustion engine, coal-fired fluidised beds, pulverised coal fired furnaces etc, incorporate source of fuel as a solid or liquid that interacts with a turbulent gas flow-field. This second phase generally considered as spherical particles (mostly droplets, bubbles, inert or combusting particles) dispersed in the continuous phase. To evaluate these processes, a comprehensive combustion model must be able to address the interaction of the mass, momentum and energy transport for continuous and discrete phase. To give the best characterisation of these phase exchanges, two main formulations have evolved and are available in most of the CFD codes (Fluent, 2007, Jones and Wille, 1996):

- Eulerian-Eulerian
- Eulerian-Lagrangian

In Euler-Euler frame, both the gas phase and the entrained particle phase are considered to be continuous in space and time by solving similar set of discretisation equations. In this frame, mainly three models are available, but offer a severe problem of numerical diffusion for dilute phase. On the contrary, Euler-Lagrange frame includes fluid phase treatment in continuum by solving the time-averaged Navier-Stokes equations, while the dispersed phase is solved by tracking a large number of particles, bubbles, or droplets through the calculated flow field. The dispersed phase can exchange momentum, mass and energy with the fluid phase. The beauty of this frame is that it assumes that the discrete phase occupies low volume

fraction and one is able to track particles at regular intervals of time with the fluid phase. Hence, it is widely adopted by engineers in modelling of spray dryers, coal and liquid fuel combustion, and some particle-laden flows. This frame can produce trajectory calculations, like discrete phase inertia, drag, momentum and heat transfer rates, mass exchange rates via volatile evolution, char combustion and so forth. This frame contains two methods, namely stochastic tracking and particle cloud, to imprint the turbulent dispersion of particles in the fluid phase.

3.8 Particle Reaction Sub Models

Modelling of combusting particles such as coal, char or liquid fuels concern processes like vaporisation, devolatilisation and char oxidation, ultimately giving rate of change of mass for particle or droplet. To model these processes an additional relationship is required for modelling. Mainly, a particle can be present in a process as inert, combusting, droplets and multi-component. According to particle type, there are different laws prevailing for computation of these sub models. Considering combustible coal particle, particle devolatilisation and char oxidation laws can be applied for the process.

Particle devolatilisation rates can be determined with single-or two-step Arrhenious reaction schemes. These approaches are fitted with empirical constants obtained from devolatilisation rate experiments for a given coal sample. The constant rate model and the chemical percolation devolatilisation model are also applicable in determining devolatilisation rate for different processes.

After the combustion, the reaction between combustible fraction and oxidiser at the surface of a combustible particle, involves balancing the rate of mass diffusion of the oxidising species to the surface of a particle. Four types of heterogeneous reaction rate models for combustible particles are available in various literatures, namely the diffusion-limited rate, the kinetics/diffusion-limited rate model, the intrinsic model and the multiple surface reaction models. The kinetics/diffusion-limited rate model is the commonly used approach and it assumes that the char oxidation rate is equal to the oxidiser diffusion rate (Fluent, 2007, Jones and Wille, 1996).

Chapter 4

Modelling Approach

In the field of Computational Fluid Dynamics, there are a variety of Commercial Codes available for different applications. To solve a problem in CFD there are three vital steps: pre-processing, choosing a solver and a post-processing. Pre-processing involves the designing of the geometry and meshing of the object. Choosing a solver enables the user to set up a model (physical and chemical models) by defining appropriate boundary conditions. Finally, post-processing includes analysing predicted results and its validation with real industrial, literature and experimental data. Validating CFD results with real plant conditions is a complicated task; certain assumptions are to be made by the user to solve any real problem in CFD. These assumptions can lead to some errors in comparing CFD results with real plant data or experimental results and leave the user uncertain about them. As mentioned in the previous chapter CFD is not a panacea for all real plant problems, it has certain limitations. In spite of these limitations, CFD has embarked upon a new era to solve fluid flow, heat transfer and chemical reactions. Directing towards the view of this project, CFD has gained special attention from Combustor Engineers for the modelling of a combustor in a power plant, and proven a very useful tool for performance improvement of optimising power plant operation.

4.1 Simulation Object and Problem Definition

Geometry for 330 MW power plant boiler and computational mesh is created using GAMBIT 2.3 pre–processor version. A simplified configuration of the boiler, with the main dimensions of the furnace, is displayed in Appendix A (Figure A.1). It has five rows of burner containing five burners in each row. A total number of 25 burners are mounted on the rear and front wall of boiler. Figure 4.1 shows the developed geometry and an example of generated computational mesh. The type of computational grid created here for the solution is tetrahedral, having 332379 finite volume cells. Unstructured mesh is adopted for this project due to the complex geometry of burner. Certain assumptions made to reduce the complexity of physical

model. Physical model domain is created up to the crossover pass and burner design is also simplified to circular object. Simplifying burner design can prevent this model to obtain effects of degree of inner, outer and primary swirl, quarl angle and entrained gas temperature. Burner flow patters are extremely sensitive to burner swirl. There could be a relation between burner swirl and deposition around burner throat. This assumption has been taken due to unavailability of industrial design data.

The mesh around the burner part is also schematically shown in Figure 4.1.

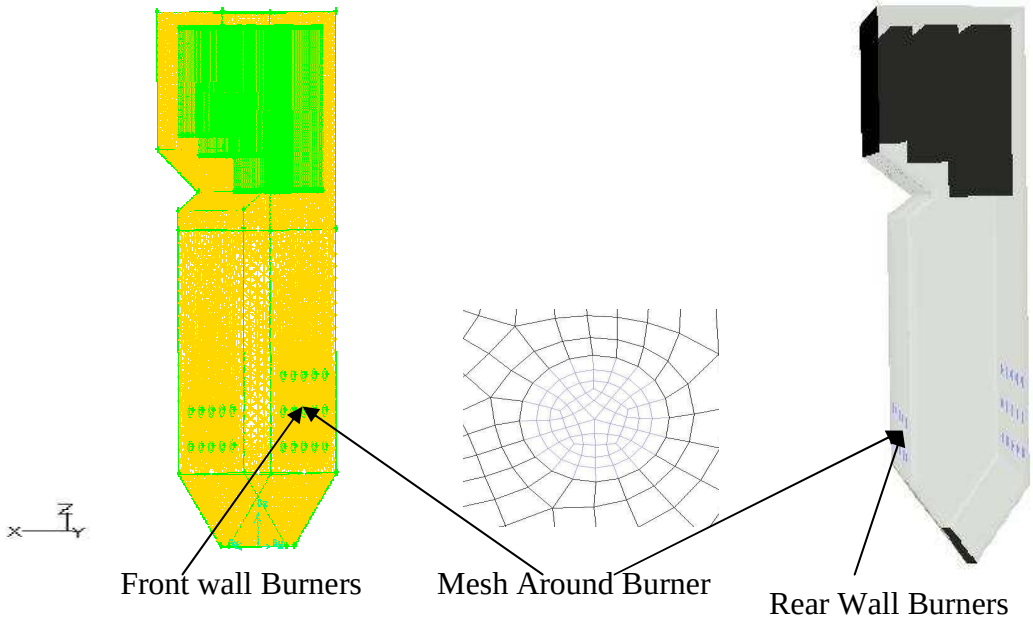

Figure 4. 1: Schematic of modelled furnace

To carry out the analysis of results up to the cross over pass, domain is extended to the mid of cross-over pass according to the actual boiler configuration. All these measures are taken to get a better understanding of the performance of a large-scale boiler and to make it possible to investigate gas flow deviation and uneven wall temperature in extended domain.

Pulverised coal combustion has been defined through the non-premixed combustion model available in it. The gas phase is described by the Eulerian approach and a Stochastic Lagrangian frame is used for discrete phase modelling. The gas phase model solves Navier-Stokes equations, coupled with appropriate equations for density and viscosity, where turbulence is modelled by $k-\varepsilon$ model (Launder and

Spalding, 1972). The required turbulent quantities at the inlet were computed using the equations provided in the literature (Fluent, 2007). The gaseous turbulent combustion is solved via non-premixed combustion with a single mixture fraction probability density function (PDF) approach. Radiation is a significant process in coal combustion; in this project P-1 radiation model is used to account for the exchange of radiation between gas and particulates, specifying composition dependent absorption coefficient through the cell based WSGGM (weighted-sum-of-gray-gases model). This model is the simplest case of P–N model, which is based on the expansion of the radiation intensity into an orthogonal series of spherical harmonics (Siegel and Howell, 1992). This model includes calculation of simple diffusion equation, which can be achieved by little computing power. In the case of coal particles combustion, coal particles devolatilise and undergo char combustion, creating a source of fuel for reaction in gas phase, where single rate devolatilisation model (Badzioch and Hawksley, 1970) and kinetic/diffusion-limited char combustion model (Baum and Street, 1971, Field, 1969) are used. As a software data input requirement, input started with choosing the pressure based solver for this case followed by enabling turbulence and energy model. To enable non–premixed combustion model, a non–adiabatic PDF table is created with single mixture fraction and the full equilibrium chemistry, where the turbulence chemistry interaction is modelled with double delta probability density function (PDF). After defining the entire species mole fraction, fuel lower calorific value and specific heat are incorporated into the table.

Properties for coal A (From Western Premier Mine), which is used for base simulation to compare the results with the literature, and actual plant data, are mentioned in Table 4.1. Simulation is carried out using two different coals, and comparisons are made with each other for temperature distribution, flow-field and combustion behaviour. Ultimate and proximate analysis for other coal B (From Griffin Ewington II Mine) is tabulated in Appendix B.

Once calculation of non–adiabatic PDF table is performed, radiation model and discrete phase model started. In the discrete phase model group injections are given according to burner location. Continuous phase turbulence determines instantaneous turbulent velocity fluctuations on the particle trajectories. The dispersion of particles

due to turbulence in the fluid phase has been predicted using the stochastic tracking model: by computing the trajectory for a sufficient number of representative particles, the random effects of turbulence on the particle dispersion and interaction with radiation is accounted for. Material types have been specified for PDF mixture and combustible particles. Boundary conditions for primary – secondary inlets, outlet and wall have been specified and detail tabulation of it provided in Appendix C (Table C.1 to Table C.6) for different cases according to Table 4.2. Coal particles are injected into the furnace from each of the Primary Air inlets. A total number of 25 injections are defined at 25 primary air inlets. Each of these injections is divided into 10 different particle sizes. Particle size distribution is calculated using a convenient method called Rossin-Rammler expression. All the models mentioned above are used widely due to the fact that they have shown remarkable efficiency in modelling of large scale utility boilers. The mathematical background of these models is provided in Chapter 3 and conceptual theory part can be found in the references (Fluent, 2007, Versteeg and Malalasekera, 2007).

Table 4. 1: Proximate and ultimate analysis of coal

Coal A (Western Premier Mine) (as received (Wt %))		
Proximate Analysis (%) As received	**Average**	**Range**
Moisture	25	22-28
Ash	8	4-10
Volatiles	29.8	22-34
Fixed Carbon	37.7	36-48
Specific Energy MJ/kg	19.6	18.8-21.5
Ultimate Analysis (%daf)		
Carbon	73.5	73-76
Hydrogen	4.8	4.2-4.9
Nitrogen	1.2	1.2-1.5
Sulphur	1.0	0.3-1.3
Oxygen	19.5	18-20
Ash Analysis (%)(db)		

SiO_2	47.3	30-55
Al_2O_3	24.8	20-30
Fe_2O_3	17.1	5-22
CaO	2.14	1-3
MgO	1.67	0.5-2
Na_2O	0.54	0.2-1
K_2O	0.73	0.3-0.9
TiO_2	1.54	1.1-2.5
Mn_3O_4	0.19	0.05-0.22
SO_3	0.90	0.3-1.8
P_2O_3	1.52	0.05-4.0
Ash Fusion Temp. (^oC)	**Average**	**Minimum**
(Reducing)		
-Deformation	1200	1100
-Sphere	1350	1200
-Hemisphere	1360	1250
-Flow	1400	1300
(Oxidizing)		
-Deformation	1300	-
-Sphere	1450	-
-Hemisphere	1450	-
-Flow	1460	-

4.2 Calculated Cases

Five different and characteristic cases of operating conditions have been determined from the available process data. Prior to that, base calculations for total air and fuel requirement are calculated using the empirical methods. Simulations runs for five different fuel loads, carried out in FLUENT.

Schematic arrangement of 25 burners, three rows on the front wall, each individual row contains five burners and two rows on the rear wall are shown in Figure 4.2. This plant is equipped with five pulverisers; each of them is feeding fuel to the associated burner row.

Table 4. 2: Different operating cases based on active burners

Burners	Full Load 3-2 Firing (100%) (CASE A) (coal A)	2-2 Firing (80%) (CASE B) (coal A)	2-1 Firing (60%) (CASE C) (coal A)	Full Load (Excess air 20%) 3-2 firing (CASE D) (coal A)	Full Load 3-2 Firing (CASE E) (coal B)
Row 1	Y	Y	Y	Y	Y
Row 2	Y	Y	Y	Y	Y
Row 3	Y	N	N	Y	Y
Row 4	Y	Y	Y	Y	Y
Row 5	Y	Y	N	Y	Y

The start–up burner is an oil–fired burner for starting up the plant firing. A basic operating condition is given for case A and E in the Appendix C (Table C.7 and C.8) for both coals.

The operational conditions of the different cases based on active burners are shown in Table 4.2, where “Y” means the burner row is in use and “N” means the burner row is completely switched off. For coal type A and B, total actual fuel consumption is plotted against the calculated values for model input (see Figure 4.3). The plot gives the scenario that calculated fuel consumption is almost similar and having standard absolute deviation around 10% to the actual data for all the feed coals. For coal type A and B, primary and secondary air flow rates as well as coal flow rates are plotted in Figure 4.4.

However, fuel slagging propensity is also calculated using various thermal indices seemed to be low to medium, which is provided in Table 4.3. In the present work case A is of great importance. Case A represents the basic operational conditions of power plant. This case is much suitable for comparison of predicted result with available literature and power plant data.

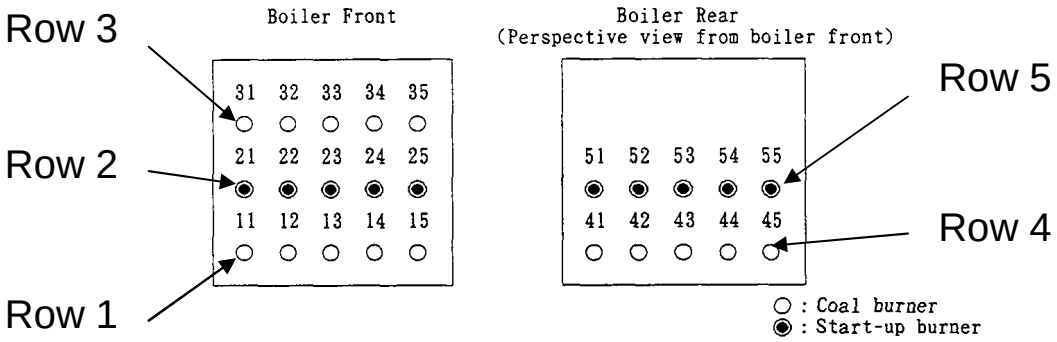

Figure 4. 2: Schematic arrangements of 25 burners on front and rear boiler walls (as received)

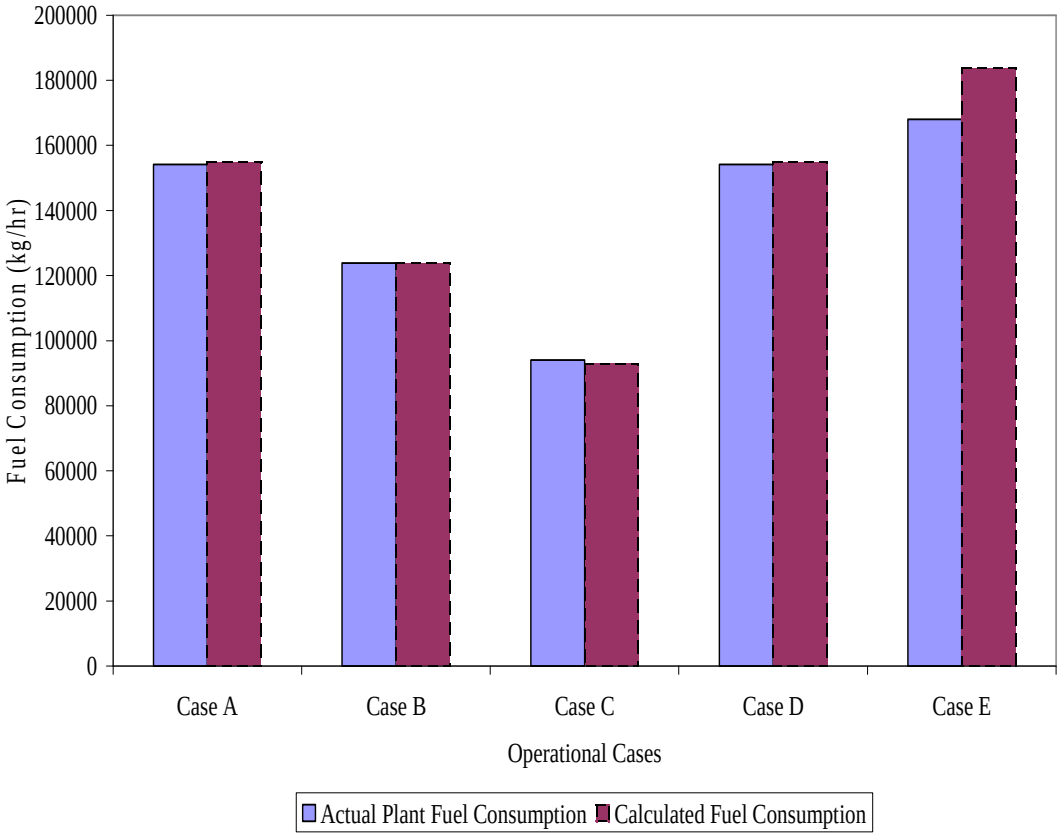

Figure 4. 3: Fuel consumption for actual plant values and calculated values for present model

4.3 Solution Procedure

The CFD commercial code FLUENT has been used for solving the governing differential equation for this pulverised coal combustion process with the unstructured mesh. It is also assumed that the flow field is at the steady-state. All the major physical processes of coal combustion are modelled with the available models in the code. The calculation strategy is simply started with the non–reacting flow field solution by disabling energy, radiation and multiphase model equations. Pressure Interpolation is set to PRESTO (Pressure staggering option) and Pressure–Velocity coupling is achieved with SIMPLEC-based algorithm (Patnakar, 1980).

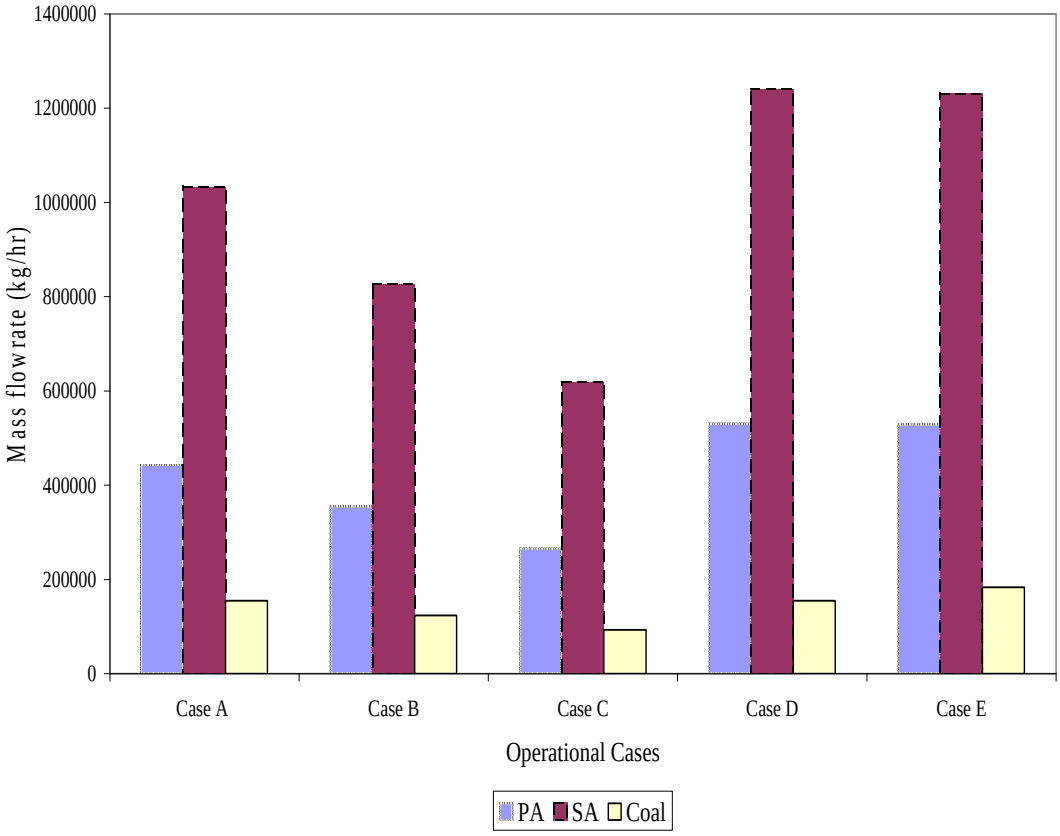

Figure 4. 4: Distribution of primary air (PA), secondary air (SA) and coal for different operational cases

Table 4. 3: Slagging indices results (Couch, 1994)

Slagging Indices	Calculated Values	Slagging Propensity[a]
Base Acid Ratio	0.29757	Low-Medium
Slagging Factor	0.003143	Low
T_{250} ^{o}C	1537.656	Low
Iron Calcium Ratio	11.19277	Low
Iron Plus Calcium Ratio	20.24	Medium-High-Severe
Silica Percentage	71.4851	Medium-high

[a] Slagging Tendency of coal is low to medium

Once the flow-field is established, all the residuals and global mass fluxes were balanced, and the results are considered converged. After that, simulations were started involving all the defined models in the problem.

The main results of the performed CFD simulation concerning 330 MW boiler consist of flow fields, particles path tracks, temperature profiles, heat flux profiles to the furnace walls, contours of O_2, CO_2 and other species concentrations, as well as areas in furnace with high propensity for clinker formation are also presented and discussed in the following chapter.

Chapter 5

Results and Discussion

The calculation has been performed on a Microsoft Windows platform with an Intel Core 2 Duo 2.13 GHz processor and 2 GB RAM. The post-processing tools of the FLUENT 6.3 code and MS office 2003 have been used for the examination of the present model results.

5.1 Different Operational Cases

As mentioned in previous chapter five cases for two different coals have been calculated for the analysis of physical processes inside the utility boiler to identify the most probable faces of the boiler to clinker formation and also the influence of temperature and species distribution on the combustion process. Hence, this chapter's itinerary is started with the temperature distribution for various cases to find out temperature distribution around burner zone and furnace exit gas temperature, species concentration through out the burner zone as well as exit of furnace. Due to unavailability of real plant data, validation is given with the existing open literature. After the validation of model, flue gas path is described with vectors on different plane for mentioned cases. Particle trajectories have been analysed from selected burners for available cases to visualise the inside behaviour of pulverised coal particles inside the furnace and influence of low as well as upper level burners on particle trajectories. Probable faces of furnace are highlighted with particular areas, where propensity clinker generation is higher. Once the areas of clinker formation are marked with relevant temperature range, discussion is provided for difficulties and its consequences, which emerges in power utilities. Governing parameters of clinker formation are identified, and its validation is given with available literature, where ever required. Result analysis is carried out using different lines and planes in the simulation object. Physical domain of the model is shown in Appendix D. Seven different planes (Figure D.1) according to the model specification are created to analyse temperatures and velocity vectors for stated cases. Species concentration is analysed on different lines, created in the object (Figure D.

2). Specifications of all the planes and lines as of the simulation object configuration are briefed in Table D.1 and D.2.

5.2 Temperature Distribution

To have a better understanding of temperature distribution in the boiler, this section is briefly mentioned with temperature distribution contours on different cross-sections and lines for all cases. Figure 5.1 is showing the temperature distribution along the cross-section A, where significant distinction in temperature range has been visualised mainly for case A, case D and case E. The highest temperature peak is in the case D (1920K); the lowest temperature peaks are in case C (1667K) and case E (1780K). From the temperature contours, it can be seen that temperature in burner quarl is too high as most of the combustion occurs mainly in the near burner region. All the volatile fraction of coal consumed within 1 to 2 m of the burner zone, while char burns at slower rate, and normally is not consumed until it reaches the furnace centre. To make the difference more clear, Temperature distributions in the region of the burners, three planes crossing each burner row has been created, namely cross-section B, C and D. Cross-sections B,C and D with the temperature contours are given in Figure 5.2. Other difference is observed in the mean temperature near burner zone (mostly 1400-1895K) for all the cases excluding case E, where in case E mean value is lower. Iso-surfaces for all cases near burner zone with the approximate average temperature range are provided in Figure 5.3. The mean temperature in burner zones for operational cases plotted and provided in Appendix E (see Figure E.1 to E.5). Figure E.1 to E.5 are the plots on line A-A*, where Figure E.6 to E.10 are for three different lines B-B*, C-C* and D-D* for temperature distribution for calculated cases. From the burner zone to exit zone the temperature gradually decreases as heat transfer takes place from the flue gas to the furnace walls, re-heaters, super-heaters and economizer. Economizer is not modelled in this study due to geometry complications. After the nose of the boiler there is considerable gas temperature deviation in the platen superheater zone. There has been substantial research done on gas temperature deviation and different researchers hold different opinions (Yin et al., 2002). As the general view for temperature deviation in boiler depends on many parameters, where the amount of combustion air and its distribution inside the boiler governs lot for combustion efficiency in boiler.

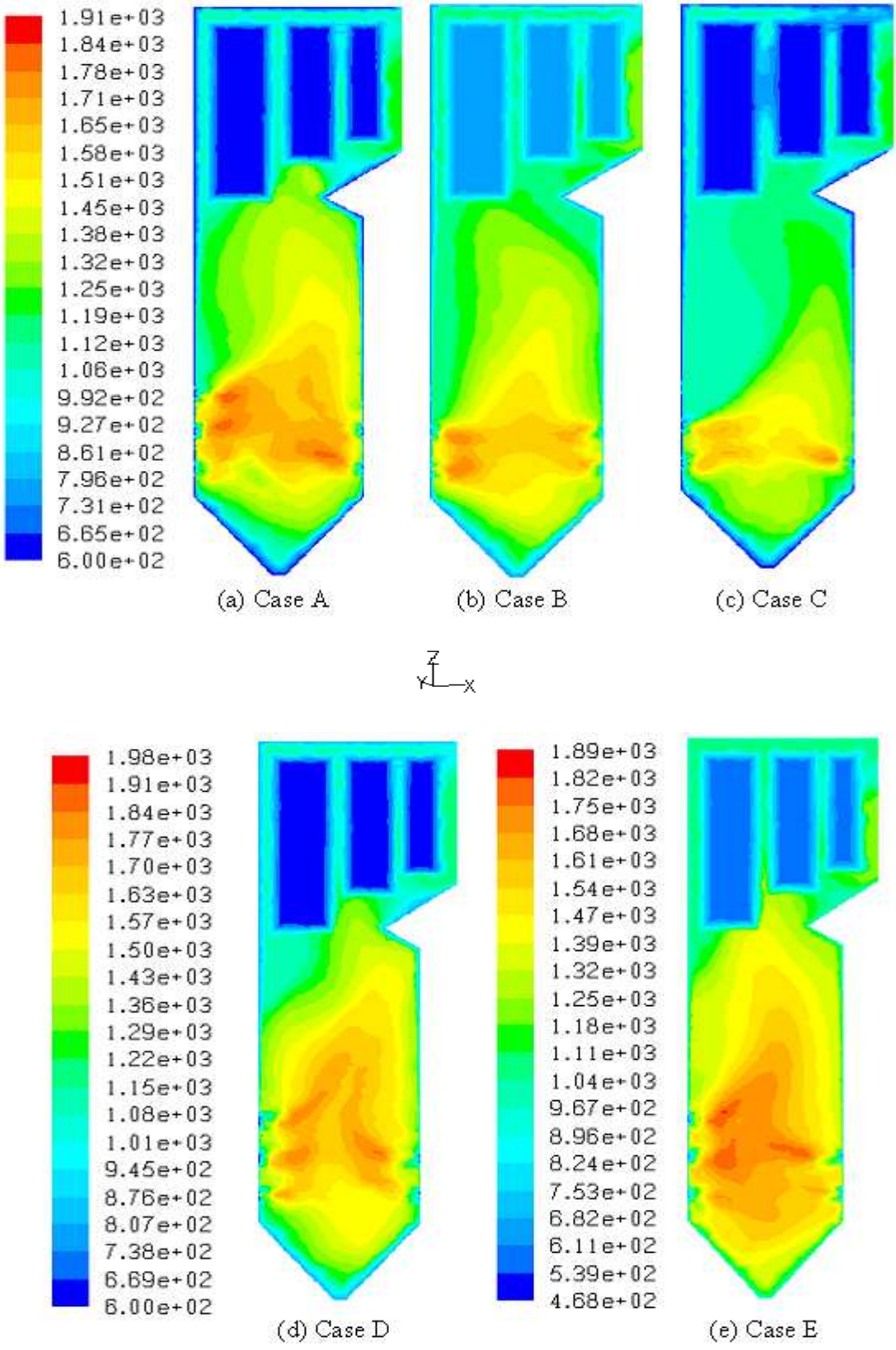

Figure 5. 1: Temperature distribution along cross-section A, for cases A to E (Y-Y planes)

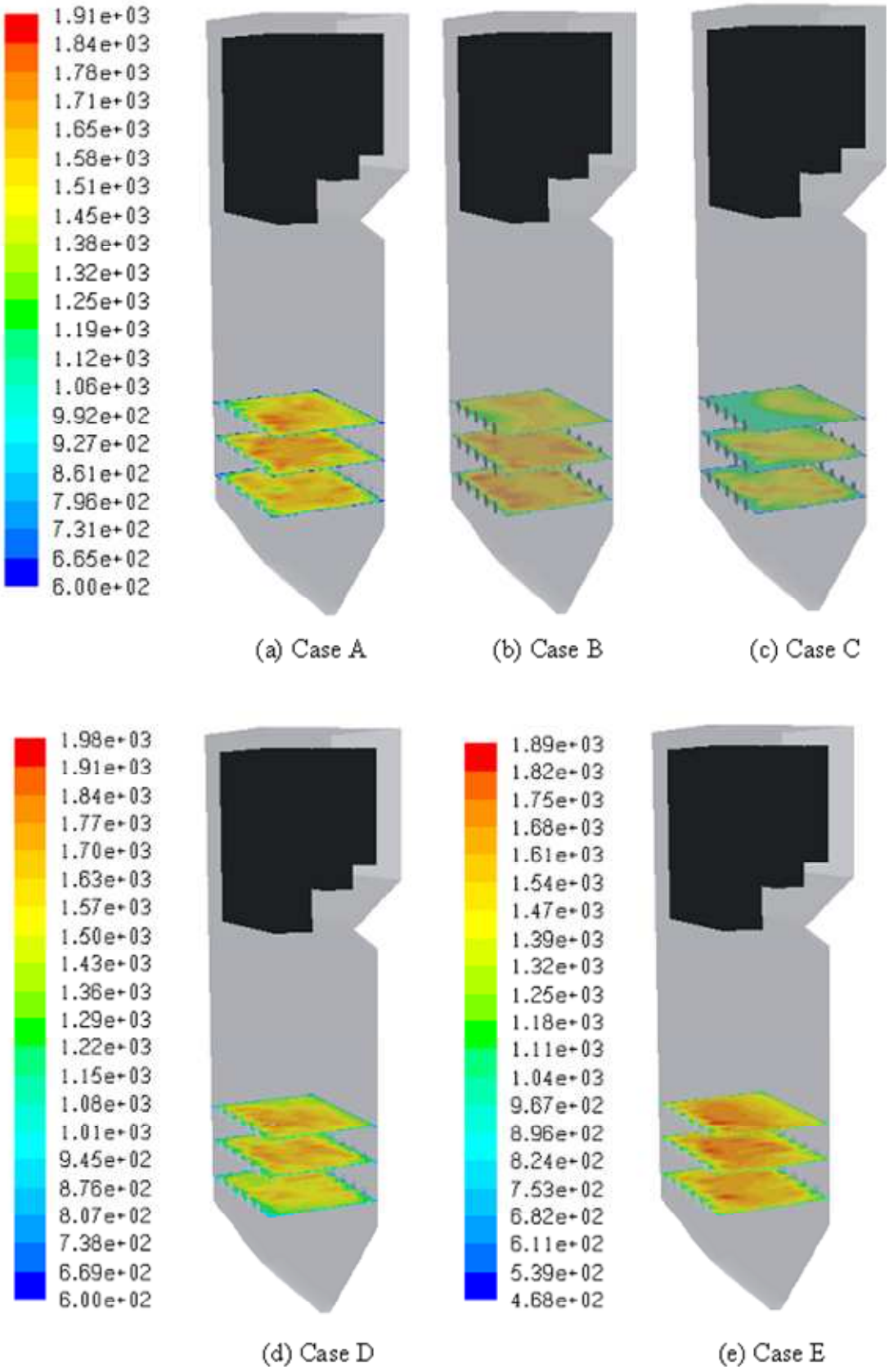

Figure 5. 2: Temperature distribution across various cross-sections B, C and D for all cases (Z-Z planes)

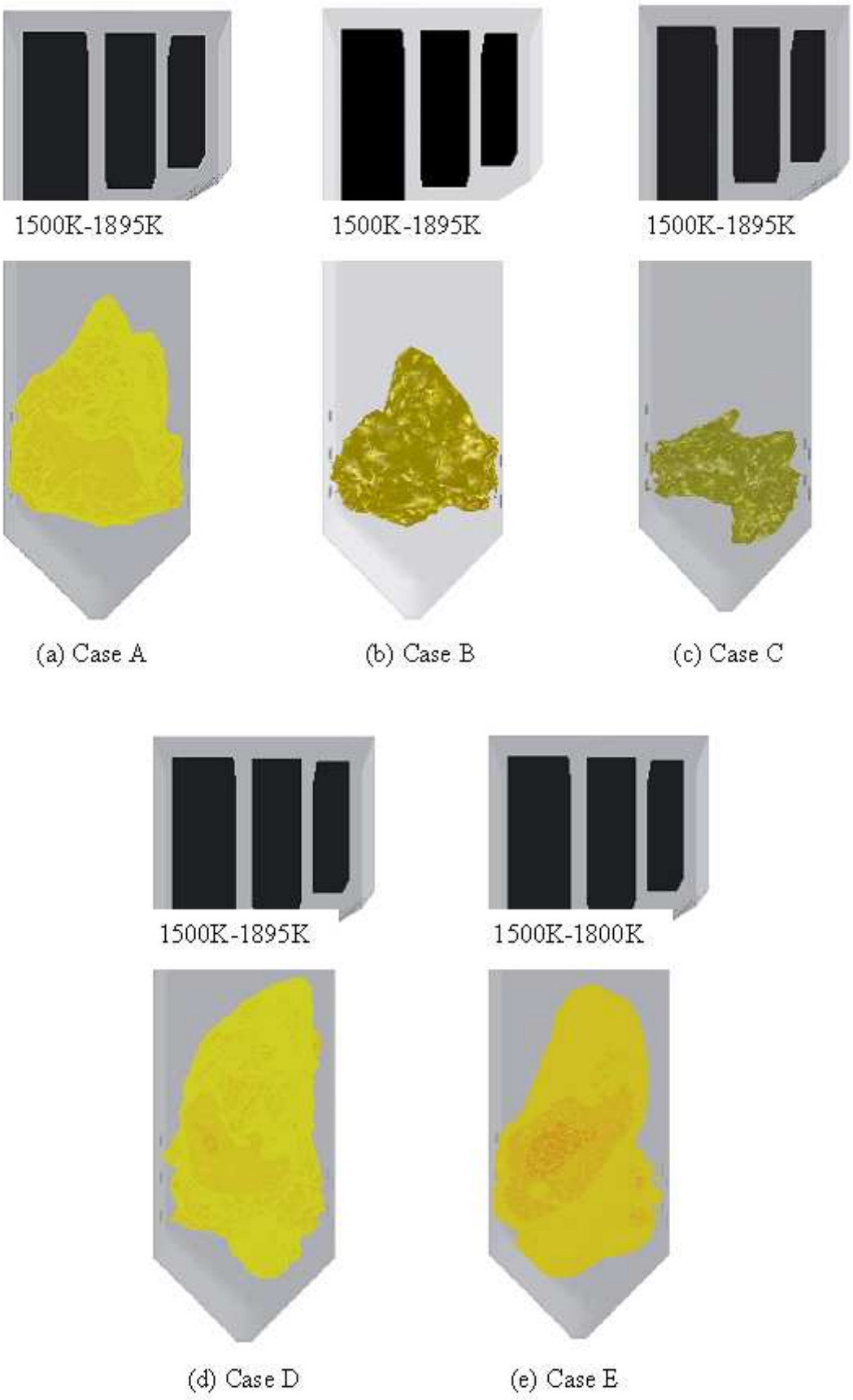

Figure 5. 3: Iso-surfaces for different cases representing average burner zone temperature

Low supply of combustion air to the upper part of burners, which are inactive, causes higher temperatures in the higher part of the furnace. Furthermore, to represent Furnace exit gas temperature (FEGT) for model, temperature plots shown in Figures E.11 to E.15. To calculate FEGT in the available model cross-section H is considered as furnace exit plane, which called cross-over pass in real plant boiler. FEGT is the most important parameter to quantify the effect of slag deposits on furnace heat absorption with constant observation. FEGT gets differ according to number of burner in service or fuel load in the boiler operation. Here, in the simulation result average FEGT for case A is 1197K, while case D is reported with 1240K. For other cases FEGT values are almost same. For the ideal boiler operation FEGT must be in between 1150-1350K according to literature and design values. Validation of current model values and its discrepancies with literature values are given later in this chapter. Heat transfer to the furnace walls from the flue gas via radiation causes temperature to decreases as gas flows upward in the furnace. As temperature level near walls is also an important parameter, which can affect the slagging potential in the furnace.

Table 5.1 is given with the summary of mean temperature, peak temperature and average FEGT for all the calculated cases. Comparison of simulation has been given afterwards followed by species distribution in this current chapter. Standard absolute deviations of the predicted results with literature data have also been tabulated, which are because of simulation accuracy and geometry configuration

Table 5. 1: Summary of mean temperature in burner zone, peak temperature and FEGT

Cases	**Mean Temperature in Burner Region(K)**	**Peak Temperature(K)**	**Mean FEGT(K)**
Case A	1716	1815	1197
Case B	1675	1760	1176
Case C	1667	1667	1160
Case D	1770	1920	1240
Case E	1690	1804	1162

5.3 Species Distribution

Appendix F, shows the O_2, and CO_2 concentration plots for calculated cases on lines A-A*, B-B*, C-C*, D-D* and E-E*, where line A-A* is a centre line in domain and line E-E* is taken as exit concentration line. O_2 and CO_2 are complementary species in coal combustion as a main product and reactant. O_2 concentration is quite high near the burner quarl, and rapidly decreases after complete combustion of fuel, which is clearly shown in plots near burner lines B-B*, C-C* and D-D* (see Figures F.1 to F.8). A steepest gradient in O_2 concentration can be seen in Figures F.1 to F.8, which is due to the rapid consumption of fuel volatile species near the burner zone. The O_2 concentration in the furnace is relatively higher near the burner quarl as because the O_2 contained in the air injected into the surface.

On the other side CO_2 concentration through out the centre line A-A* is maximum, and respectively O_2 concentration nearly zero (represented in Figures F.9 to F.12). With the concentration of CO_2, one general phenomenon observed that areas with maximum concentration of CO_2 shows higher temperature, where oxygen is consumed quickly during the combustion process. Analysing species concentration and temperature distribution in the boiler, can be use to identify the fuel-lean and fuel-rich regions in the combustor. To evaluate the prediction for species concentration at cross-over pass line E-E* has been created. O_2 and CO_2 concentrations are plotted in Figures F.13 to F.16 for the predicted cases. CO_2 concentrations in the boiler can also be useful for the prediction and comparison of NO_x formation issues in boiler. NO_x formation model is not taken in this study due to complexity of given problem. Predicted specie concentration values have been compared with literature and given in next section of this chapter.

5.4 Comparison with literature and other Resource

Every research needs to be compared and evaluated to check its practical feasibility. Hence comparison of present model is provided with literature available. For comparison of temperature with available design and reference values, case A is selected. All the values reported here, are taken as mean values across the cross-section A (refer Appendix D, Figure D.1). Temperature is an important parameter to check in furnace operation. Deviation in furnace temperature with reference to its design values leads to unnecessary problem in utility operation. For comparison of different parameters selected literatures are mentioned in Table G.1(Appendix G), which suits best to the current study for comparison. First temperature comparison is provided in Figure 5.4 across cross-section A for the current case to the literature (Xu et al., 2001). Afterwards, comparison has been given for temperature at near burner region (see Figure 5.5).

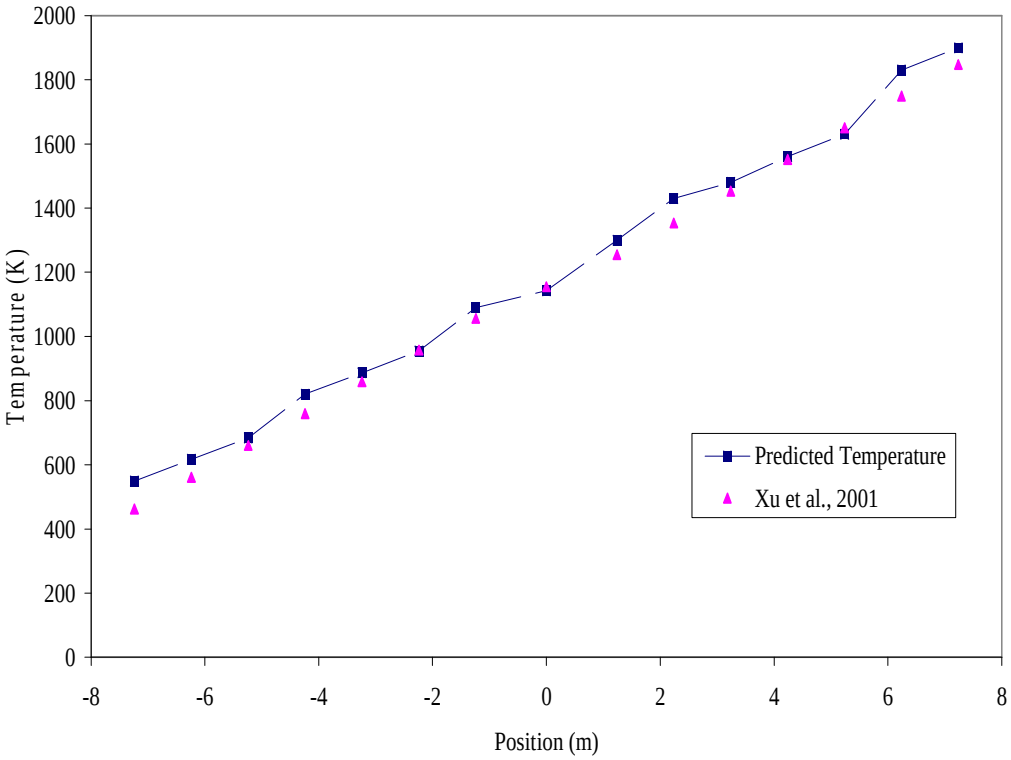

Figure 5. 4: Temperature comparison with reference across cross-section A (Std.Abs.Dev. < 2.5%)

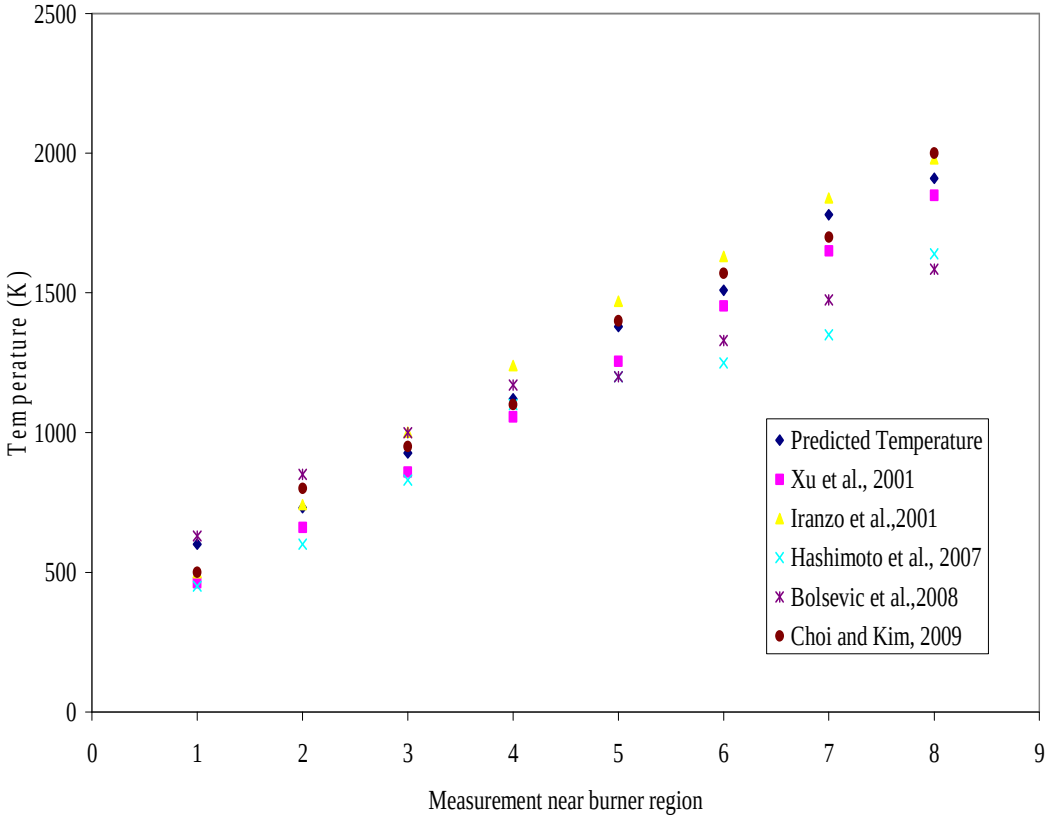

Figure 5. 5: Temperature comparison with literature values near burner region (Std.Abs.Dev. < 8%)

Mostly temperature near burner region predicted and cited in references are quite nearer, which ever the discrepancies have been reported, can be due to the different geometry configuration and different model inputs. Also the comparison has been made for case D, which is excess air case in present study, plotted against literature over fire air case (see Figure 5.6). Species concentrations also compared at different locations (Figure 5.7, 5.8 and Table 5.2) and furnace exit temperature values are mentioned in Table 5.3. Calculated radiation heat flux to the wall in current case is shown in Figure 5.9, as well as total heat transfer to the furnace walls is reported and compared in Table 5.4. Comparison of heat flux with real plant data can be made in future to evaluate the possible improvements in the heat transfer through water walls, and consequently on boiler efficiency.

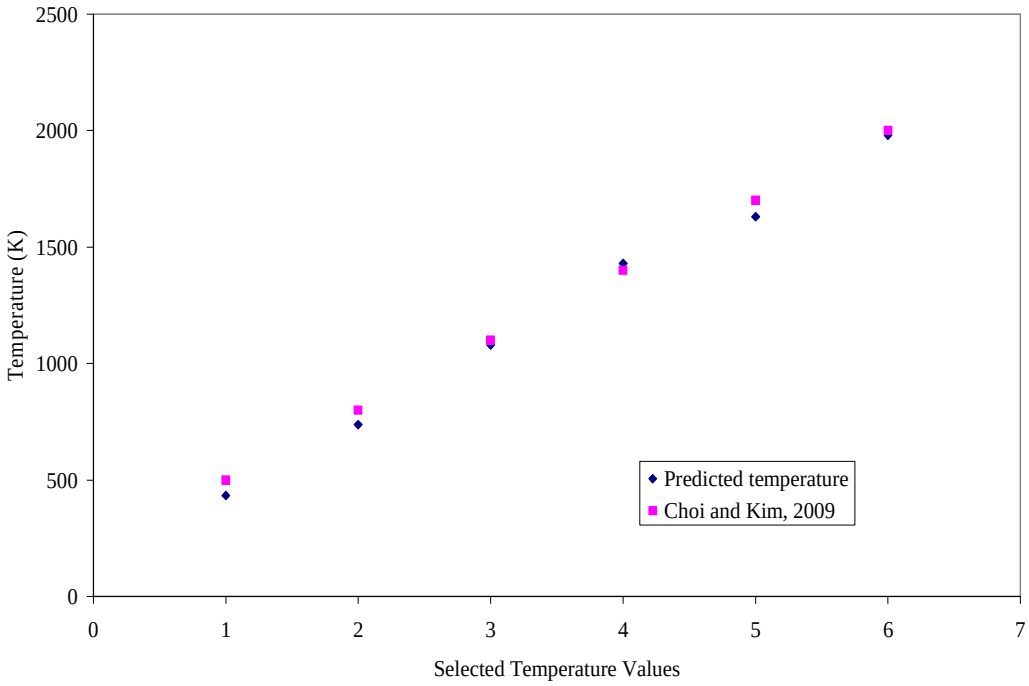

Figure 5. 6: Temperature for case of over fire air according to literature (present study, excess air) (Std.Abs.Dev. = 3.425%)

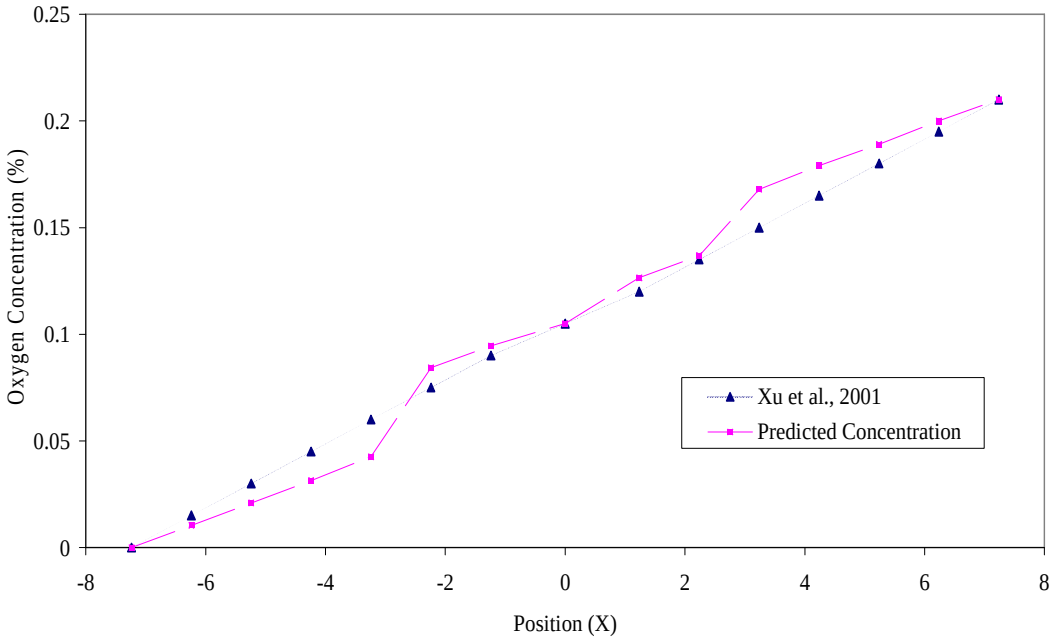

Figure 5. 7: Comparison of O_2 concentration through cross-section A (Std.Abs.Dev. = 0.001%)

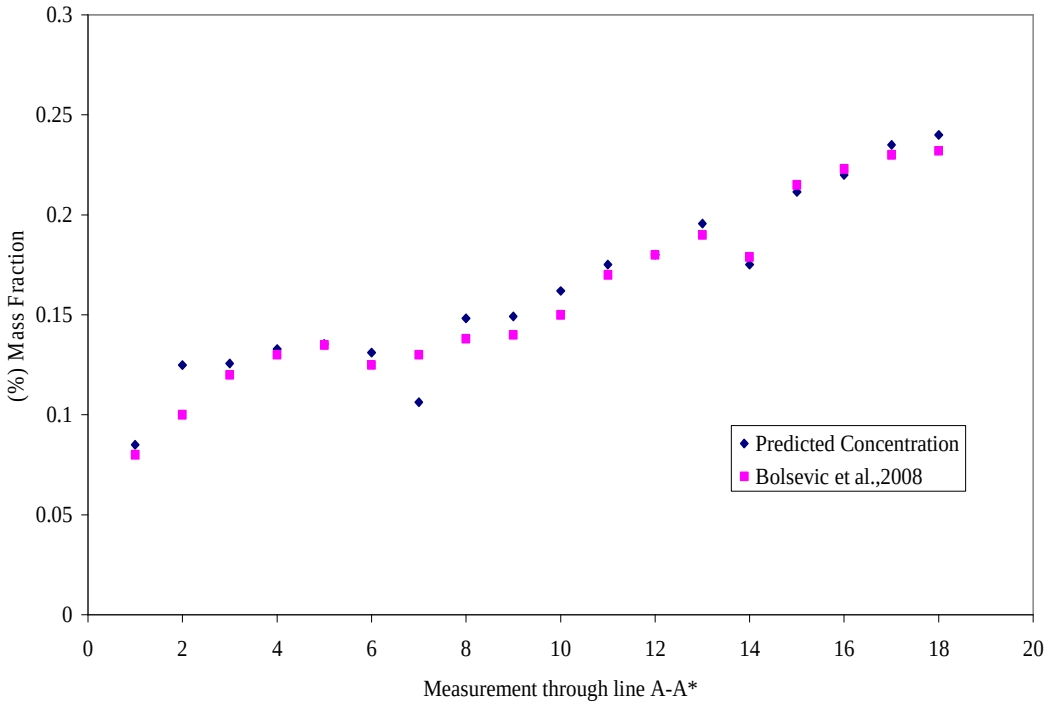

Figure 5. 8: Comparison of CO_2 concentration through line A-A* (Std.Abs.Dev. = 2.31%)

Table 5. 2: Species concentration (%)

Current Study/References	Predicted O_2 /CO_2 (%)	Measured O_2 and CO_2 (%)
Current Study	2.1/12.56	-
(Xu et al., 2001)	1.9/-	3.5/-
(Choi and Kim, 2009)	2.61/13.31	-
(Iranzo et al., 2001)	-	-
(Belosevic et al., 2008)	7/15	

Table 5. 3: Furnace exit gas temperature (K)

Current Study/References	Predicted FEGT (K) (Std.Abs.Dev. < 10%)	Measured FEGT
Current Study	1197	-
(Xu et al., 2001)	1316	1287
(Choi and Kim, 2009)	1509	1485
(Iranzo et al., 2001)	1477	-
(Belosevic et al., 2008)	1294.564	-

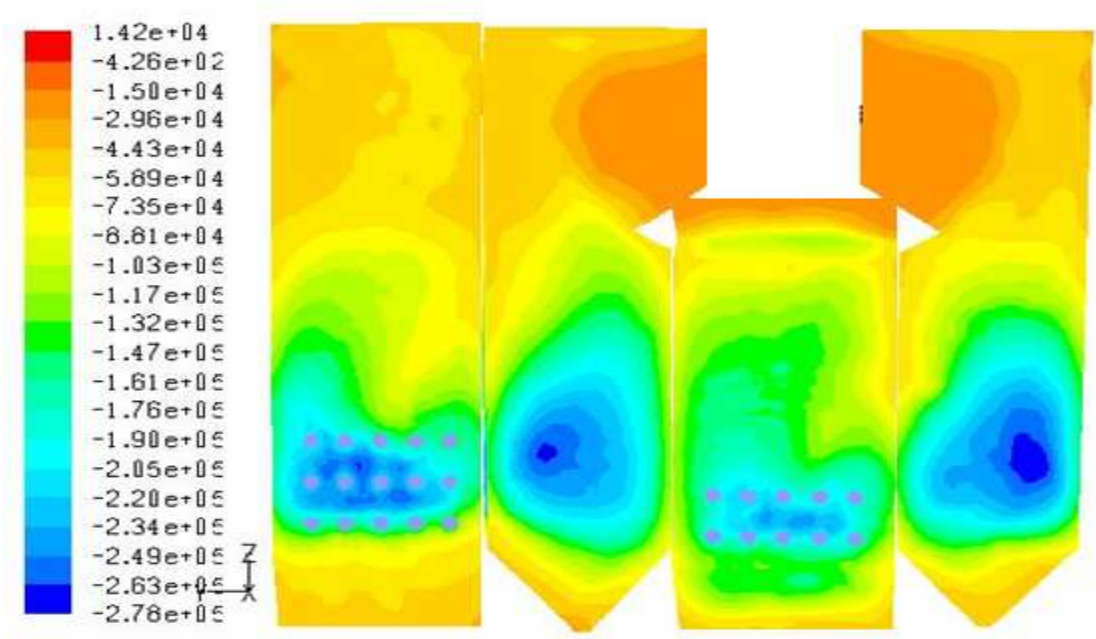

Figure 5. 9: Radiation heat flux (w/m^2) to the walls

Table 5. 4: Heat transfer to walls (W)

Current Study/References	**Heat Transfer to the Furnace Walls(W) (Predicted)(Std.Abs.Dev<10%)**	**Measured**
Current Study	3.43×10^5	-
(Xu et al., 2001)	3.01×10^5	3.30×10^5

5.5 Flow Fields, Particle Tracks and Areas of Clinker Formation

5.5.1 Flow fields

The velocity distribution and vectors in cross sections along the furnace height, for case A are shown in Figure 5.10, where rest of the cases are depicted in Appendix H (refer Figures H.1 to H.4 for cases B, C, D and E respectively). Schematic of velocity vectors along six different cross-sections B, C, D, F, G and H (Figure D.1) are shown for all cases.

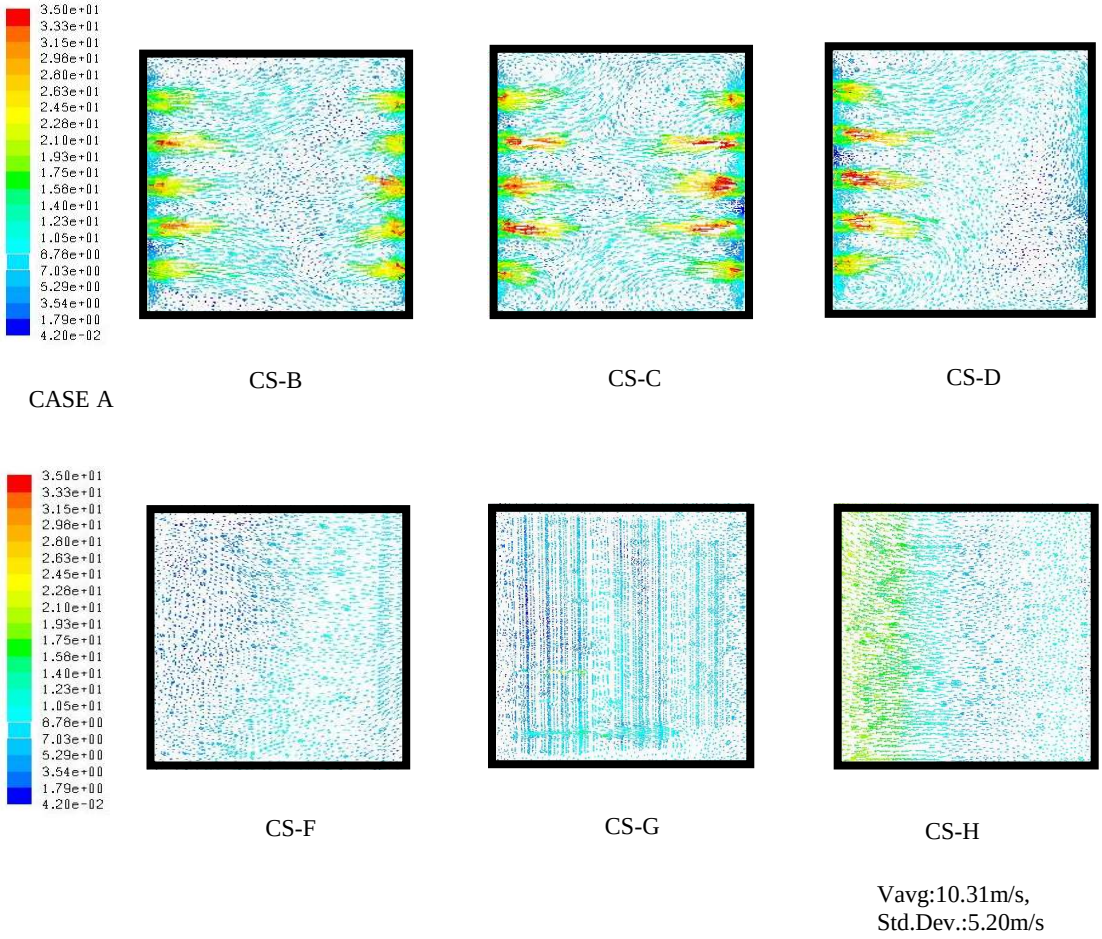

Figure 5. 10: Flow fields on different cross-sections for case A

It is observed that the flow enters through the burners and part of the flow goes downward along the furnace wall into the ash hopper, and then travels upwards towards the burner region and lastly passing by the nose to platen heaters and exits

the furnace in crossover pass. The flow fields along the burner region seem very active compared to other parts of boiler. Dramatic interaction of flow can be seen from burner region (Figure 5.10 and Figures H.1 to H.4, cross-section B, C and D) to the nose of boiler, apart from that, when it approaches towards cross-over section of boiler, flow is becoming more flat with uniform velocity distribution (Figure 5.10 and Figures H.1 to H.4, cross-sections F, G and H). Due to the rigorous turbulent interaction around burner region of flow is obtained with the maximum velocity in cases A, D and E in range of 55-60m/s at certain points. Average velocities for all cases are in the range of 25-28m/s near burner region (plotted in Figure H.5). At the cross-section H velocity for case A and case D, are 10.31m/s and 10.63m/s with standard absolute deviation around 5m/s observed cases (see Figure H.6).

5.5.2 Particle tracks and areas of clinker formation

The particle tracks provide further insights in the boiler. Some particle tracks have been released from selected burners and are shown in Appendix I. Each of the figures is provided with analysed burner trajectories, which has high propensity for causing clinker formation on furnace walls. The entire cases have been given the burner numbers according to the Figure 4.2. Also Table 5.5 is formulated with all the selected burners for mentioned cases and observed travelling path of particles. For calculated cases, it has been revealed that particle path inside the boiler differs due to the changing flue gas path. The particles injected from the lower burners, initially goes towards ash hopper and bottom of the furnace, eventually travel up through the high-temperature and swirling flow combustion zone can be seen in Figures 5.11 to 5.15 mostly for burners 11, 12 and 13. While some of the particles from burners 51, 52, 52 and 23 are directly shoots up on the front wall, than redirecting towards centre burner zone and goes upward. On other side, coal particles from the upper level burners pass around the burner region travels towards superheater panel (see burners 21, 22, 23, while 32 and 33 in case C). Some of them deviates towards nose and goes to top of the superheater panel.

The particles representing short residence time can be cause of carbon presence in the ash at the furnace outlet because they travel very fast from the combustion zone without complete combustion. The particles from low level burners have higher residence time compare to the particles fed from the higher level burners. Coal

devolatilisation and char combustion take place while the coal particles are travelling around the furnace. The maximum residence time of coal particle observed 42s in case A, while case B is reported with 48s. Due to the recirculation flow in case C higher residence time is shown with 60s for particles, which travels to hopper section after colliding with the incoming flow of opposite burner particles, and make the flow like spider's nest. In general, it is known that all fuel species except char are consumed very quickly in the furnace. However, char burns at a slower rate and is consumed in the central region of the furnace. In this calculation, the conversion ratio of the combusting particles is approximately 100%. This dictates that the present combustion process offer sufficient time even for char conversion.

Table 5. 5: Predicted average residence time and relevant burner numbers for different cases

Calculated Cases	**Relevant Burners***	**Average Residence Time of Streams Reaching Exit Plane (s)**
Case A	12 and 13	8.43
	21 and 22	7.32
	31 to 35	4.46
	52 and 53	5.52
	42 and 43	9.78
Case B	21 and 22	7.20
	11, 12 and 13	14.40
	41, 42 and 43	16.80
	51 and 52	7.90
Case C	22, 23 and 24	10.80
	41 and 42	15.80
	11, 12 and 13	13.30
Case D	32 and 33	5.10
	51 and 52	9.45
	41 and 42	14.90
	21, 22 and 23	7.89
	11 and 12	18
Case E	31, 32 and 34	2.34
	11 and 12	11
	41 and 42	13.40
	22, 23 ,24 and 25	6.23
	52 and 53	7.97

* all the burner numbers are given in the similar fashion as shown in Figures 5.11 to 5.15, from left hand side to right hand side starting from top to bottom, for respective cases

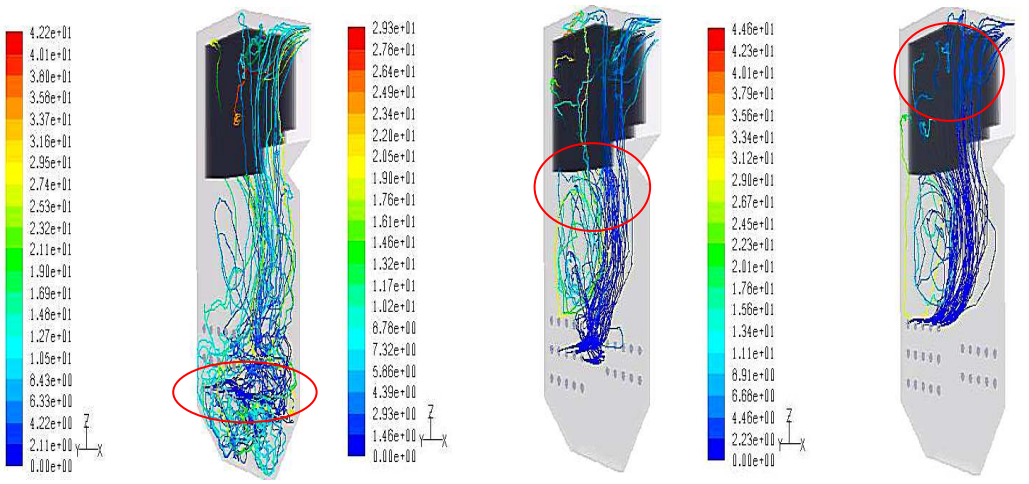

Burner 12 and 13

Burner 21 and 22

Burner 31,32,33,34 and 35

Probable zones of clinker formation

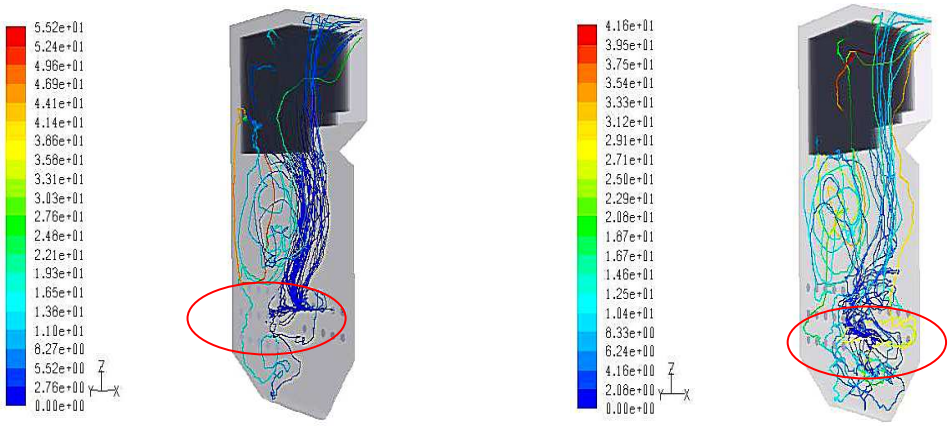

Burner 52 and 53

Burner 42 and 43

Figure 5. 11: Particle trajectories for selected burners for case A

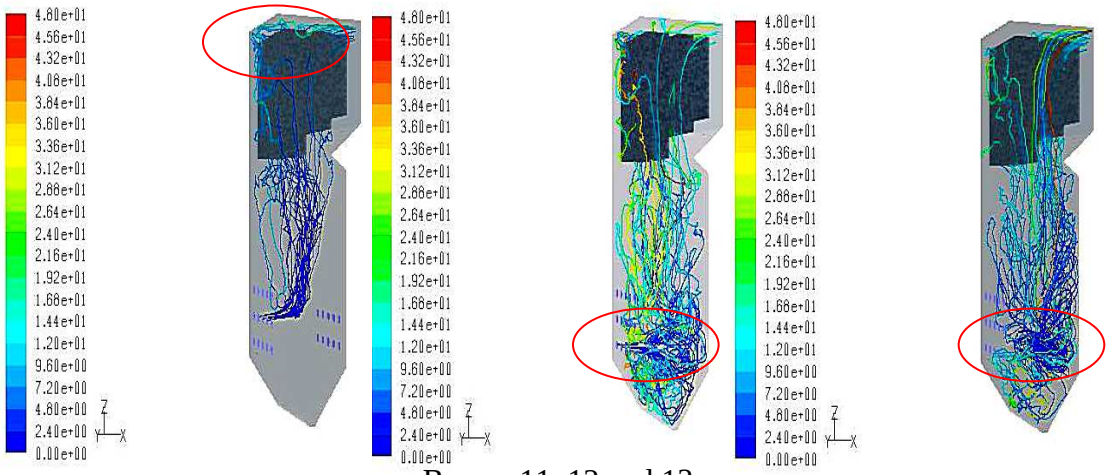

Burner 21 and 22 Burner 11, 12 and 13 Burner 41, 42 and 43

Probable zones of clinker formation

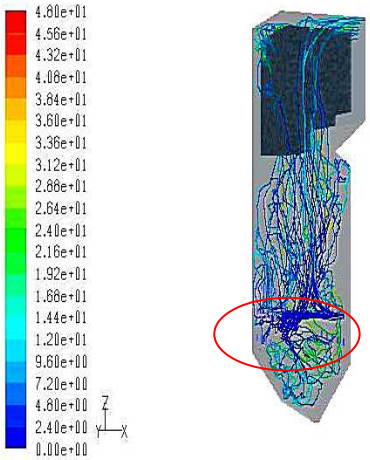

Burner 51 and 52

Figure 5. 12: Particle trajectories for selected burners for case B

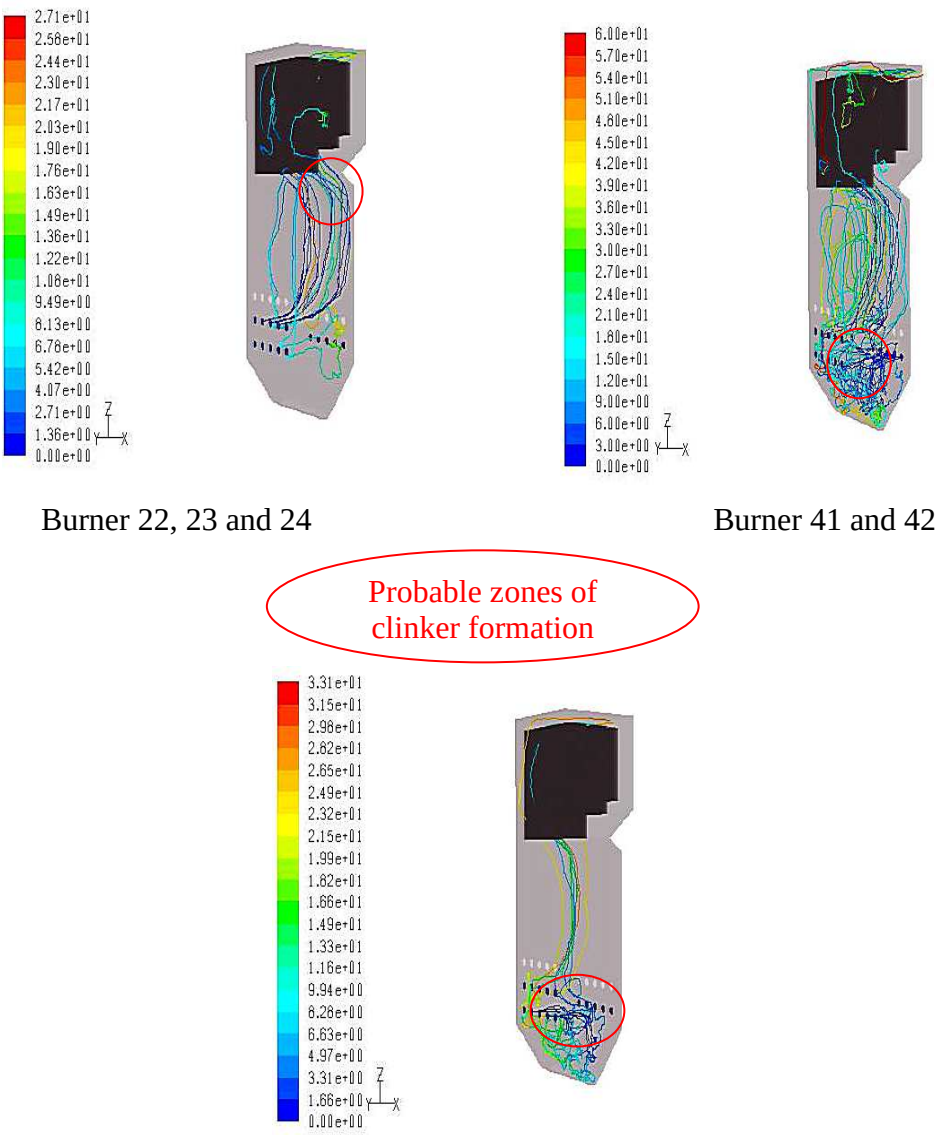

Figure 5. 13: Particle trajectories for selected burners for case C

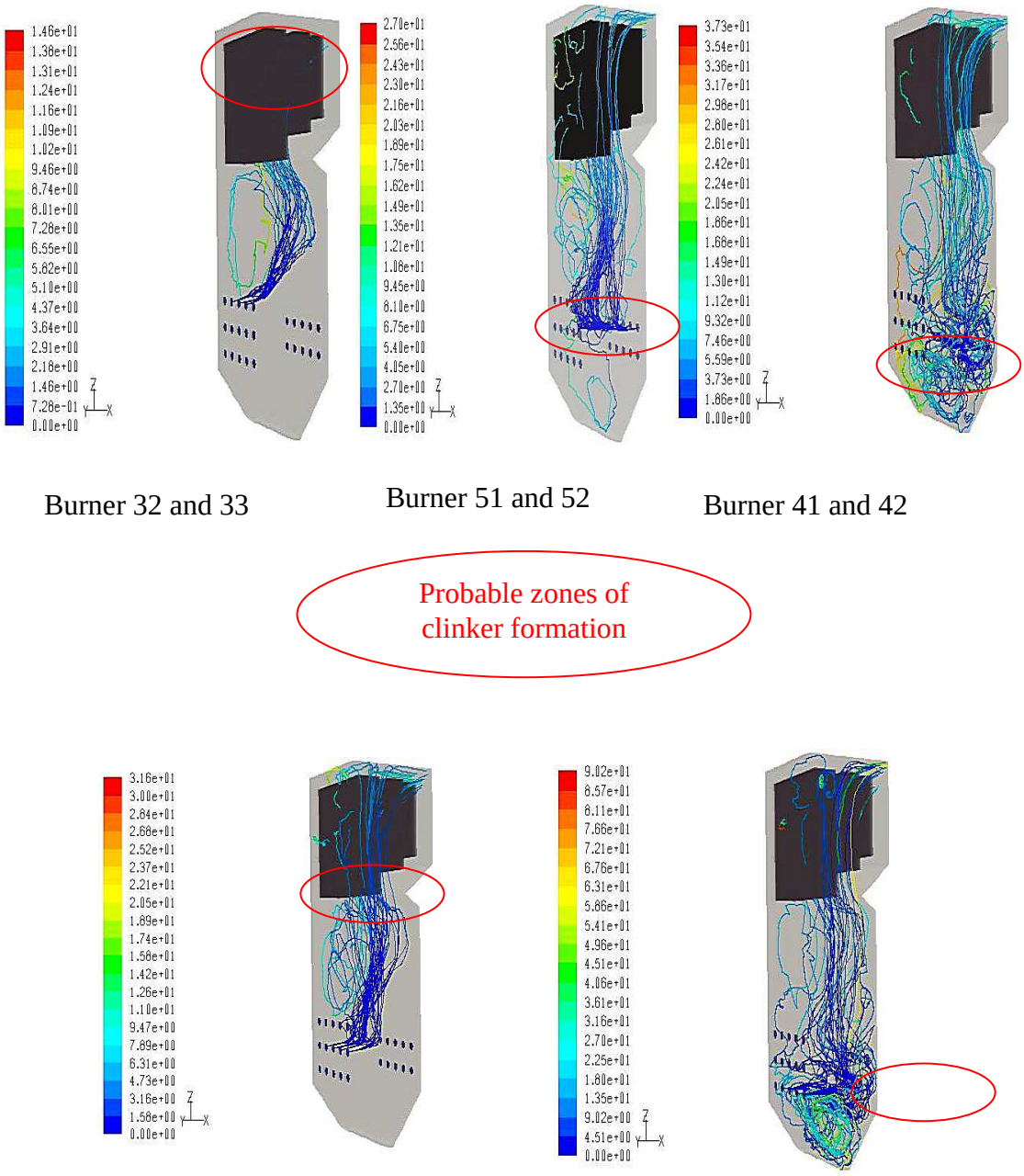

Figure 5. 14: Particle trajectories for selected burners for case D

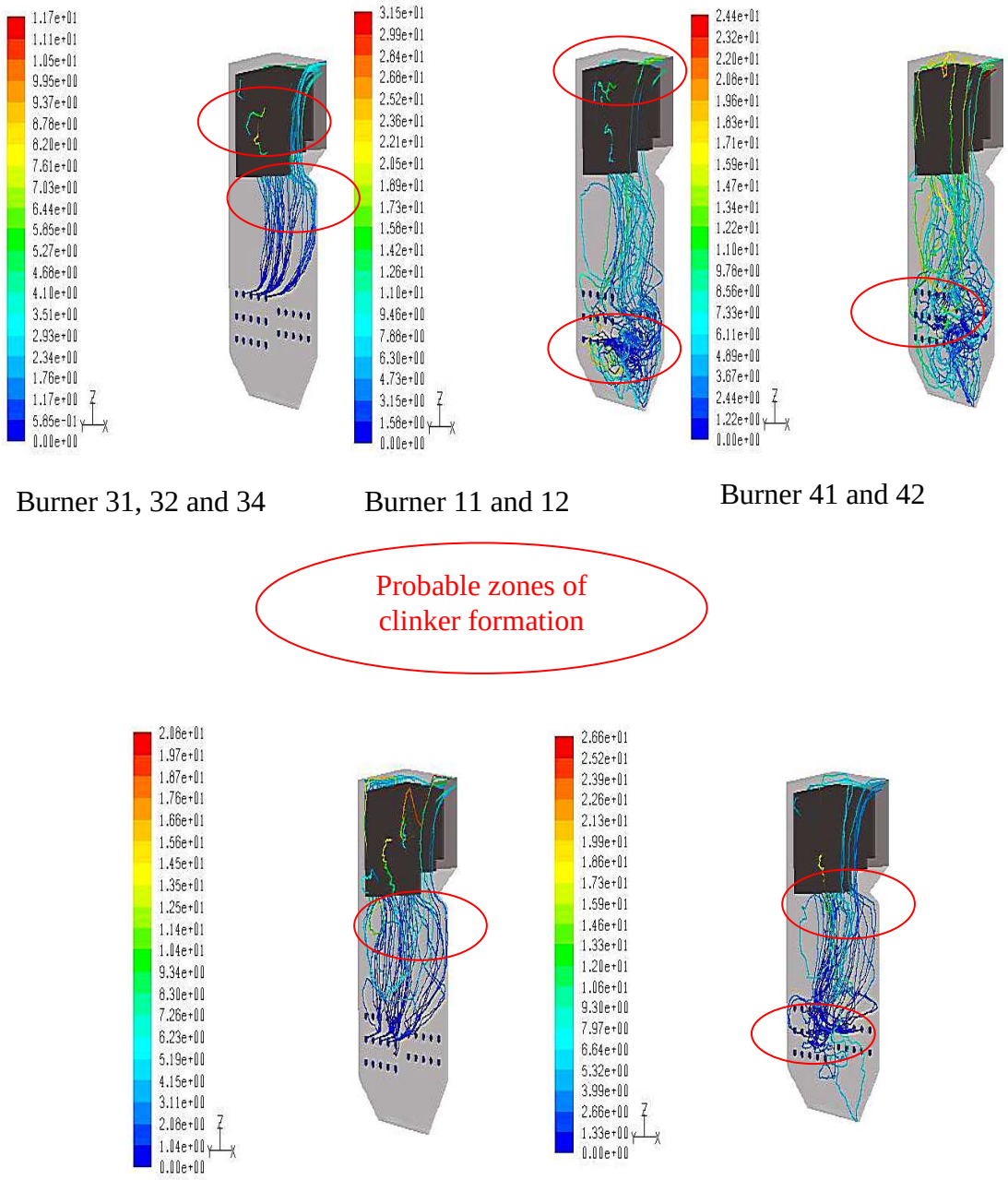

Figure 5. 15: Particle trajectories for selected burners for case E

Typically in the opposite wall-fired furnace three types of particle travelling paths observed in the present study, which causes large deviation in particle trajectories and modify the coal burnout behaviour. Particles which are coming out from the lower level burner, shows this effect stronger. In addition, interaction between the inlet flows from neighbour burners and particles coming out of the opposite burner and their interaction are significant enough to distort the coal particles trajectories. The ash melting temperature of coal particles represents the slagging potential in the boiler. Ash particles in the area of hot spots where melting temperature is reached can adhere to the wall where initial deposit layer is already exists. At this stage deposition will depend on the adhered slag viscosity, weather the incoming particle will stick or bounce off. Particles from some burners come out in combustion zone, and directly shoot up towards opposite side wall and platen superheater. Particle behaviour of this type in boiler leads to excessive slagging on furnace wall, burner 'eyebrows' and platen superheater surface, leaves power utility to unnecessary maintenance, ash hopper explosions, tube rupture and large amount of clinkers on the furnace walls.

Clinkers are mainly a mass formed on furnace walls due to the low fusion temperature of ash present in coal. Those clinkers are rough and strong-bonded with surface in appearance. Presence of silica, calcium oxide, magnesium oxides and other mineral matters in ash lead to a low fusion temperature. These minerals in ash differ as feed coal changes to other. Fused clinker on the furnace walls has tendency to grow and generally sticks to the host surfaces rather than cold surfaces. Hence, clinker accumulation in furnace depends on quality of coal, ash fusion temperature according to the boiler operating conditions.

Ash melting behaviour is a dominant parameter in generating clinkers as it follows mineral distribution of coal and existing temperature conditions in the boiler. Hence, analysing temperature distributions of particle streams in the boiler can prove to be valuable for power utilities to adopt corrective measures for clinker formation on the furnace walls. To justify above comments, Figures 5.11 to 5.15, are marked with areas as identified highly probable zones for clinker formation in different cases, which are briefly described in Table 5.6 as an outcomes of clinker formation in power utilities with the average temperature range of particles. Tabulated operational

difficulties in Table 5.6 for the power utilities, are agreed well with real plant observation (refer Figure 2.4) and discussion in open literature.

In addition to the probable spots for clinker formation on the furnace walls, governing parameters for clinker accumulation is provided in Table 5.7. This information is very useful for power utilities to analyse the areas where particles have short residence time, or impacting particles and building up clinkers on furnace walls. Further, it can assist operators to opt for intelligent sootblowing operation by optimising its frequency.

Table 5. 6: Information on probable spots of clinker formation on the furnace walls

Burner Nos	Relevant Cases	Summary of Observed Particle Trajectory path	Predicted Zone of Clinker Formation	Operational Difficulties
52 **51** **53**	**cases A, B, D and E** **case D** **case A and E** **(Temperature range 1160 to 1630K)**	Most of the streams impacts on front wall between first and second row In case A, fewer streams from burner 52 and 53 travel towards ash hopper, while most of them going upwards to superheater tubes and after crossing it gets the exit Another scenario is seen in case B, where streams from burner 52 straight away impacts on opposite burner wall as well as quarl and rest of them goes towards boiler nose to superheater tubes and going out For case D and E trajectories are same as case A	Clearance between first row and second row on front wall Corner of boiler nose and rear wall, superheater tubes	Damaging burner quarl of the burner rows, blockage of air and coal flow, forming uneven situation in burner region Chances of hanging clinker at the corner of boiler nose and superheater tubes
43 **41** **42**	**case A and B** **cases B, C, D and E** **all cases**	More streams towards front wall second burner row and others after impacting comes back towards rear wall of the ash pan Streams from burner 41 coming up to the centre of the burner and goes upward, among those streams some show recirculation after combustion	Directly towards quarl of burner 21 Front wall first two burner rows Ash hopper front wall	Can block the burner and big clinker formation chances, leads to ash hopper explosions, and distort the flame stability Chocking of ash hopper and burner quarl

	(Temperature range 1230 to 1580K)	zone near front wall Overall path of streams for all cases remains mostly the same except case C, where half of the streams going towards ash hopper		
12 **11** **13**	**all cases** **all cases except case A** **cases A, B and C** **(Temperature range 1430 to 1680K)**	Many streams directly goes to ash pan wall on the rear wall, after that moves around burner zone chaotically due to recirculation flow All the cases represents streams with same travel path, except case C, where some of the streams going towards burner 41 and 42	On the ash pan rear wall and around eyebrow of burner 41 and 42	High velocity of particles can cause abrasion of surface
31 to 35 **32 and 33** **31, 32 and 34**	**case A** **case D** **case E** **(Temperature range 1080 to 1450K)**	All the streams travels straight up with the rear wall and impinge on nose of furnace, and again deviates towards superheater tube bank on front wall, and goes up to the wall of boiler drum and last exits the domain. Some of the streams in case A shows recirculation, where case D and E are same without recirculation paths	On the nose surface, corner of nose wall and rear furnace wall Puncture of superheater tubes and wear of upper wall	Particles with high temperature can accumulate and form initial slag, as consequence loss of heat transfer and corrosion to the wall Particles with high velocities towards superheater tubes can cause piercing

21 and 22 **23** **24** **25**	**cases A, B, and D** **cases C, D and E** **case C and E** **case E** **(Temperature range 1090 to 1360K)**	Mostly all the streams travels in similar fashion, parallel to the front wall, and collides to the furnace tubes Another path observed in case B and E, where few particle streams directly hits to the upper wall of furnace Instead of going in parallel to the front wall, in case C and E, a group of particle streams flows towards rear wall first and than to corner of boiler nose and travel through superheater tube bank to the exit	Tubes of platen superheater Abrasion of upper wall of boiler nose Corner of boiler nose	Deposition between tube spacing, sometimes tube rupture due to particle impingement and loss to steam production. Wear on boiler upper plate and damaging leftover tubes in cross-over pass, where particle velocities are high
Specifications: **Front wall** **Rear wall**		First Row – (11 to 15) Second Row – (21 to 25) Third Row – (31 to 35) First Row – (41 to 45) Second Row – (51 to 52)	(Mounted through +Y to –Y axis in constructed domain) (Provided temperature range is based on the average values of the particle streams)	
Note: **Refer Figure 2.4, photographs of clinkers in actual plant operation, which justifies the above predicted results.**				

Table 5. 7: Governing parameters for clinker accumulation on probable surface of furnace walls

Probable Spots of Clinker on the Furnace Walls	Governing Parameters For Clinker Accumulation
Clearance between first row and second row on front wall **Corner of boiler nose and rear wall, superheater tubes**	Temperature at walls nearer to ash fusion temperature and stickiness of incoming particles Stickiness of adhered layer on the furnace walls, deviation of particle streams velocity, which leads trapping in the ash pan region
Directly towards quarl of burner 21 **Front wall first two burner rows**	Temperature of particles and particle streams sensitive to burner levels due to burner aerodynamics (Boyd and Kent, 1994)
On the ash pan rear wall and around eyebrow of burner 41 and 42	Particle size distributions and their relevant impaction rate and angle to the surface as well as particles in reducing environment
On the nose surface, corner of nose wall and rear furnace wall **Puncture of superheater tubes and wear of upper wall**	Particle impaction on the surface having initial deposit layer, temperature and thickness of deposit and particle residence time
Tubes of platen superheater **Abrasion of upper wall of boiler nose** **Corner of boiler nose**	Short residence time of particles, higher local temperature

Chapter 6

Conclusions and Recommendation

6.1 Conclusions

Optimisation of pulverised coal combustion is vital in today's global climate, due to stricter emission policies imposed by government across the globe and boiler maintenance requirements. Clinker formation on furnace walls is the foremost issue faced by many power utilities in present times. According to the various power utilities' experience and survey, deposition in coal-fired furnaces leads to billions of dollars in maintenance around the world. Hence, in the present study the CFD code has been used to model the utility boiler with the aim to identify the regions of wall of furnace with high propensity to clinker accumulation and conclusions drawn from the current study are given below.

6.1.1 Model development and simulation for different operational cases

- For this purpose, 3D model of boiler has been created with actual plant dimensions.
- The simulation run has been carried out with a boiler in five different scenarios with various burner configurations as well as fuel loads.
- Calculations for these five different operational cases have been done in the accordance with real plant process data.
- Calculated air flow and feed coal are almost same to the received industrial data.

6.1.2 Model results and validation

Temperature distributions, species concentration and heat transfer

- Different parameters like temperature distribution near the burner, at the exit and on the superheater panel, species concentration and heat transfer to the furnace walls have been observed.

- Some phenomena have been visualised in different cases in terms of temperature distributions. Temperature distribution in boiler is a very important parameter which influences ash deposition on furnace walls and radiation zones. Due to uneven temperature distribution there are chances of excessive ash deposition and which can dominate big clinker formation on furnace walls.
- Detail phenomena of coal combustion in large scale boilers have been understood through CFD simulations and its practical implications to power utilities have been discussed to mitigate utility problems.

Comparison of predicted results with literature data

- At present, due to lack of real plant data, calculated data have been compared with literature values. Comparisons are made with important process parameters like temperature, species concentration, FEGT and heat transfer to the furnace walls, which are congruent with literature values.
- The calculated values from the present model are consistent with the comparison of parameters depicted in the available literature. Standard absolute deviation is less than 10% for all results, where temperature profiles near the superheater region showed some discrepancies as the models of superheaters and reheaters have not been considered as a heat sink.
- Detailed descriptions of particle path lines are provided for calculated cases with different air flow configuration; there have been dramatic changes visualised in cases with higher air flow compared to lower air flow. There are three main types of flow patterns observed in this current study which is discussed in previous chapter. Main variations have been viewed in the particles streams which are coming out from the lower level burner, and these streams can be responsible for uneven flow distributions in the boiler.

6.1.3 Identification of clinker formation regions

- Analysed particle trajectories and detailed information gives a clear indication of probable clinker formation spots in the furnace.
- All the flow patterns of the particle's travelling path dictate the clinker accumulation faces inside the boiler during different operations.

- Probable spots of clinker deposition on the furnace walls creates some operational difficulties like damaging burner quarl, blockage of air and coal flow, ash hopper explosions and loss to heat transfer, which causes steam production loss.
- The suggested wall surfaces could be beneficial for power plant engineers to identify ash deposition mechanism as well as low temperature eutectics from interaction of mineral matter present in flow gases. This study can provide the strong platform to study the series of mechanism for clinker formation.
- In the view of this issues arising in boiler, some governing parameters for them are discovered and mentioned in present study.

Findings from this investigation will give a better understanding of particle travel path inside a boiler which can provide utility engineers with a means for mitigating the clinker formation issues as well as possible visualisation of clinker growth on probable faces inside a furnace during time to time plant operation. This can lead to further recommendation for making this model very effective in real plant operation. Nevertheless, CFD modelling is presently quite useful as a utility problem solver, as investigated in the current study.

6.2 Recommendation

Future work can be done with making the present 3D model more precise with grid size and using alternative combustion models as well as it can be utilised to study other important phenomena like NO_X-emissions in boiler. Submodels and parameters like different particle size and air fuel ratio can be changed according to the industrial process requirement. To develop a model which precisely predicts clinker formation requires boiler specified data related with ash chemistry which is unavailable in the present case. There is a possibility to relate this work with those prescribed ash deposition mechanisms. Predicted gas velocities, particle trajectories and temperature profile would also be useful to pursue further detailed research on deposition mechanisms.

Detail chemical analysis of ash and modelling of ash formation could be a leading way towards the development of submodels for clinker formation and hooking it with a developed CFD model. Development of clinker formation sub model will

require, additional experiments to determine the factors such as initial ash deposition layer, thickness of deposited layer, sintering behaviour of coal particles and its residence time in boiler.

It is also viable to study the aerodynamics of burners in the present study with the help of utility engineers. Aerodynamics of burners will show temperature of particles and particle streams which are sensitive to burner levels. Plant experience from several similar utilities from firing different coals can also strengthen the model which is also developed in the current work. This will enable to formulate a generalised model which will be significant help to practice engineers.

Appendix A

Model Configuration

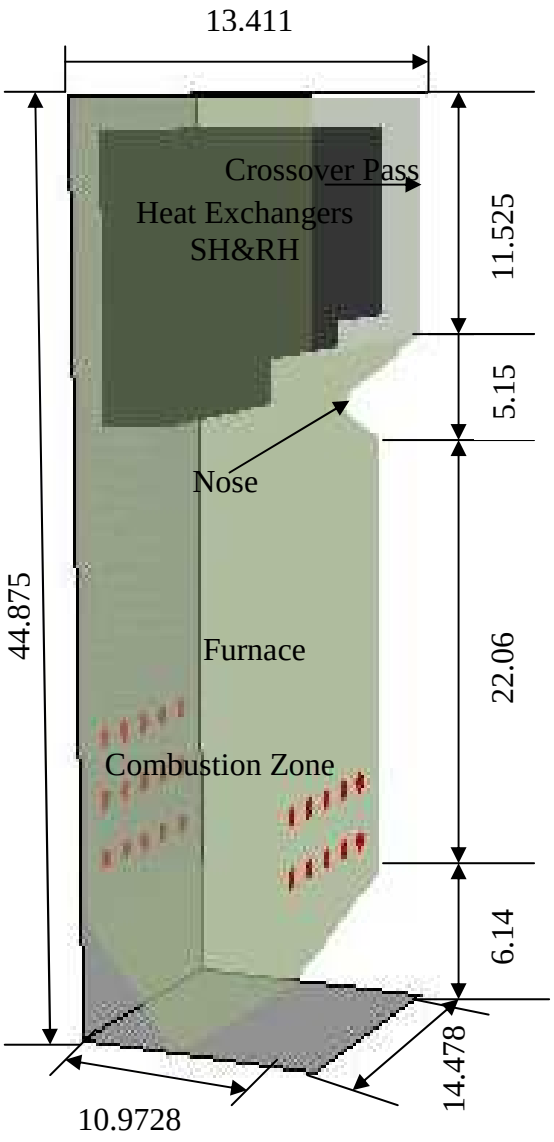

Figure A. 1: Major dimensions (all in meter) reported for created boiler model

Appendix B

Coal Properties for Coal Type B

Coal Type B (Griffin Ewington II Mine) (As received in (Wt %))		
Proximate Analysis (%) As received	**Average**	**Range**
Moisture	25	23-27
Ash	10.5	8-14
Volatiles	25.5	23.5-27.5
Fixed Carbon	40	36-42
Specific Energy MJ/kg	19.2	18.8-20.5
Ultimate Analysis (%)(d.a.f)		
Carbon	75.5	75-76.5
Hydrogen	4.7	4.6-4.9
Nitrogen	1.4	1.4-1.5
Sulphur	0.7	0.6-1.07
Oxygen	17.7	16.8-18.0
Ash Analysis (%)(d.b.)		
SiO_2	51.4	47-59
Al_2O_3	33.5	31-36
Fe_2O_3	7.4	5-10
CaO	1.8	0.4-2.1
MgO	0.86	0.2-1.1
Na_2O	0.24	0.02-0.3
K_2O	0.33	0.2-0.4
TiO_2	0.99	0.4-2.0
Mn_3O_4	0.07	0.06-0.08
SO_3	0.21	0.06-0.35
P_2O_3	1.60	0.65-2.15
Ash Fusion Temp. (^oC)	**Average**	**Minimum**

(Reducing)		
-Deformation	>1600	1420
-Sphere	>1600	1470
-Hemisphere	>1600	1540
-Flow	>1600	1560
(Oxidizing)		
-Deformation	>1600	>1460
-Sphere	>1600	-
-Hemisphere	>1600	-
-Flow	>1600	-

Appendix C

Boundary Conditions

Table C. 1*:* Boundary conditions for case A

CASE A - coal A	
Primary Air Flow rate	123 kg/s
Secondary Air Flow rate	287 kg/s
Total Coal Flow rate	43 kg/s

Table C. 2: Boundary conditions for case B

CASE B - coal A	
Primary Air Flow rate	98.4 kg/s
Secondary Air Flow rate	229.6 kg/s
Total Coal Flow rate	34.4kg

Table C. 3: Boundary conditions for case C

CASE C - coal A	
Primary Air Flow rate	73.8 kg/s
Secondary Air Flow rate	172.2 kg/s
Total Coal Flow rate	25.8 kg

Table C. 4: Boundary conditions for case D

CASE D - coal A	
Primary Air Flow rate	147.6 kg/s
Secondary Air Flow rate	344.4 kg/s
Total Coal Flow rate	43 kg/s

Table C. 5: Boundary conditions for case E

CASE E - coal B	
Primary Air Flow rate	147 kg/s
Secondary Air Flow rate	342 kg/s
Total Coal Flow rate	51 kg/s

Table C. 6: Model inputs for all cases

Primary Air Temperature	**333K**
Secondary Air Temperature	633K
Primary Air Inlet H_D (m)	0.15
Primary Air Inlet T.I. (%)	3
Secondary Air Inlet H_D (m)	1.03
Secondary Air Inlet T.I. (%)	3
Outlet H_D (m)	12.83
Outlet T.I. (%)	8-10
Wall emissivity	0.8
Outlet emissivity	1

Table C. 7: Calculated air and coal flow rates for 330MW power plant using coal type A[a] (case A)

Power Plant Capacity	**330MW**
Coal Type A (WESTERN PREMIER MINE)	Sub-Bituminous
Calorific Value of Fuel	5135 kcal/kg
Coal Flow Rate	43 kg/s
Primary air mass flow rate	123 kg/s
Secondary air mass flow rate	287 kg/s
Primary Air Velocity[b]	14.21 kg/s
Secondary Air Velocity[b]	18.66 m/s
Coal flow Rate for Injections	1.72 kg/s

Table C. 8: Calculated air and coal flow rates for 330MW power plant using coal type B[a] (case E)

Power Plant Capacity	**330MW**
Coal Type B (GRIFFIN EWINGTON II MINE)	Sub-Bituminous
Calorific Value of Fuel	4299 kcal/kg
Coal Flow Rate	51 kg/s
Primary air mass flow rate	147 kg/s
Secondary air mass flow rate	342 kg/s
Primary Air Velocity[b]	17 kg/s
Secondary Air Velocity[b]	22.25 m/s
Coal flow Rate for Injections	2.04 kg/s

[a] all the values for flow rates reported in the above table is solely calculated with empirical formulas.

[b] These values is determined for the model input (calculated as a function of mass flow rate, density and inlet section area).

Appendix D

Post-Processing Planes and Lines in Simulation Object

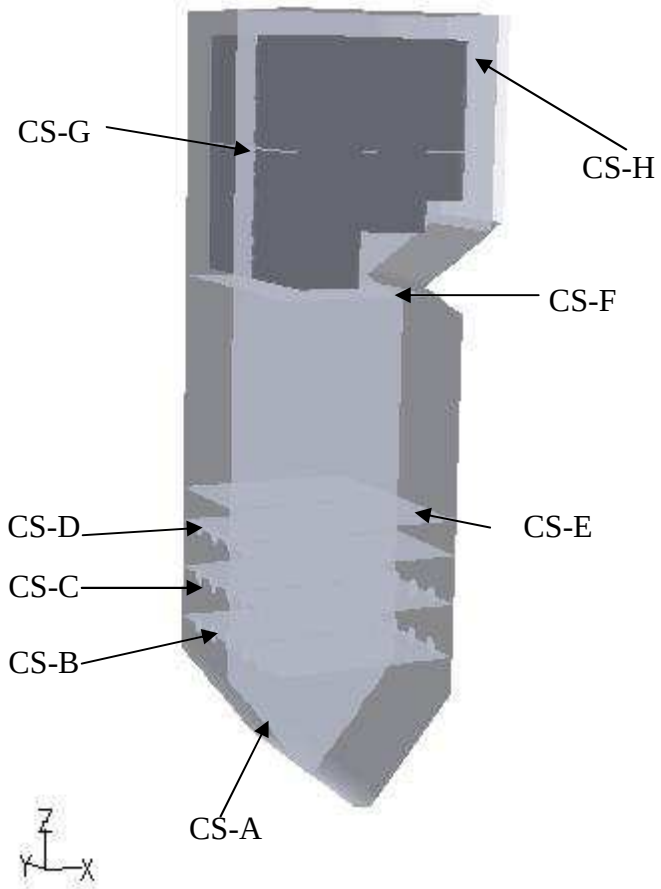

Figure D. 1: Geometry showing different cross-sections for result representations (CS – Cross-section, specifications of locations are given in Table D. 1)

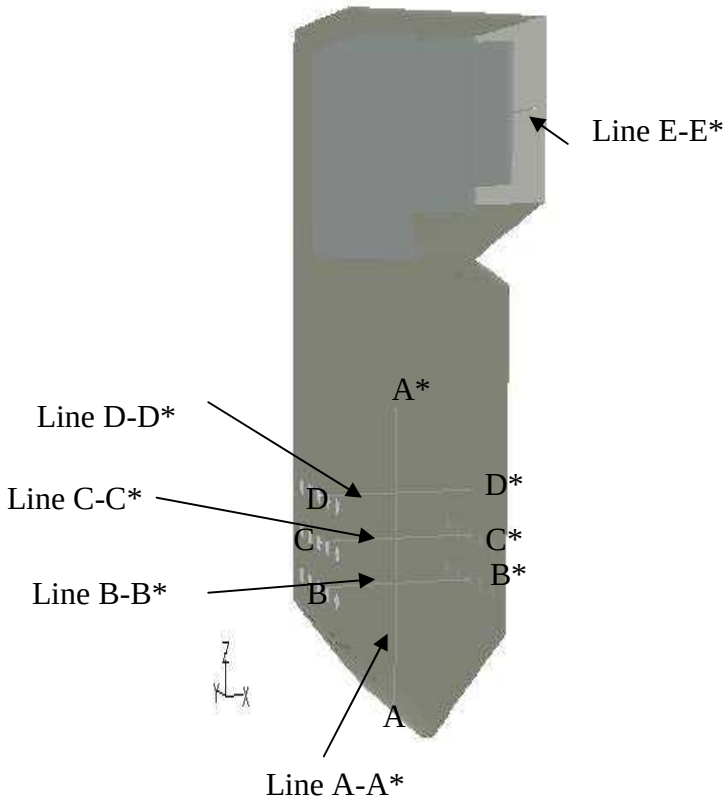

Figure D. 2: Geometry showing different lines for result representations (Specifications are given in Table D. 2)

Table D. 1: Specifications for different cross-sections and lines in geometry

Cross-Sections	**Appropriate Specification in Geometry**
CS-A	Plane on Y-axis, X=0 and Z=0
CS-B	Crossing first burner row on both sides, Z=8.301786m
CS-C	Crossing second burner row on both sides, Z=11.44313m
CS-D	Crossing third burner row on front wall, Z=14.31513m
CS-E	After combustion zone, Z=16.37938m
CS-F	Near boiler nose, Z=29.30338m
CS-G	Crossing superheater tubes, Z=37.24625
CS-H	Measurement of FEGT, X=7.187184m

Table D. 2: Specifications for different cross-sections and lines in geometry

Lines	**Appropriate Specification in Geometry**
Line A-A*	Vertical line from ash hopper to combustion zone, Z=0 to 20m
Line B-B*	Z=8.35m
Line C-C*	Z=11.35m
Line D-D*	Z=14.35m
Line E-E*	X=7.187184m,Z=39.131m

Appendix E

Temperature Distributions

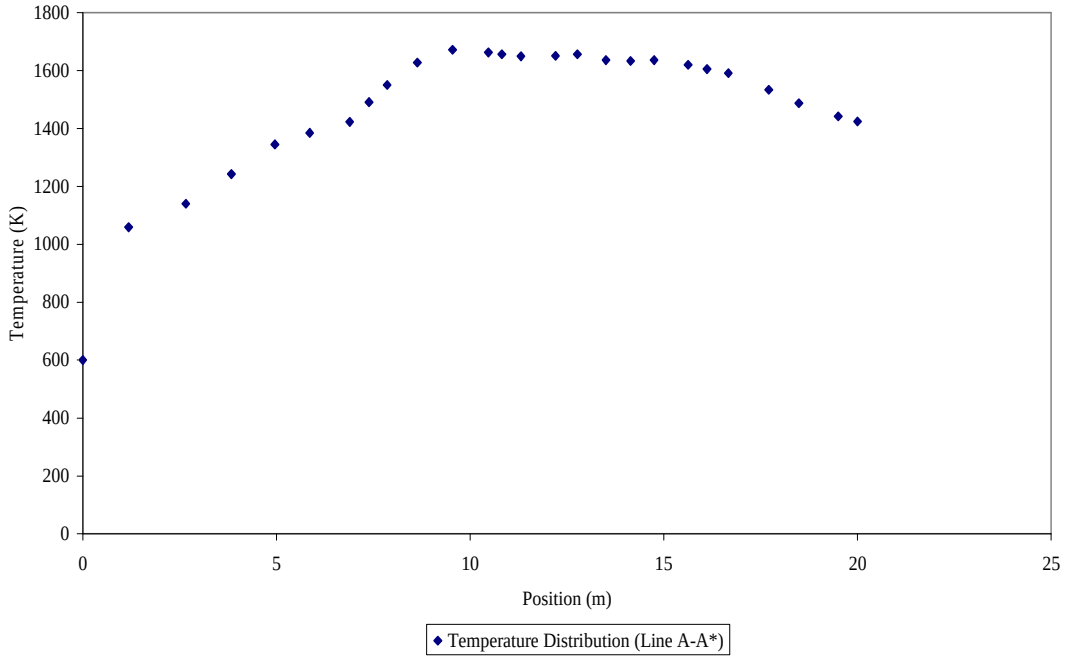

Figure E. 1: Temperature distribution for case A on line A-A*

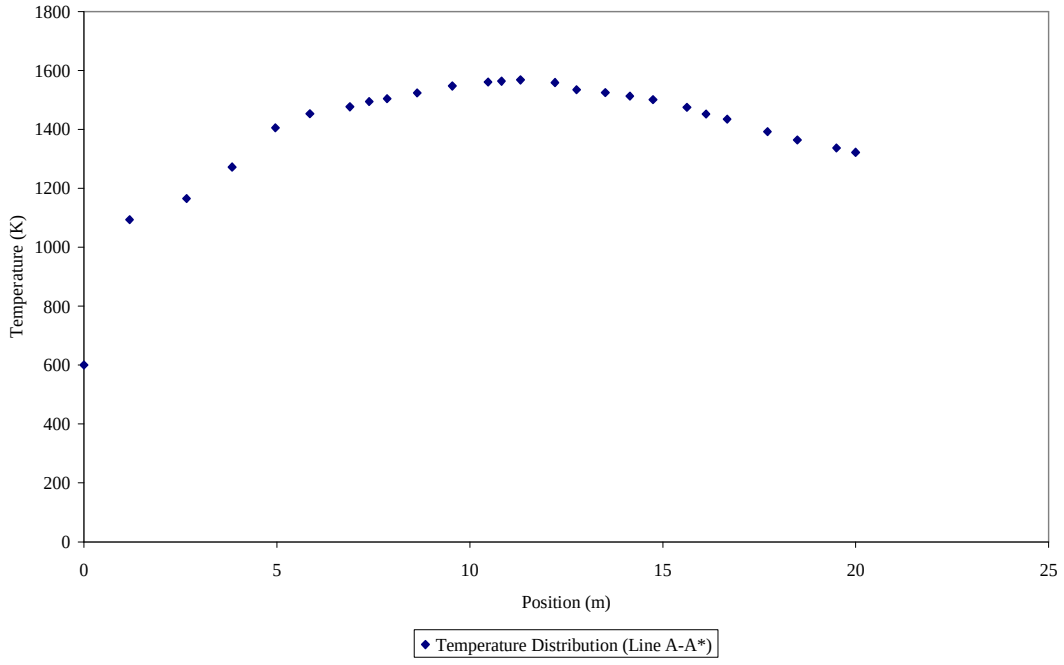

Figure E. 2: Temperature distribution for case B on line A-A*

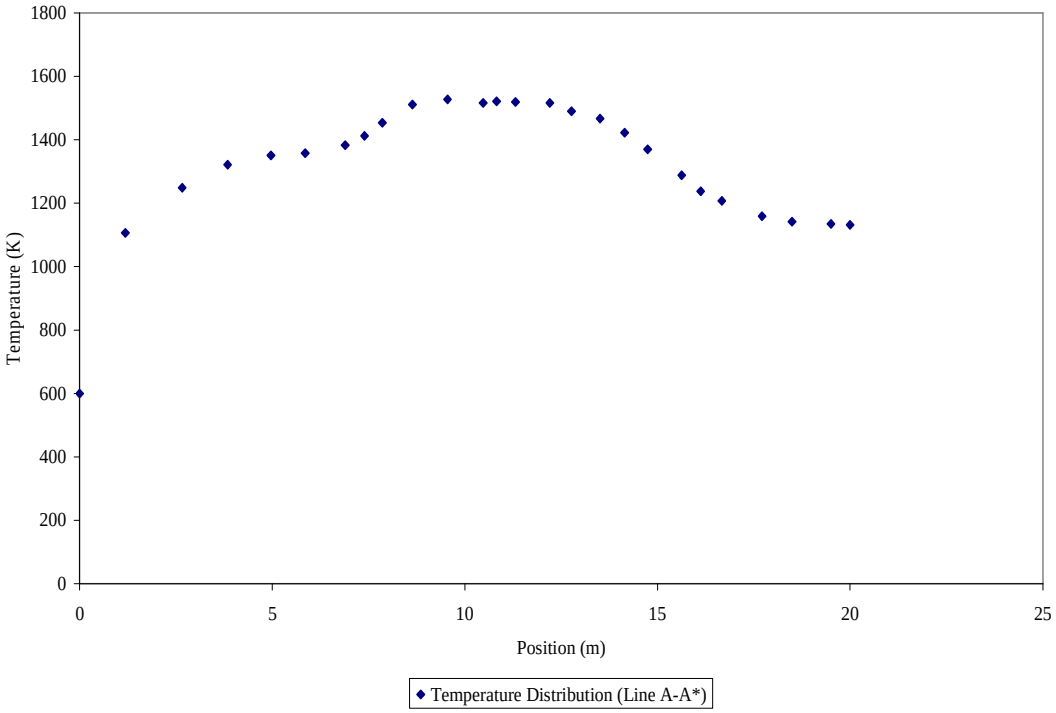

Figure E. 3: Temperature distribution for case C on line A-A*

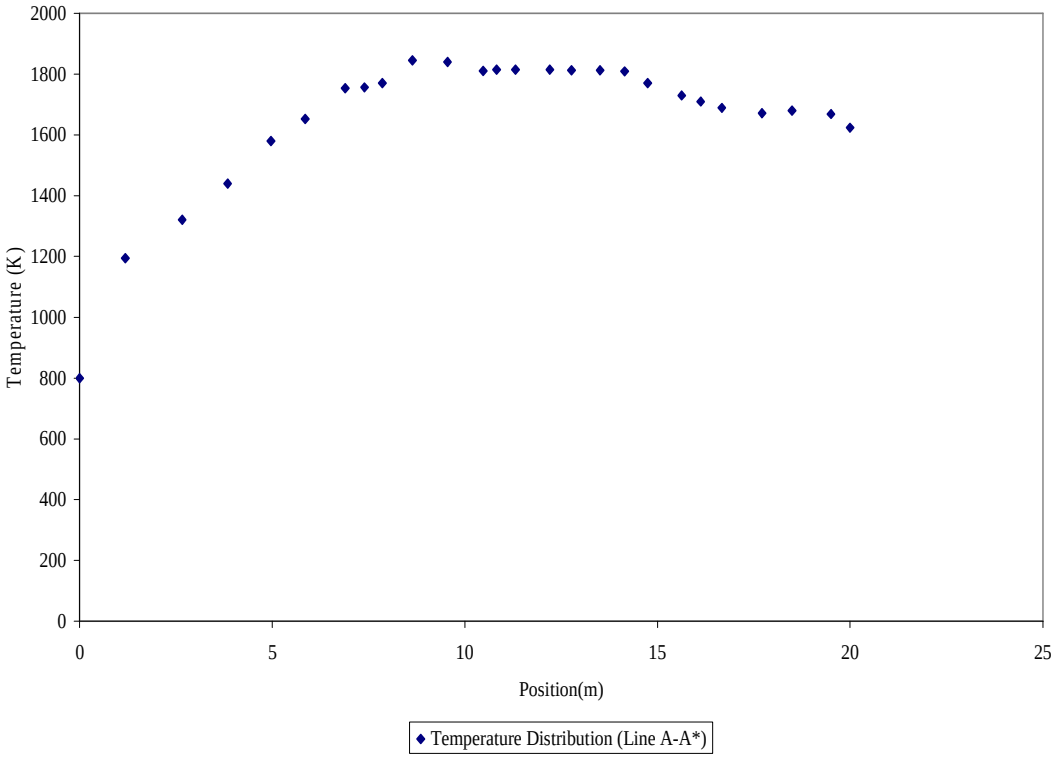

Figure E. 4: Temperature distribution for case D on line A-A*

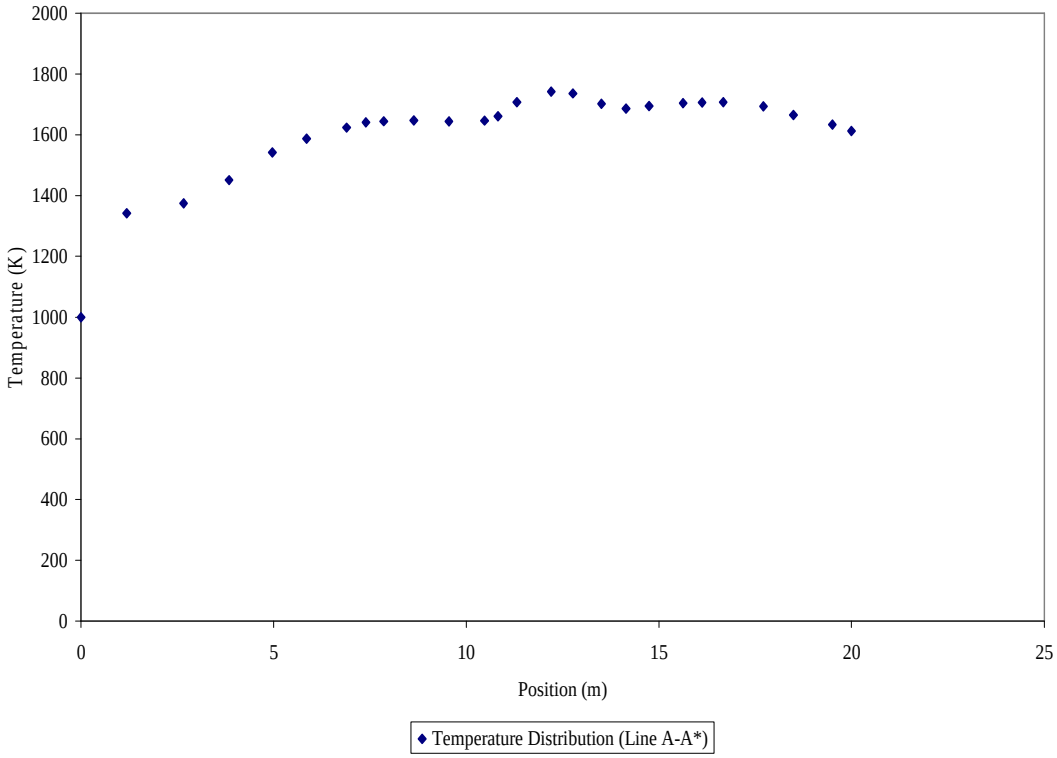

Figure E. 5: Temperature distribution for case E on line A-A*

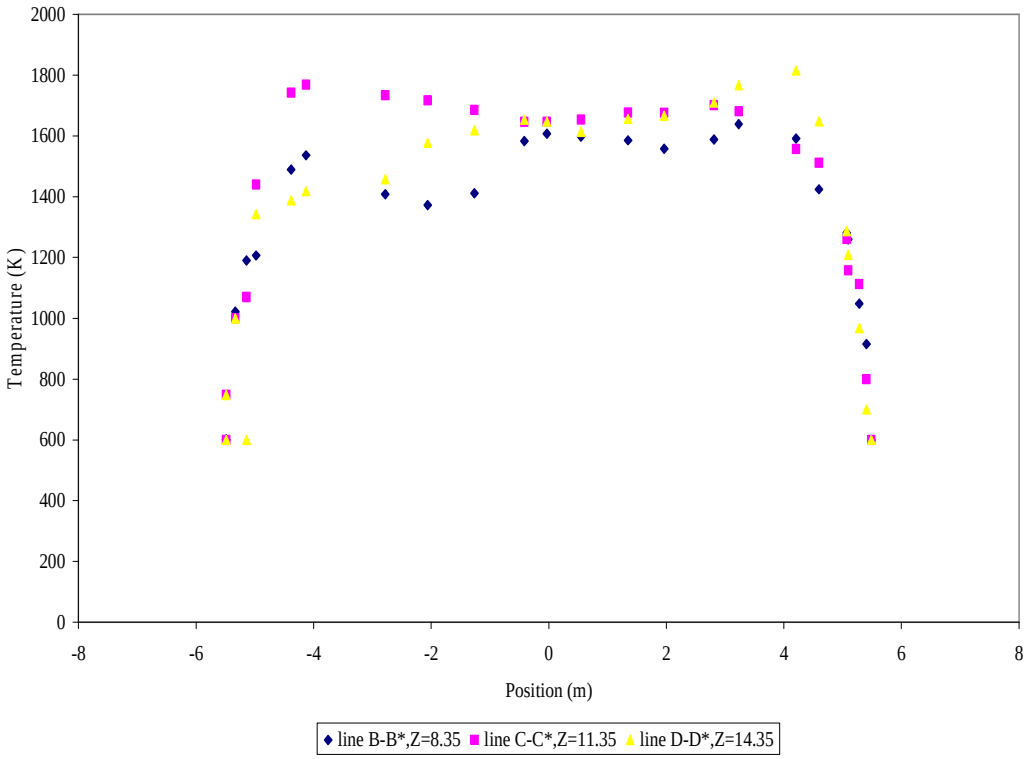

Figure E. 6: Temperature distribution for case A on three lines near burner

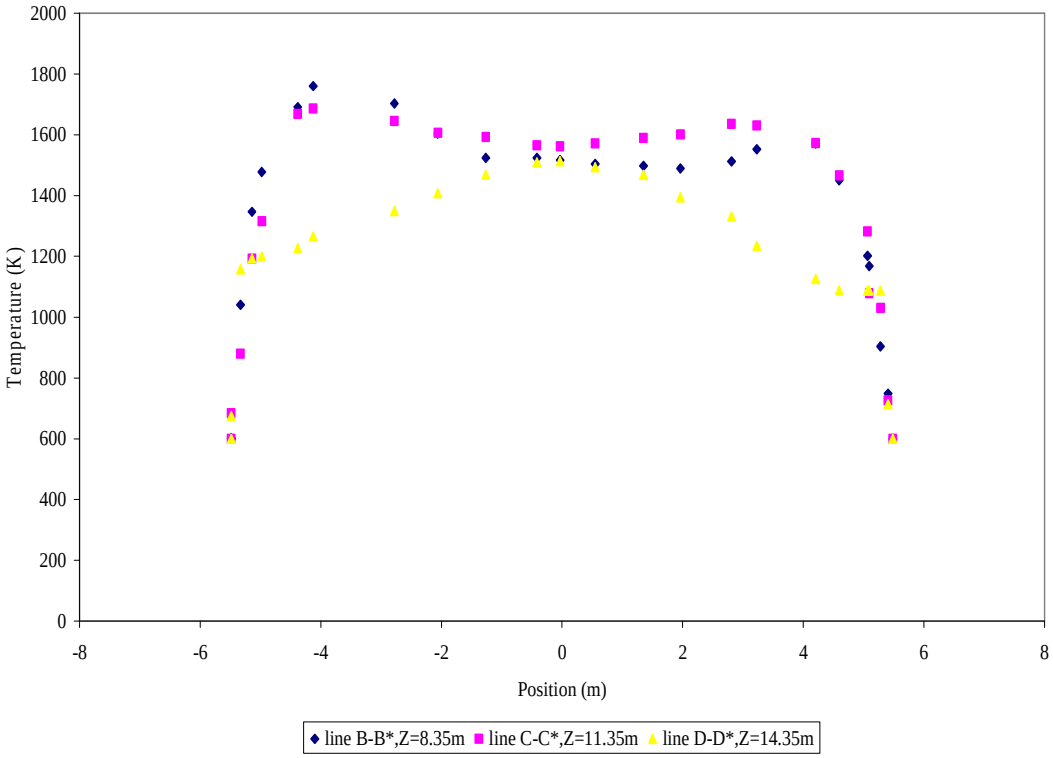

Figure E. 7: Temperature distribution for case B on three lines near burner

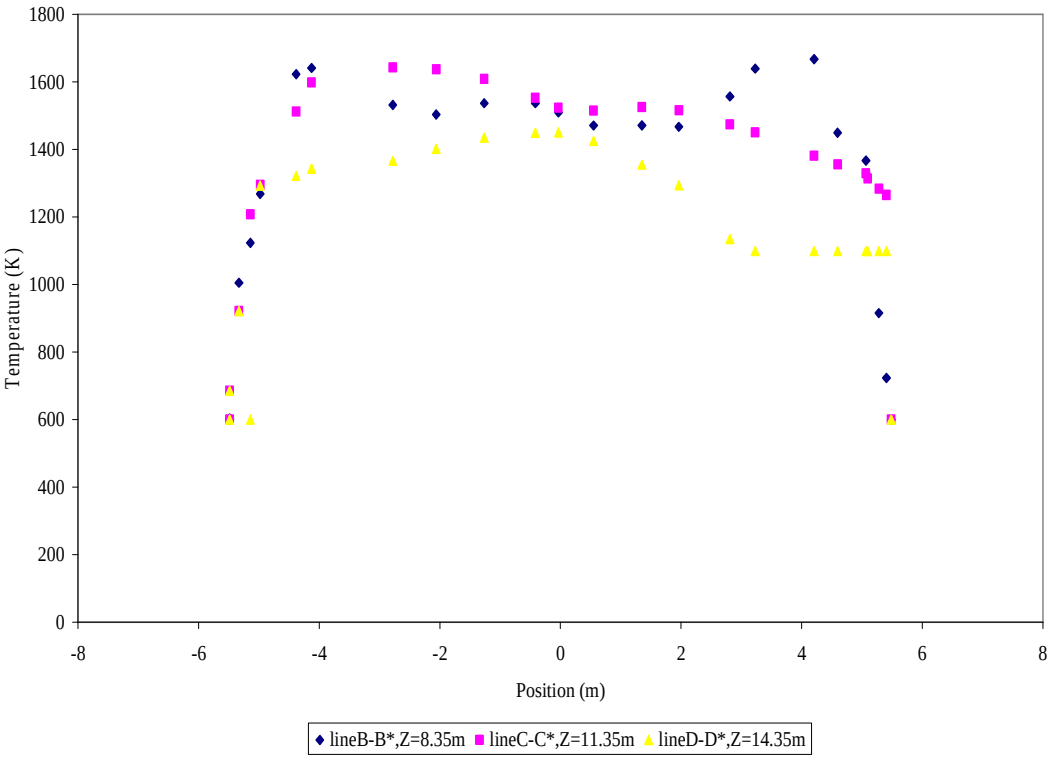

Figure E. 8: Temperature distribution for case C on three lines near burner

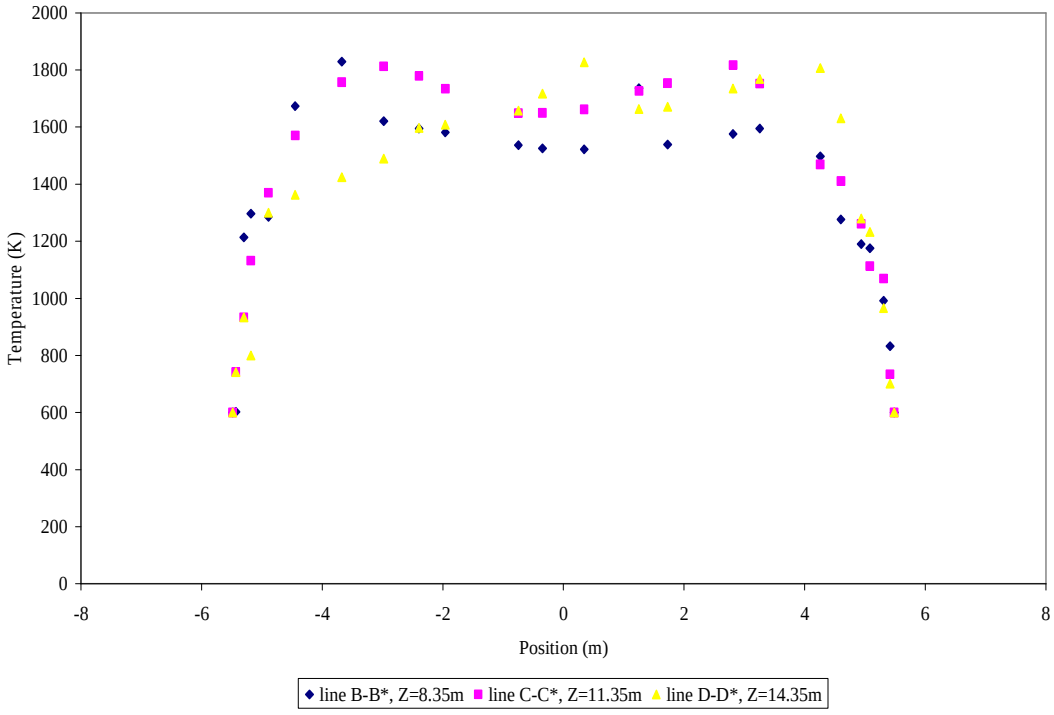

Figure E. 9: Temperature distribution for case D on three lines near burner

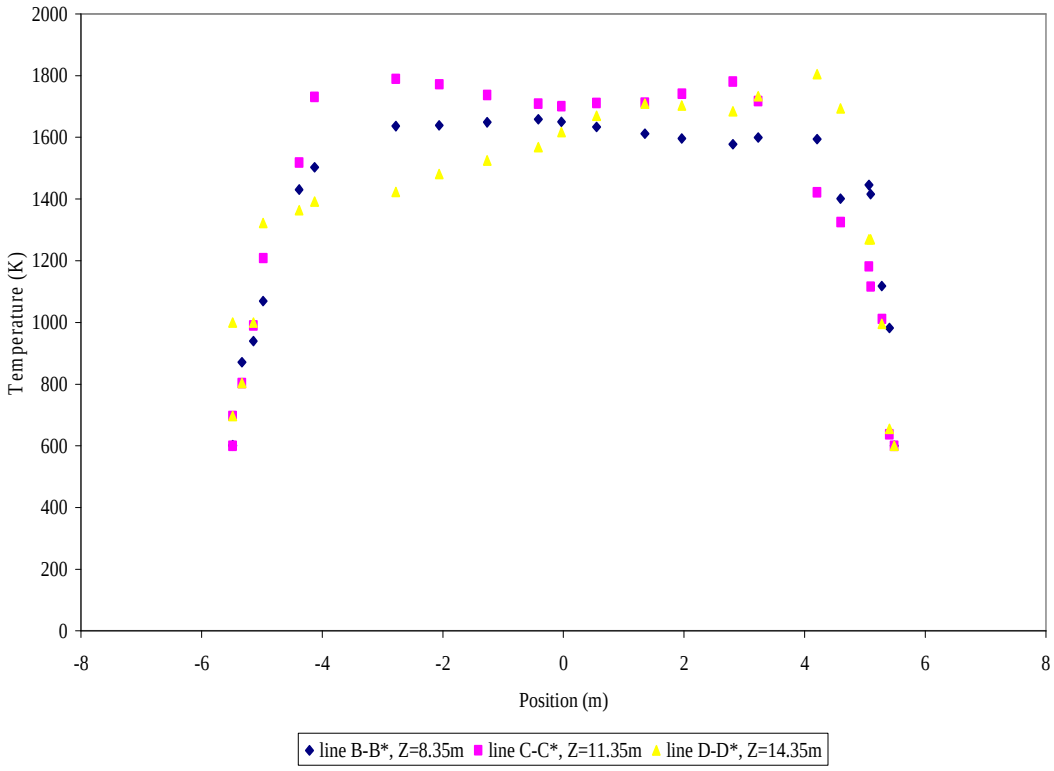

Figure E. 10: Temperature distribution for case E on three lines near burner

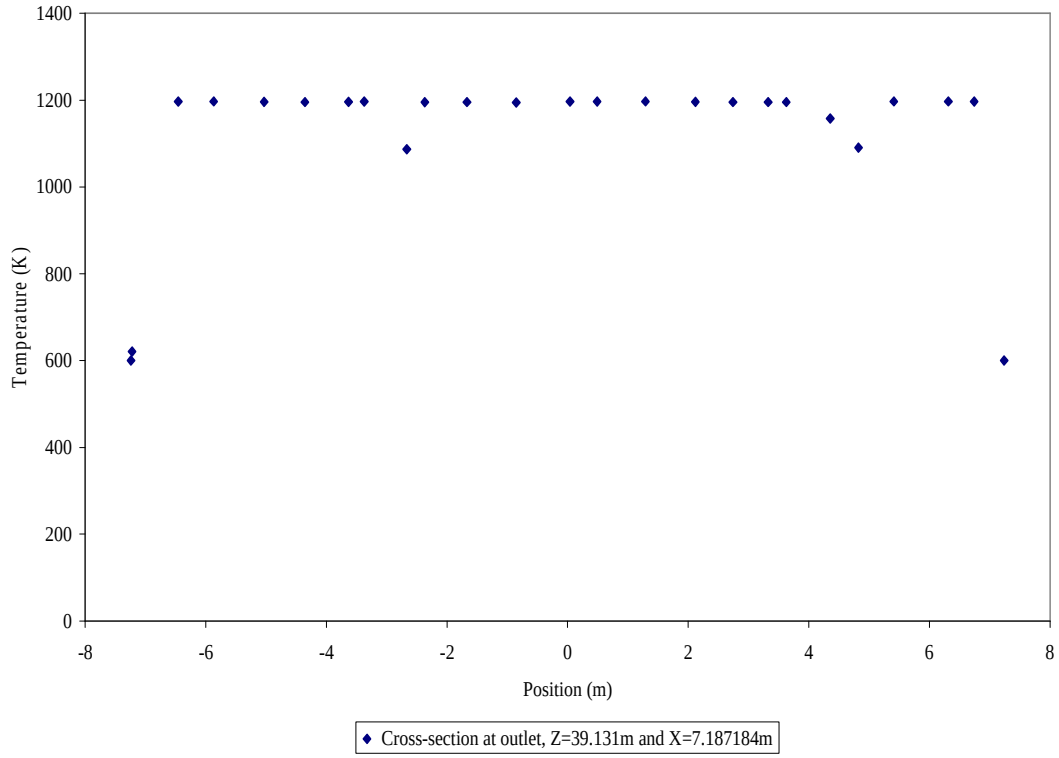

Figure E. 11: Temperature distribution for case A on CS-H

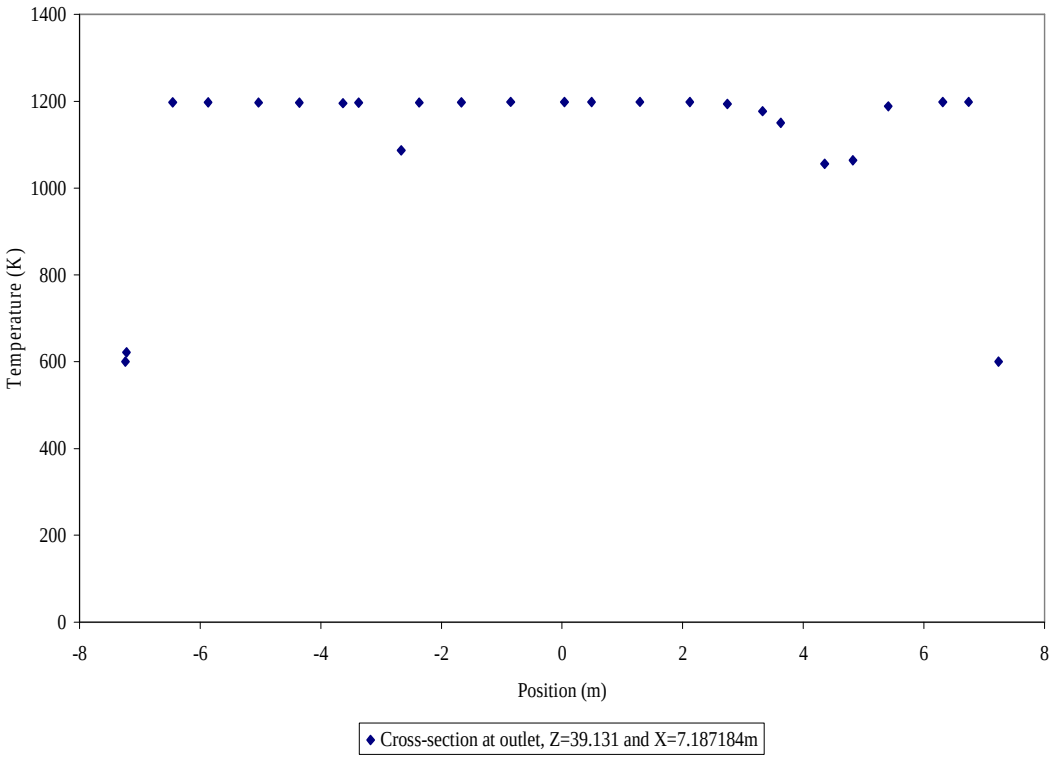

Figure E. 12: Temperature distribution for case B on CS-H

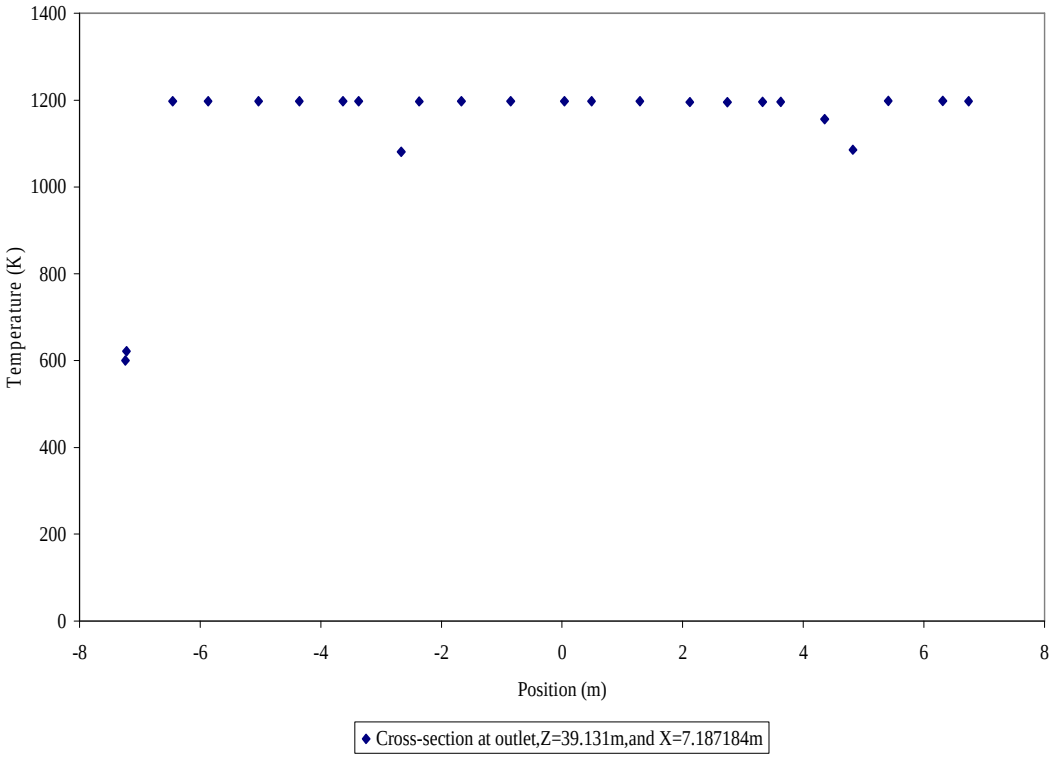

Figure E. 13: Temperature distribution for case C on CS-H

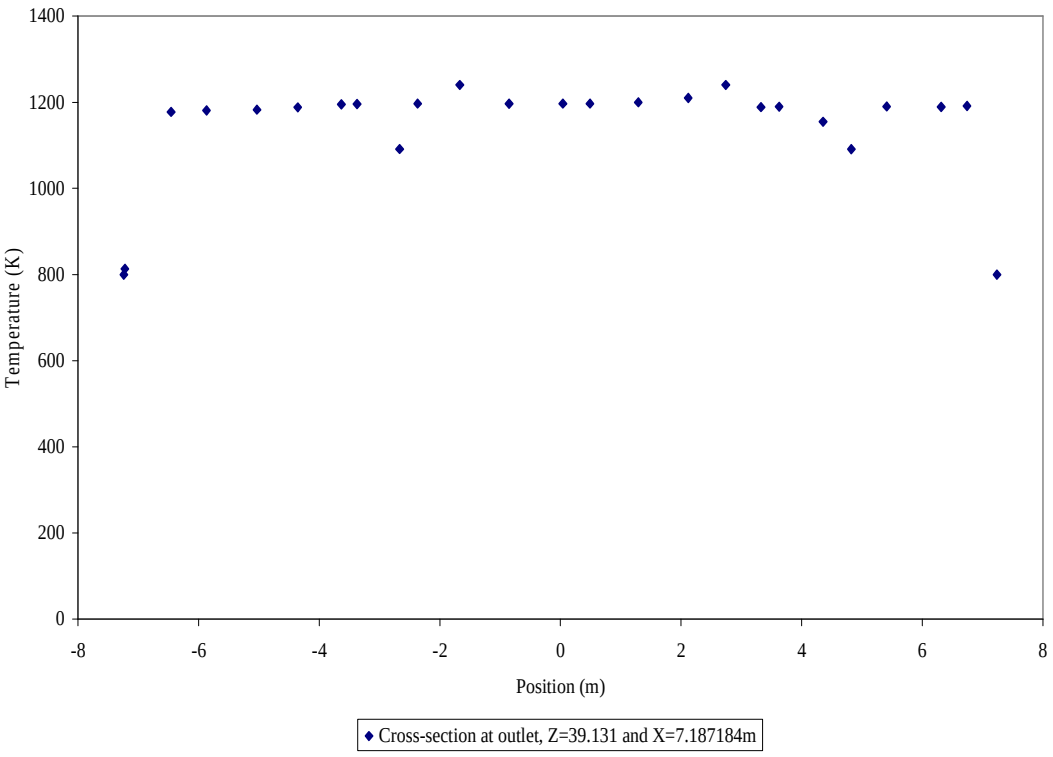

Figure E. 14: Temperature distribution for case D on CS-H

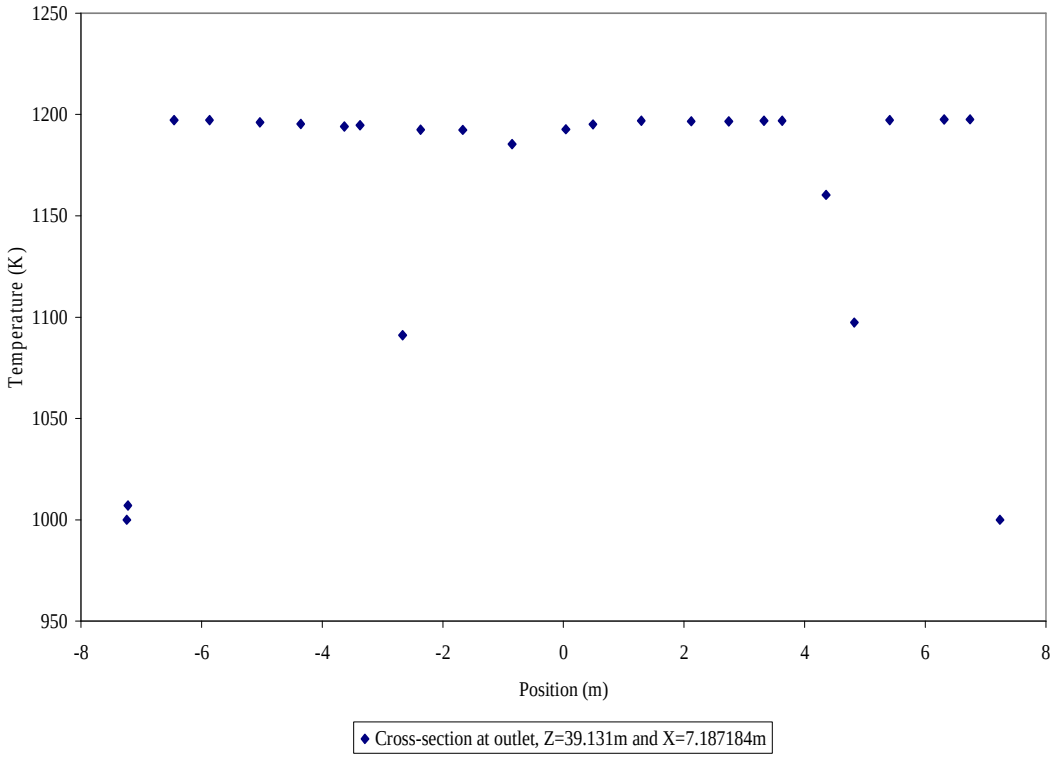

Figure E. 15: Temperature distribution for case E on CS-H

Appendix F

Species Concentration

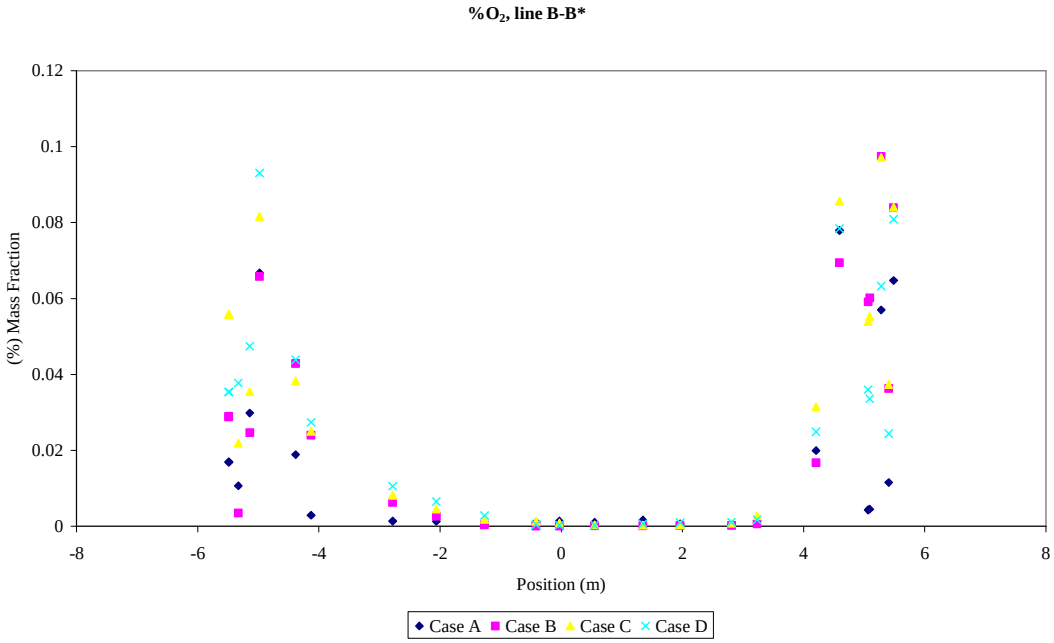

Figure F. 1: % O_2 on line B-B* for cases A, B, C and D

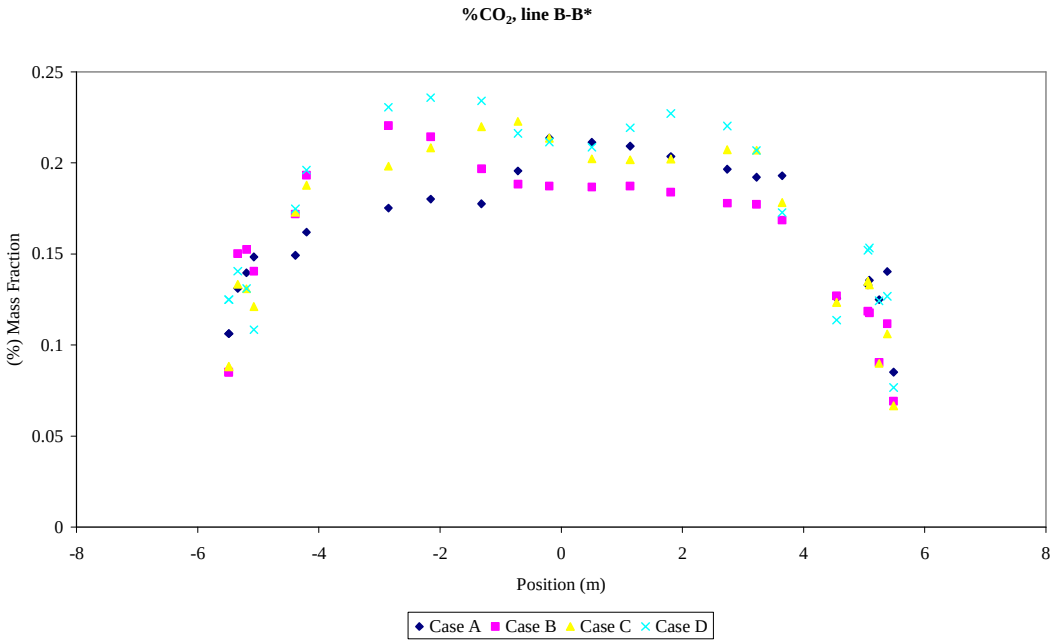

Figure F. 2: % CO_2 on line B-B* for cases A, B, C and D

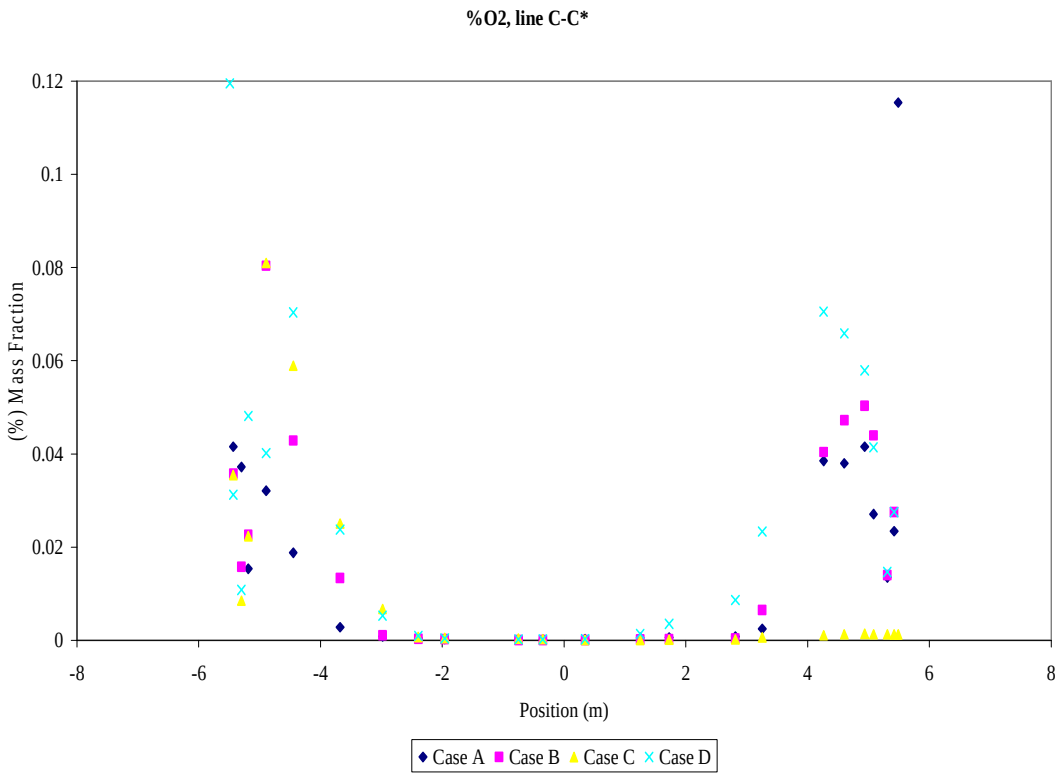

Figure F. 3: % O_2 on line C-C* for cases A, B, C and D

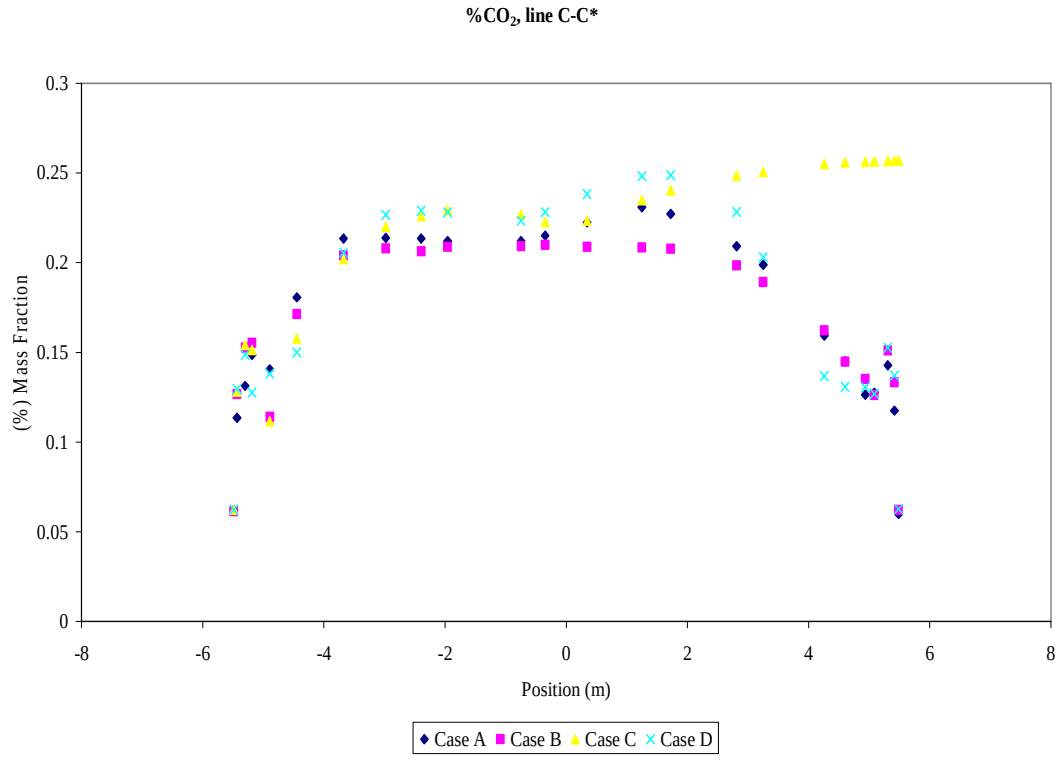

Figure F. 4: % CO_2 on line C-C* for cases A, B, C and D

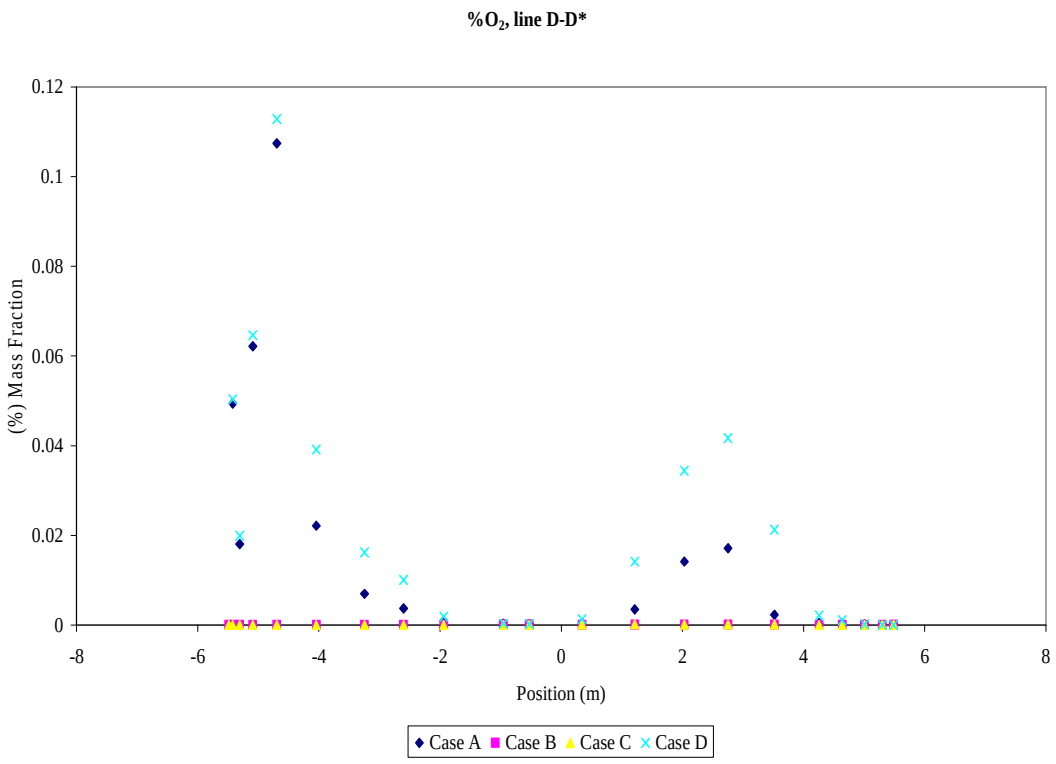

Figure F. 5: % O_2 on line D-D* for cases A, B, C and D

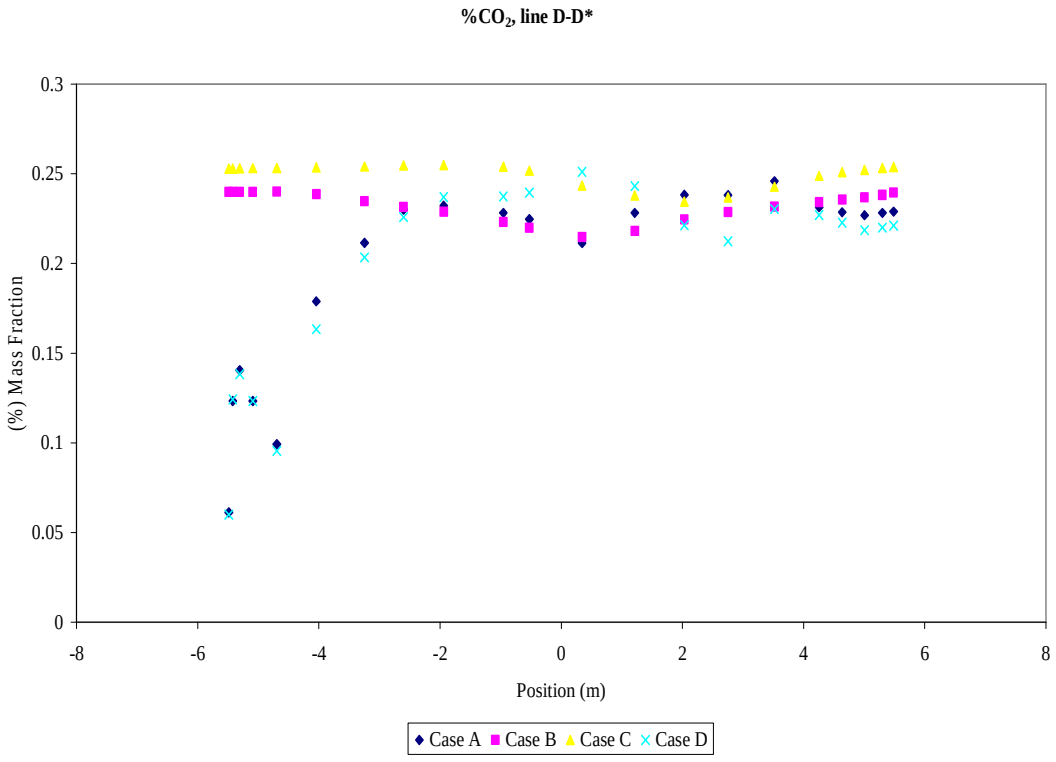

Figure F. 6: % CO_2 on line D-D* for cases A, B, C and D

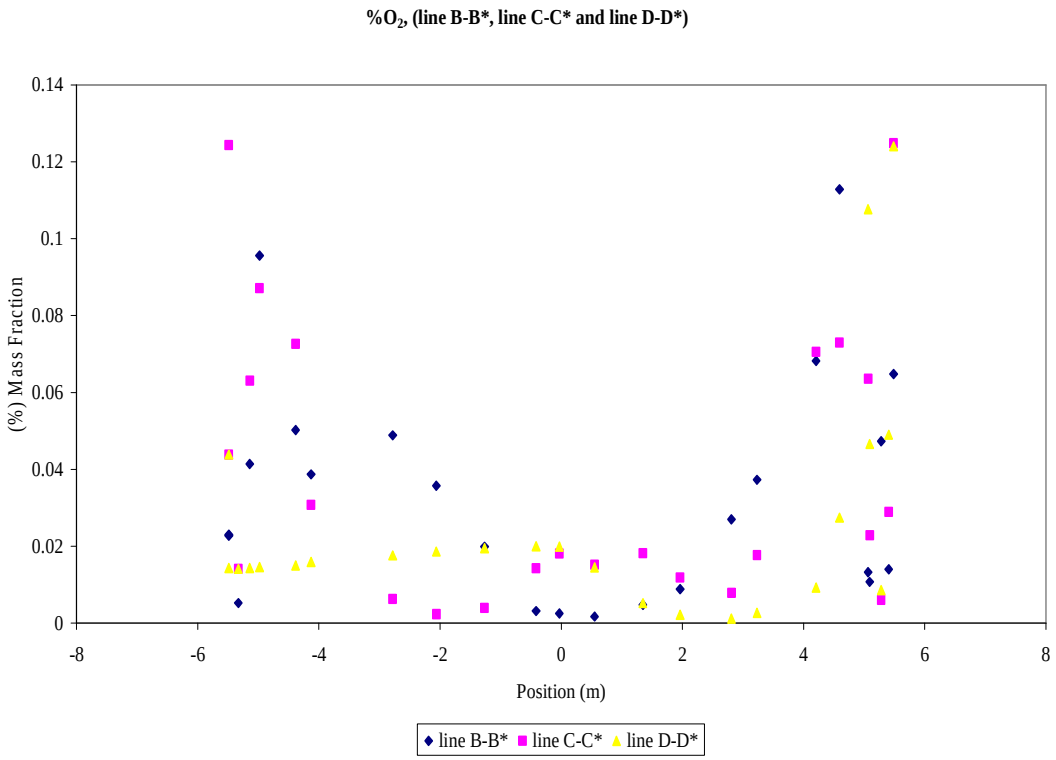

Figure F. 7: % O_2 on line B-B*, line C-C* and line D-D* for case E

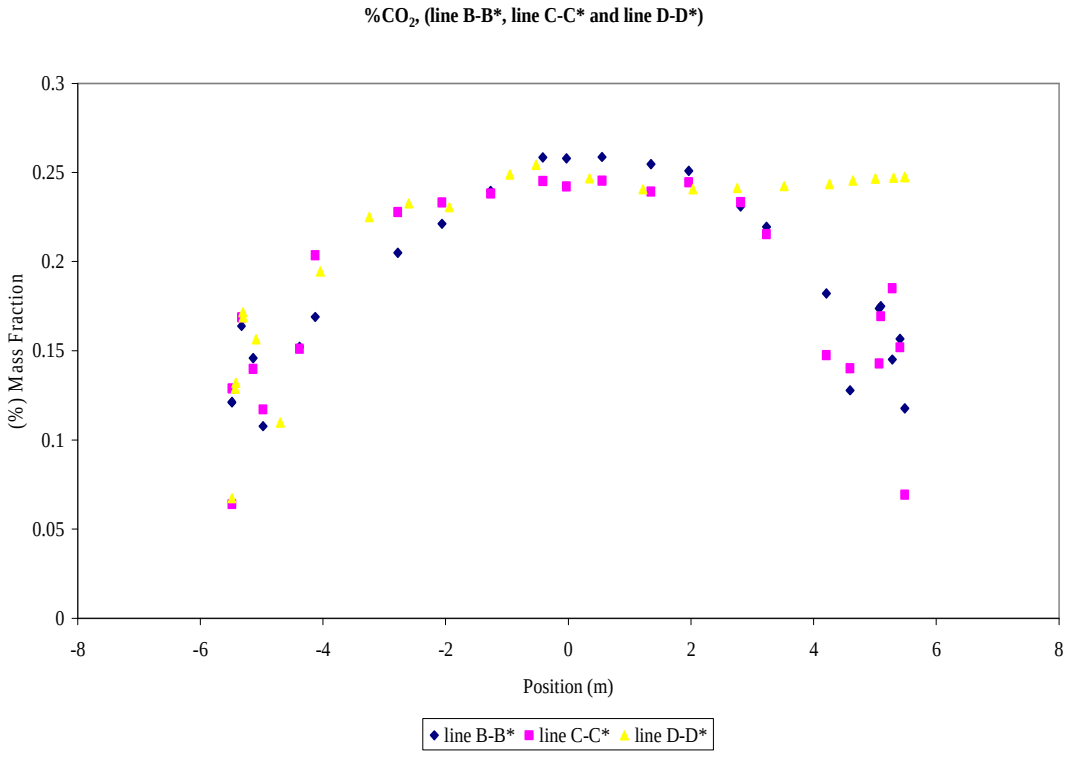

Figure F. 8: % CO_2 on line B-B*, line C-C* and line D-D* for case E

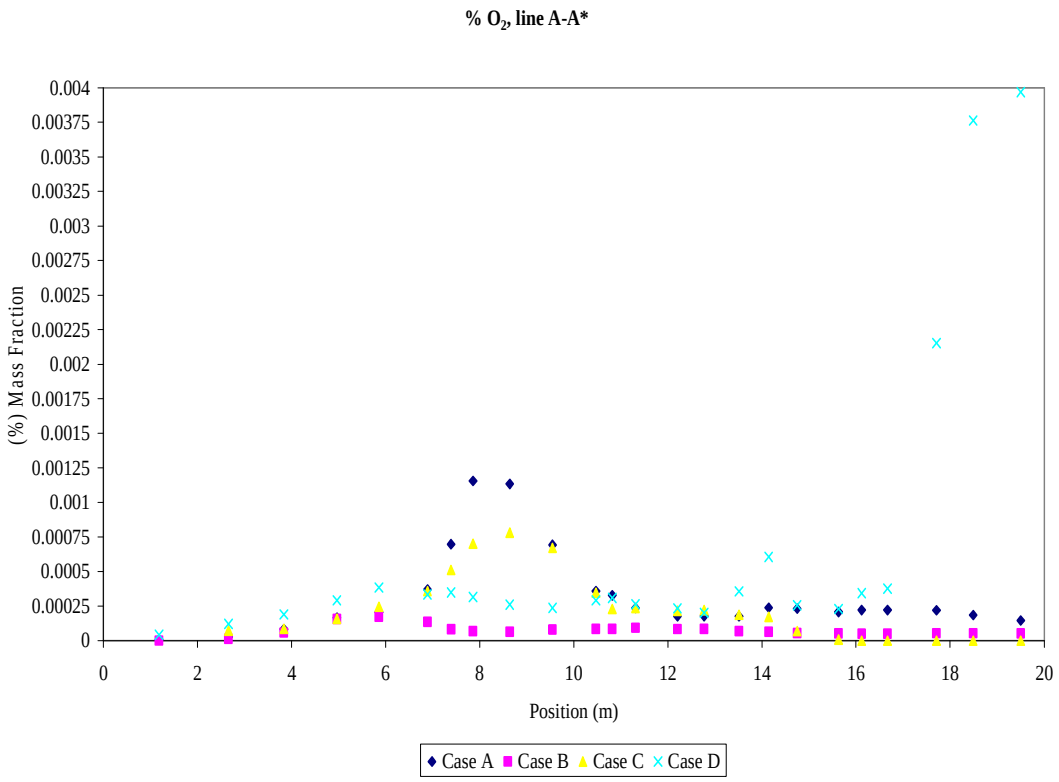

Figure F. 9: % O_2 on line A-A* for cases A, B, C and D

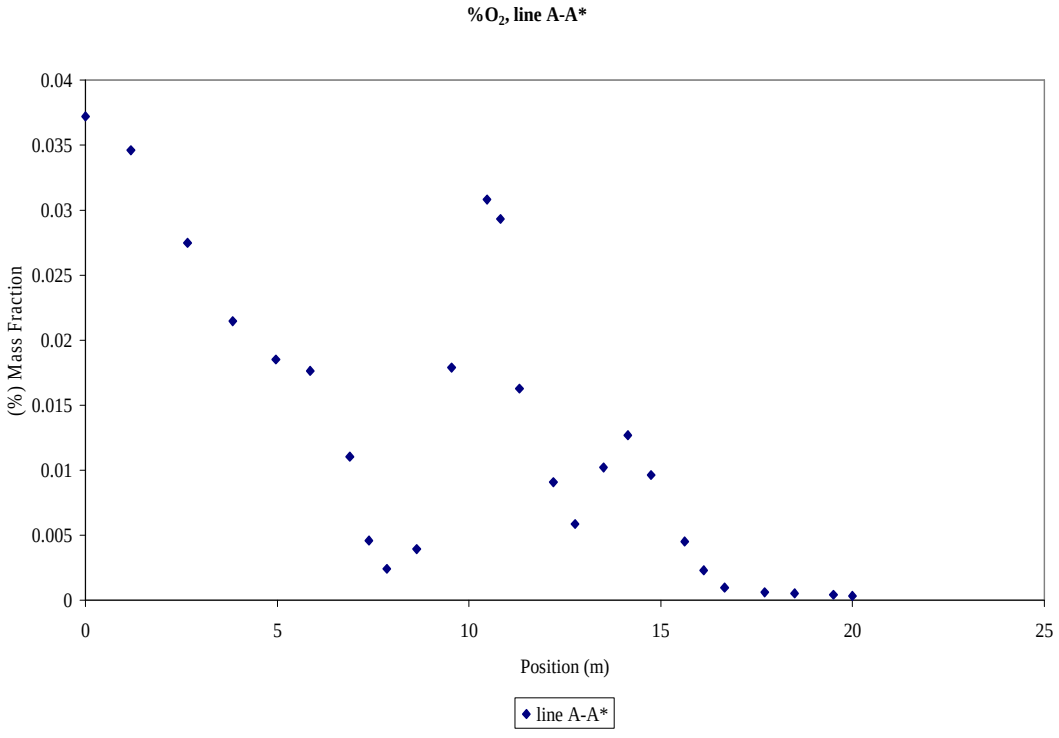

Figure F. 10: % O_2 on line A-A* for case E

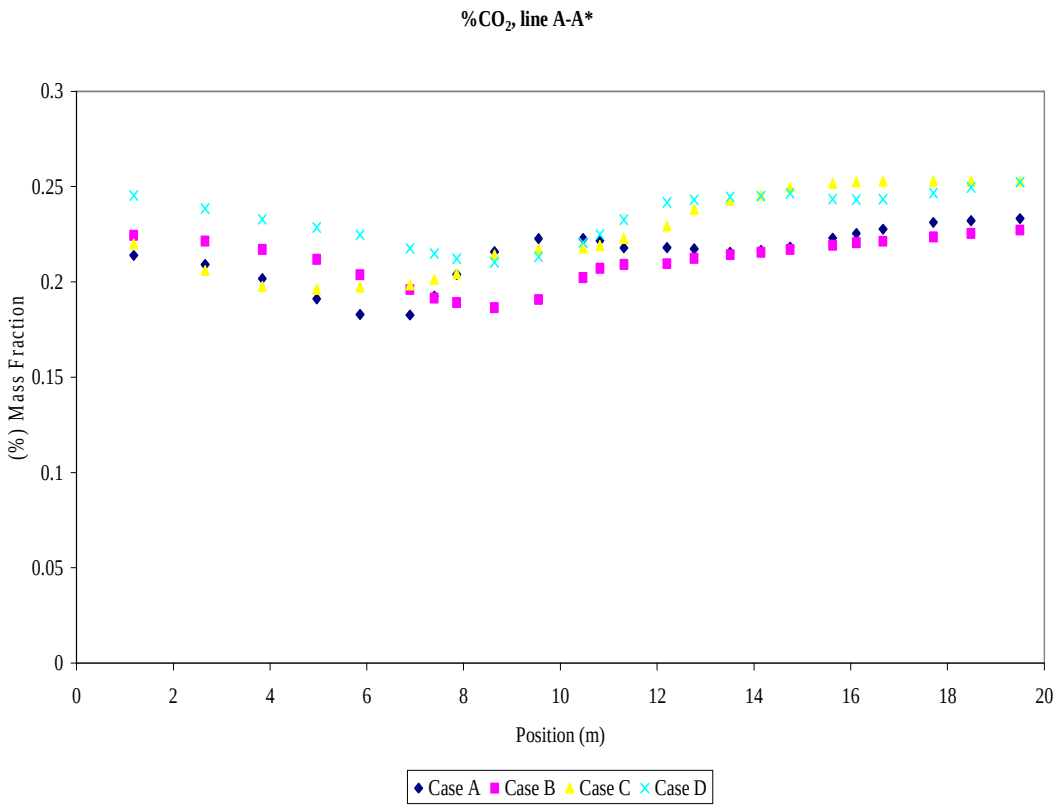

Figure F. 11: % CO_2 on line A-A* for cases A, B, C and D

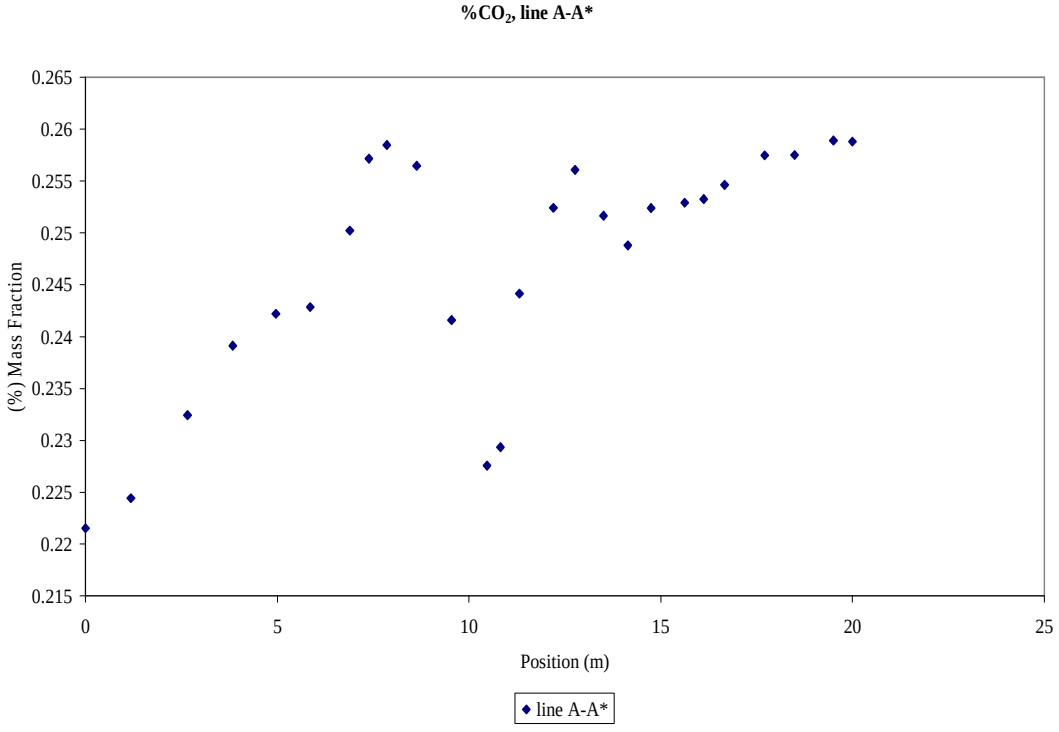

Figure F. 12: % CO_2 on line A-A* for case E

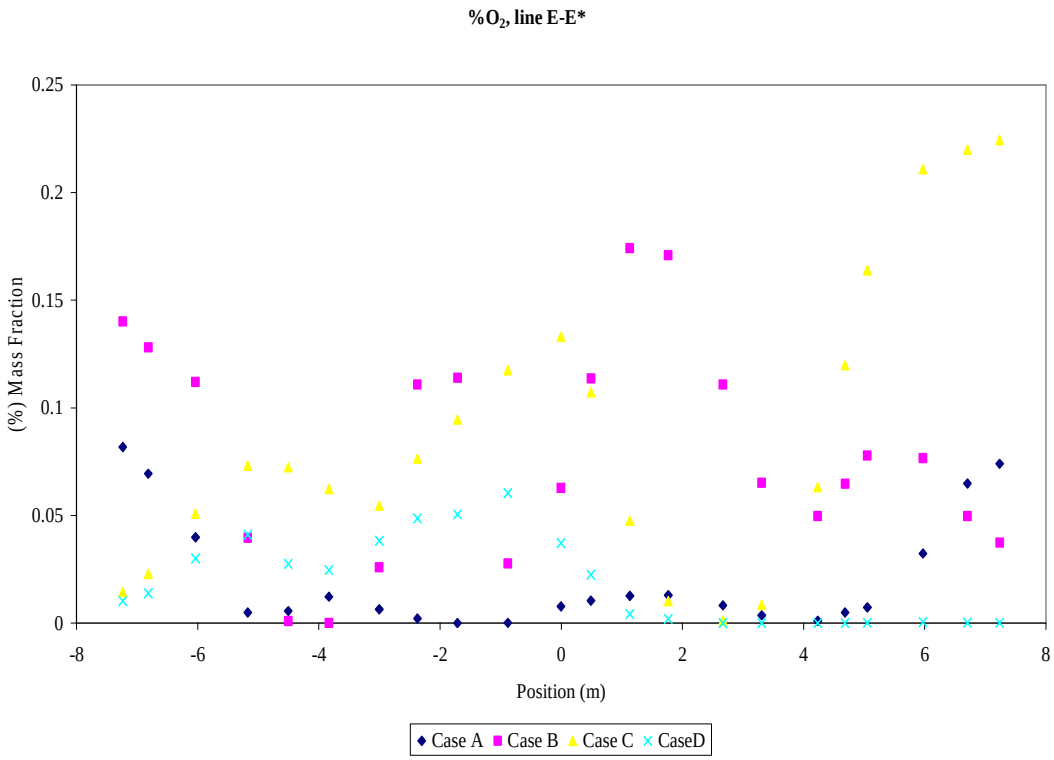

Figure F. 13: % O2 on line E-E* for cases A, B, C and D

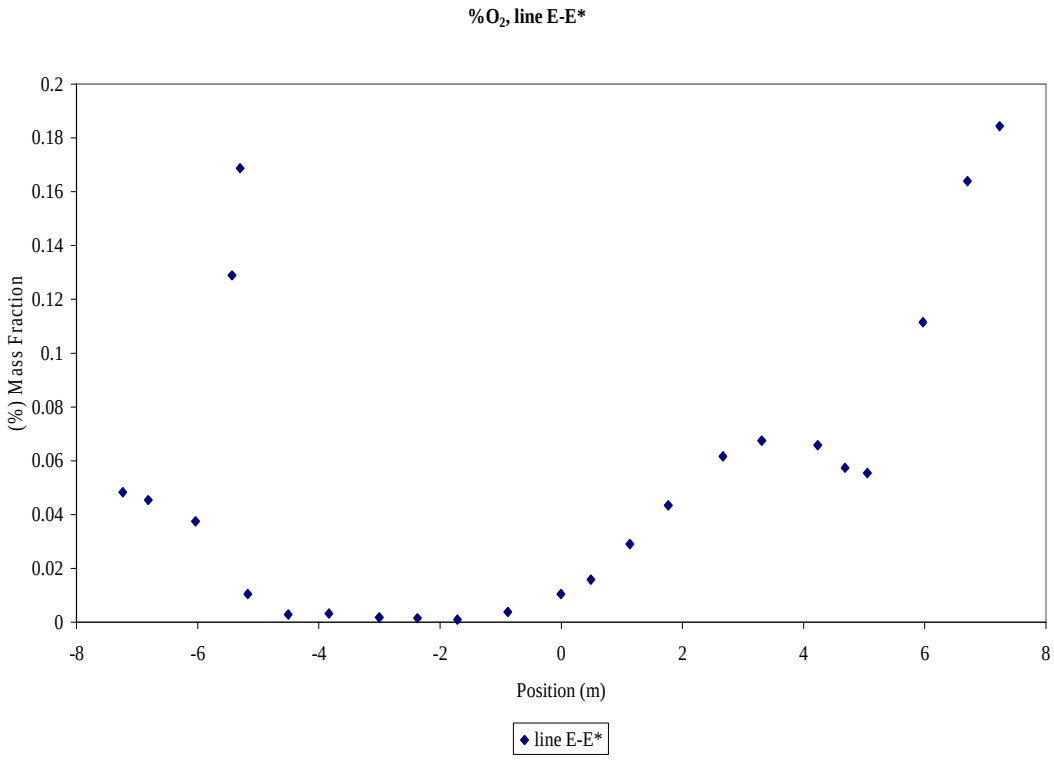

Figure F. 14: % O_2 on line E-E* for case E

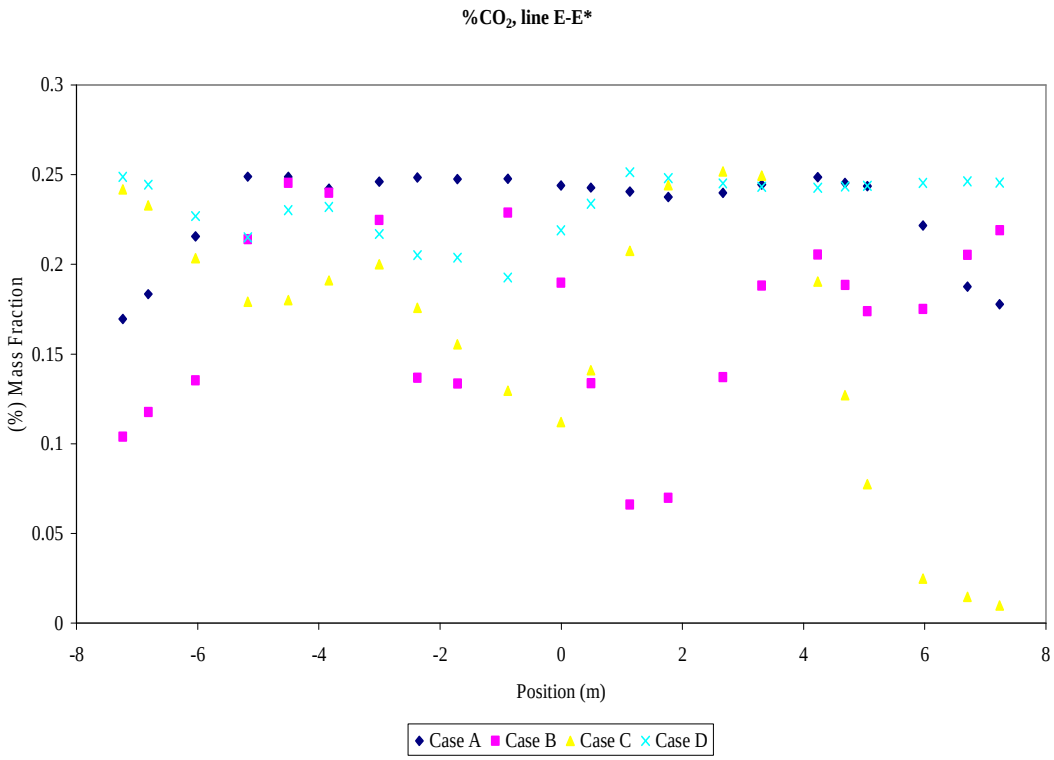

Figure F. 15: % CO_2 on line E-E* for cases A, B, C and D

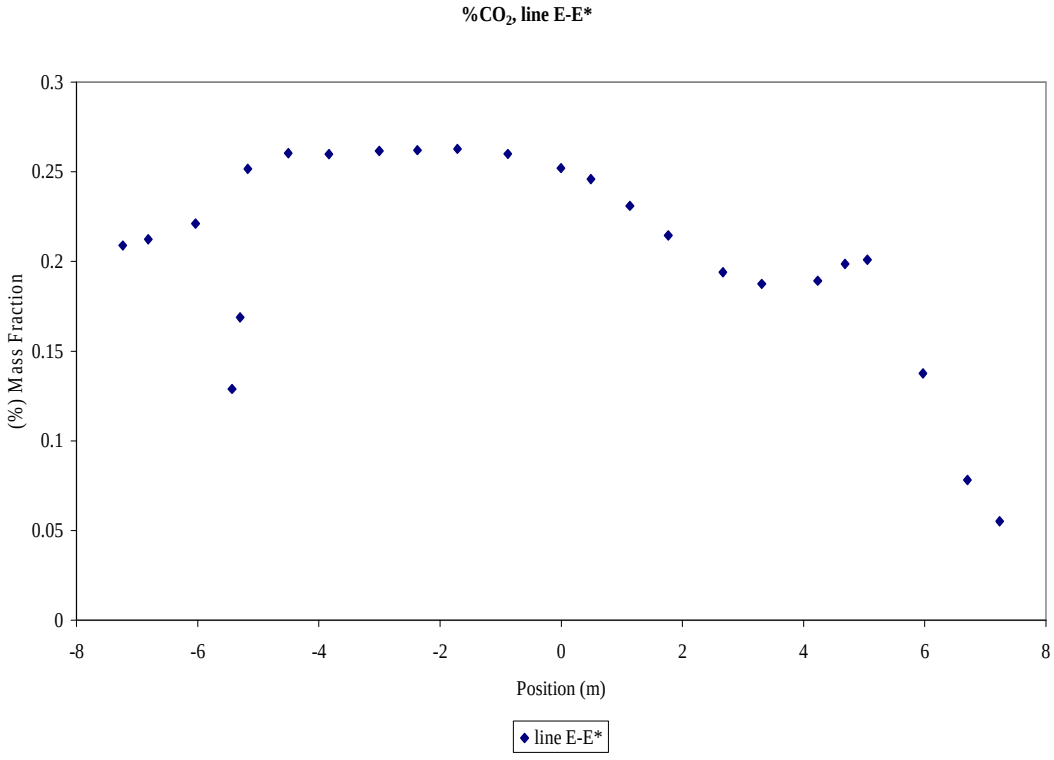

Figure F. 16: % CO_2 on line E-E* for case E

Appendix G

Selected Literature for Model Comparison

Table G. 1: Summary of literatures, taken as reference for comparison of present model

No.	Literature Citation	Modelling/ Experiment Validation	Utility Scale	Type of Coal
1	(Xu et al., 2001)	Real plant	300MW, front-wall furnace	-
2	(Hashimoto et al., 2007)	Experimental	100kg/h, experimental furnace	Bituminous
3	(Belosevic et al., 2008)	Real plant	350MW, tangentially-fired furnace	Serbian lignite Kostolac-Drmno
4	(Choi and Kim, 2009)	Real plant	500MW, tangentially-fired furnace	Bituminous
5	(Iranzo et al., 2001)	Real plant	350MW, front-wall fired	Sub-bituminous

Appendix H

Flow Fields along Various Cross-sections

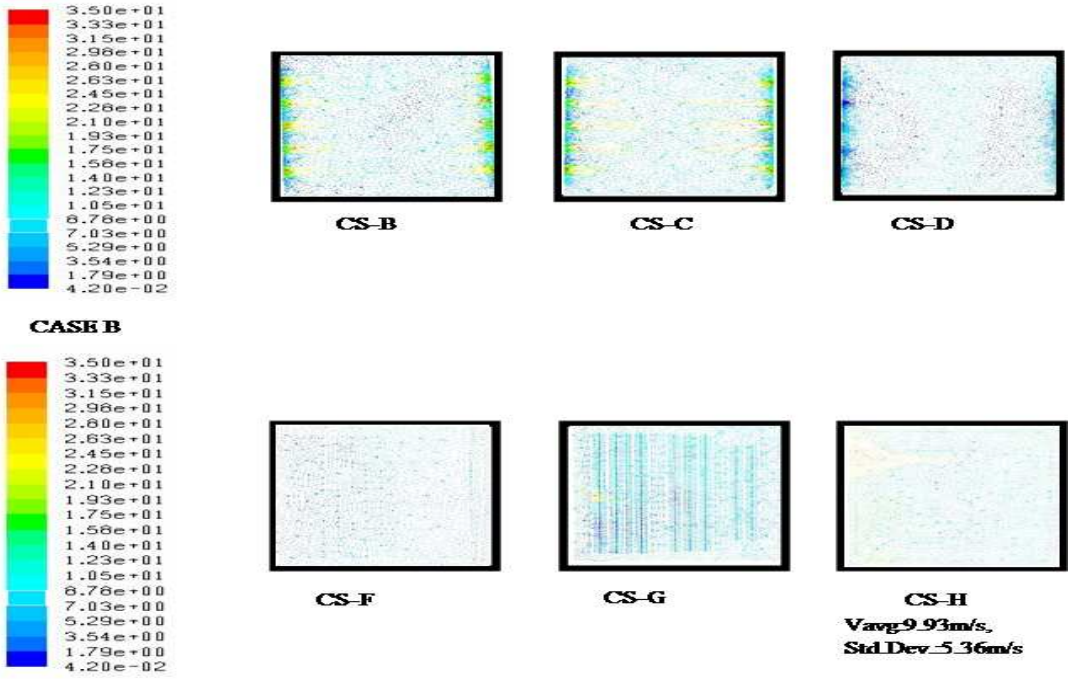

Figure H. 1: Flow fields on different cross-sections for case B

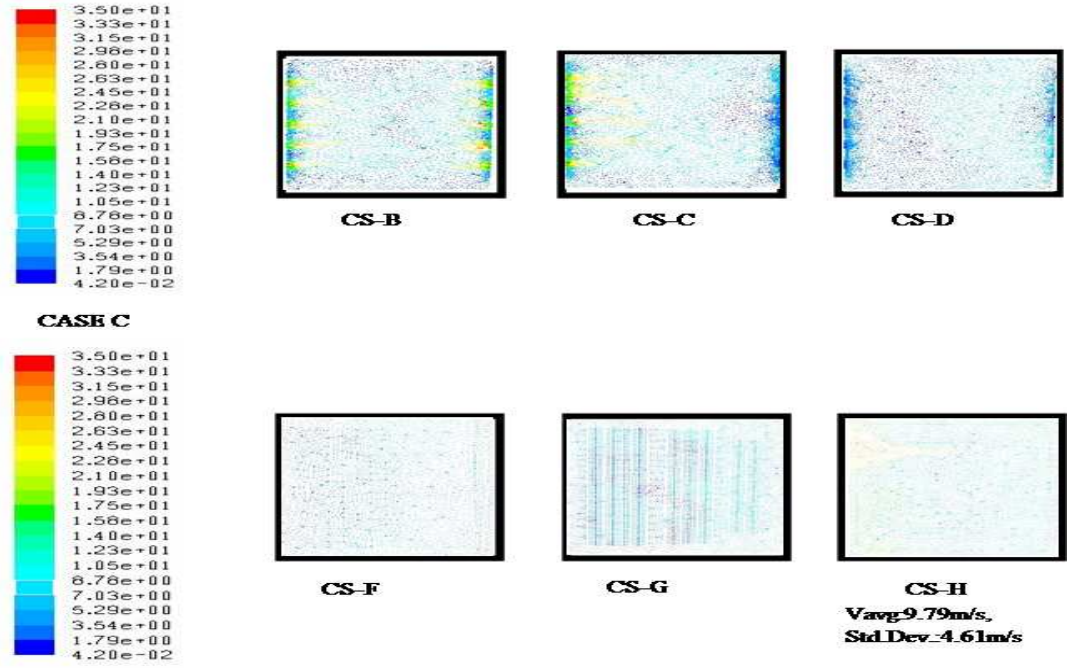

Figure H. 2: Flow fields on different cross-sections for case C

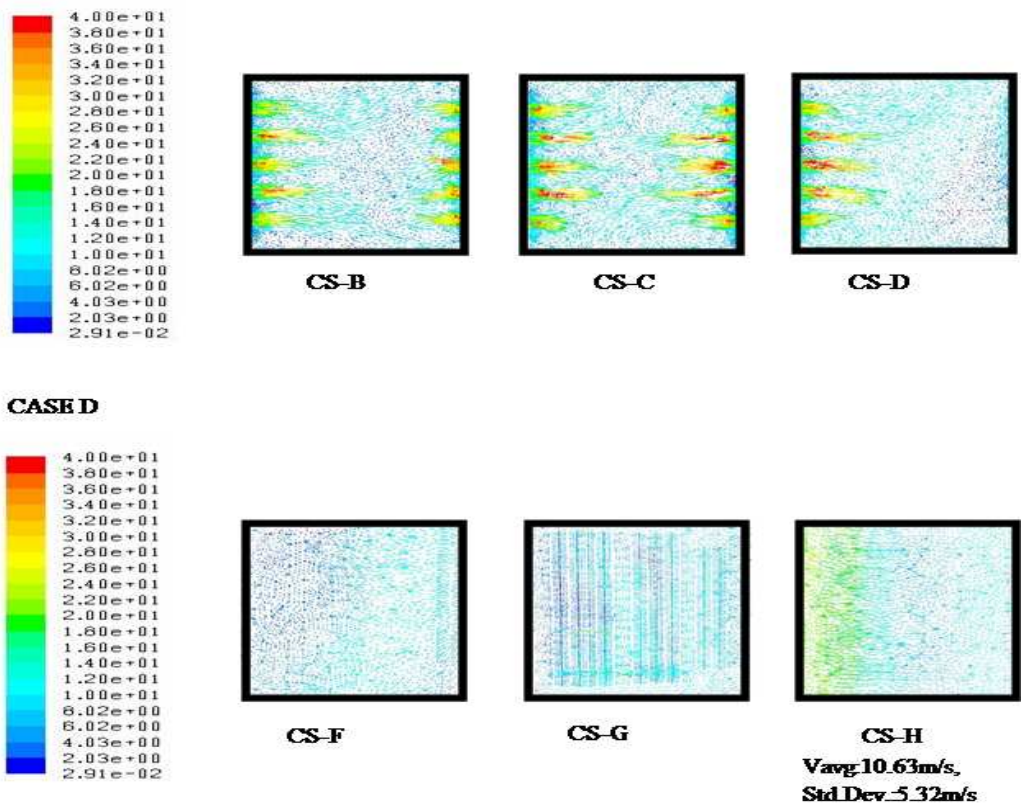

Figure H. 3: Flow fields on different cross-sections for case D

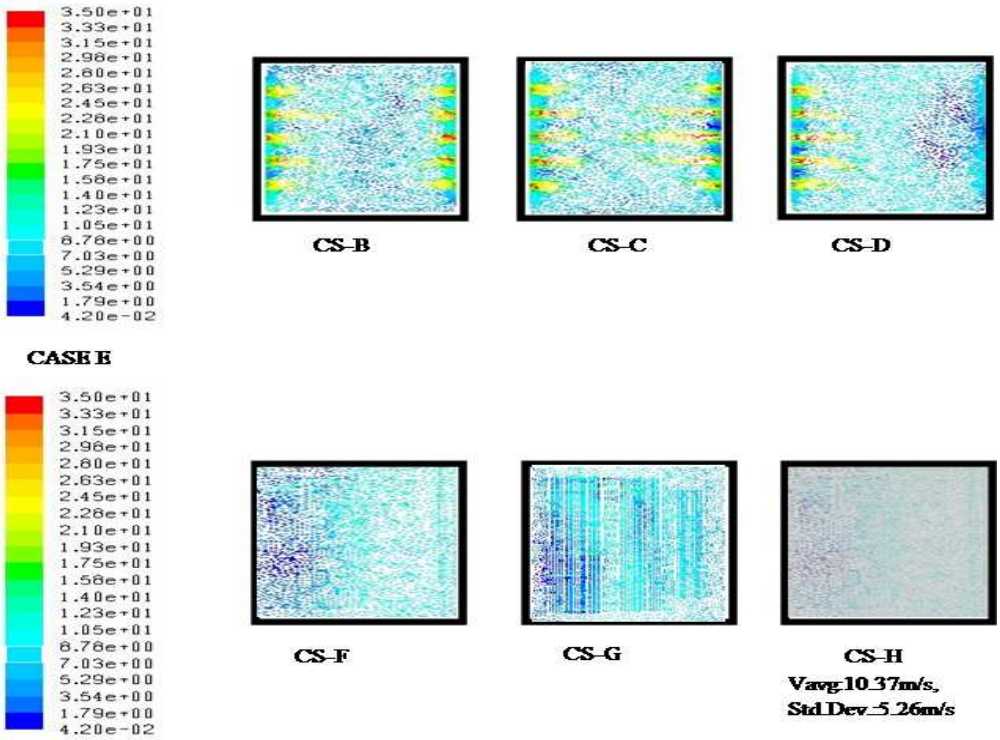

Figure H. 4: Flow fields on different cross-sections for case E

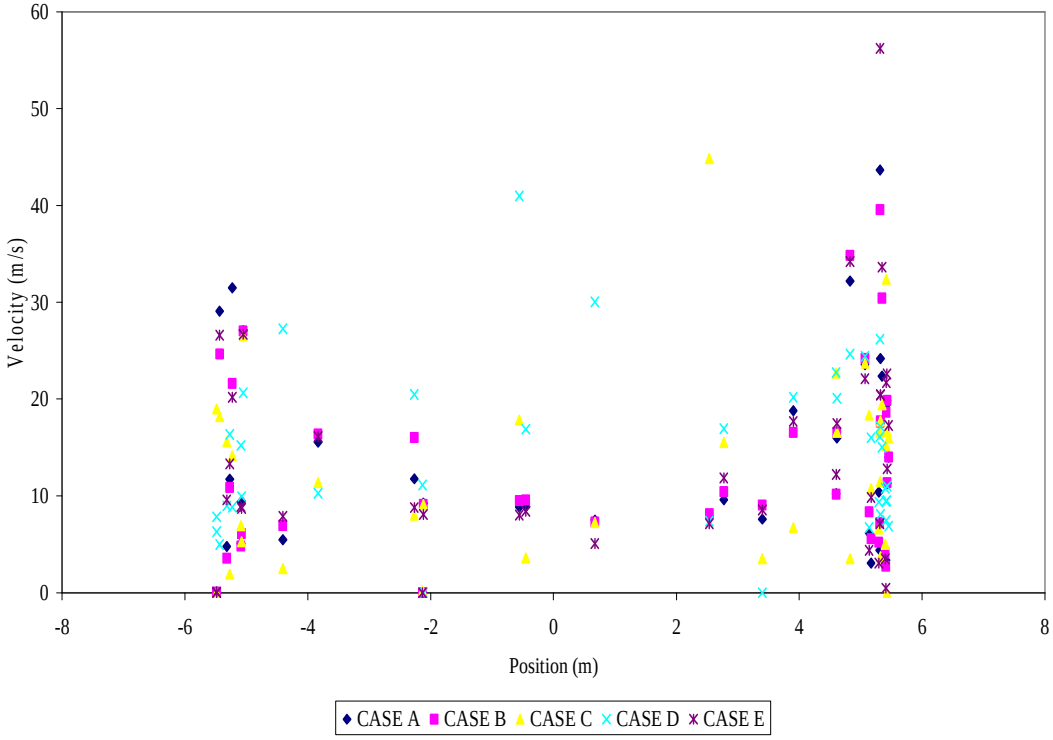

Figure H. 5: Flow fields for all cases on cross-section B

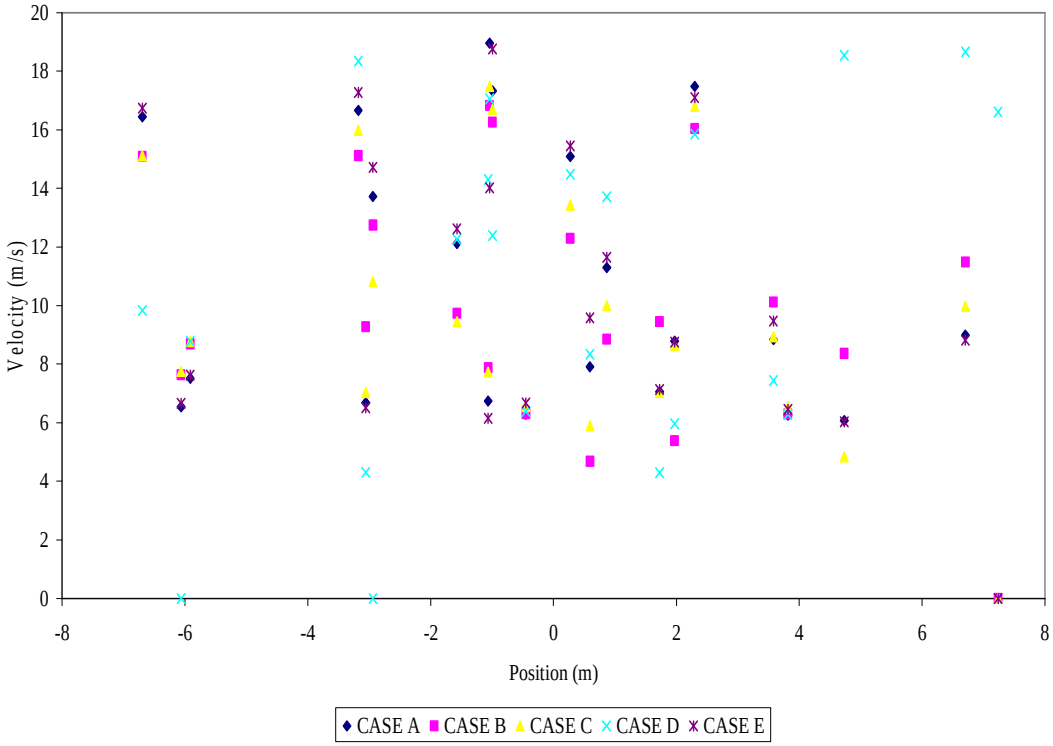

Figure H. 6: Flow fields for all cases on cross-section H

References

Badzioch, S & Hawksley, PGW, (1970) Kinetics of Thermal Decomposition of Pulverized Coal Particles. *Industrial & Engineering Chemistry Process Design and Development*, 9, 521-530.

Bashir, A., Awais, MM & Shamail, S, (2004) CFD based combustion modeling for industrial scale combustors. *Multitopic Conference*, 2004. Proceedings of INMIC 2004. 8th International.

Baukal, CE, Gershtein, VY & Li, X, (2000) *Computational Fluid Dynamics in INDUSTRIAL COMBUSTION*, CRC Press.

Baum, MM & Street, PJ, (1971) Predicting the Combustion Behaviour of Coal Particles. *Combustion Science and Technology*, 3, 231 - 243.

Baxter, LL, (1990) The evolution of mineral particle size distributions during early stages of coal combustion. *Progress in Energy and Combustion Science*, 16, 261-266.

Baxter, LL & Desollar, RW, (1993) A mechanistic description of ash deposition during pulverized coal combustion: predictions compared with observations. *Fuel*, 72, 1411-1418.

Belosevic, S, Sijercic, M, Oka, S & Tucakovic, D, (2006) Three-dimensional modeling of utility boiler pulverized coal tangentially fired furnace. *International Journal of Heat and Mass Transfer*, 49, 3371-3378.

Belosevic, S., Sijercic, M., Tucakovic, D & Crnomarkovic, N, (2008) A numerical study of a utility boiler tangentially-fired furnace under different operating conditions. *Fuel*, 87, 3331-3338.

Bird, RB, Stewart, WE & Lightfoot, EN, (1960) *Transport phenomena*, New York, Wiley.

Boyd, RK & Kent, JH, (1988) Three-dimensional furnace computer modelling. *Symposium (International) on Combustion*, 21, 265-274.

Boyd, RK & Kent, JH, (1994) Comparison of large scale boiler data with combustion model predictions. *Energy & Fuels*, 8, 124-130.

Boyd, RK & Lowe, A, (1990) Clinker formation on refractory surfaces in pulverised fuel boilers. 90 pt 3 ed. Barton, Aust, Publ by IE Aust.

Boysan, F, Ayers W.H, Swithenbank J, and Pan, Z, (1981) , Three-Dimensional Model of Spray Combustion in Gas Turbine Combustors, *AIAA Paper*, St. Louis, MO, 1-7.

Bryers, RW, (1995) Fireside Slagging, Fouling and High - temperature Corrosion of Heat Transfer Surface Due to Impurities in Steam Raising Fuels. *Progress in Energy and Combustion Science*, 29-120.

Carpenter, AM, (1995) Coal Blending for Power Staitons. London:*IEA Coal Research*.

Charon, O, Sarofim, AF & Beér, JM, (1990) Distribution of mineral matter in pulverized coal. *Progress in Energy and Combustion Science*, 16, 319-326.

Choi, CR & Kim, CN, (2009) Numerical investigation on the flow, combustion and NOx emission characteristics in a 500 MWe tangentially fired pulverized-coal boiler. *Fuel*, In Press, Corrected Proof.

Couch, G, (1994) Understanding slagging and fouling in pf combustion. *IEA Coal Research*, London.

Desollar, RW, (1995) Reseach needs of the power industry, in Application of Advanced Technology to Ash-related Problems in Boilers. *Engineering Foundation Conference*. Waterville Valley, NH.

Eaton, AM, Smoot, LD, Hill, SC & Eatough, CN, (1999) Components, formulations, solutions, evaluation, and application of comprehensive combustion models. *Progress in Energy and Combustion Science*, 25, 387-436.

Erickson, TA, Allan, SE, Mccollor, DP, Hurley, JP, Srinivasachar, S, Kang, SG, Baker, JE, Morgan, ME, Johnson, SA & Borio, R, (1995) Modelling of fouling and slagging in coal-fired utility boilers, *Fuel Processing Technology*, 44, 155-171.

Fan, J, Qian, L, Ma, Y, Sun, P & Cen, K, (2001a) Computational modeling of pulverized coal combustion processes in tangentially fired furnaces. *Chemical Engineering Journal*, 81, 261-269.

Fan, J. R., Zha, X. D., Sun, P. & Cen, KF, (2001b) Simulation of ash deposit in a pulverized coal-fired boiler. *Fuel*, 80, 645-654.

Field, MA, (1969) Rate of combustion of size-graded fractions of char from a low-rank coal between 1200°K and 2000°K. *Combustion and Flame*, 13, 237-252.

Filkoski, RV, Belosevic, SV, Petrovski, IJ, Oka, SN & Sijercic, MA, (2007) Computational fluid dynamics technique as a tool for description of the phenomena occurring in pulverized coal combustion systems. *Proceedings of the Institution of Mechanical Engineers*, 221, 399.

Fluent (2007) Fluent 6.3 Users Guide.

Gorner, K & Zinser, W, (1988) Prediction of Three-Dimensional Flows in Utility Boiler Furnaces and Comparison with Experiments. *Combustion Science and Technology*, 58, 43-57.

Harris, CK, Roekaerts, D & Rosendal, FJJ, (1996) Computational Fluid Dynamics for Chemical Reactor Engineering. *Chemical Engineering Science*, vol.51, 1569-1594.

Hashimoto, N, Kurose, R, Tsuji, H & Shirai, H, (2007) Numerical Analysis of Pulverised Coal Combustion in a Multiburner Furnace. *Energy and Fuels*, 21, 1950-1958.

Hatt, RM, (1990) Fireside deposits in coal-fired utility boilers. *Progress in Energy and Combustion Science*, 16, 235-241.

Huffman, GP, Huggins, FE, Shah, N & Shah, A, (1990) Behavior of basic elements during coal combustion. *Progress in Energy and Combustion Science*, 16, 243-251.

Hurley, JP & Schobert, HH, (1992) Ash formation during pulverized subbituminous coal combustion. 1. Characterization of coals, and inorganic transformations during early stages of burnout. *Energy & Fuels*, 6, 47-58.

Iranzo, I, Domingo, E, Cortés, C, Arauzo, I, (2001) Combustion characterisation of a pulverised coal utility boiler bases on CFD techniques, *Presentación O Comunicación En Congreso O Conferencia*, Centro de Investigatción del Rendimiento de Centrales, Eléctricas (CIRCE), Spain.

Jones, WP & Kakhi, M, (1998) Pdf Modeling of Finite-rate Chemistry Effects in Turbulent Nonpremixed Jet Flames. *Combustion and Flame*, 115, 210-229.

Jones, WP & Whitelaw, JH, (1982) Calculation methods for reacting turbulent flows: A review. *Combustion and Flame*, 48, 1-26.

Jones, WP & Wille, M, (1996) Large-eddy simulation of a plane jet in a cross-flow. *International Journal of Heat and Fluid Flow*, 17, 296-306.

Kær, SK., Rosendahl, LA & Baxter, LL, (2006) Towards a CFD-based mechanistic deposit formation model for straw-fired boilers. *Fuel*, 85, 833-848.

Kays, WM, (1994) Turbulent Prandtl number-where are we? *Transactions of the ASME. Journal of Heat Transfer*, 116, 284-95.

Korytnyi, E, Saveliev, R, Perelman, M, Chudnovsky, B & Bar-Ziv, E, (2009) Computational fluid dynamic simulations of coal-fired utility boilers: An engineering tool. *Fuel*, 88, 9-18.

Launder, BE (1989) Second-moment closure: present... and future? *International Journal of Heat and Fluid Flow*, 10, 282-300.

Launder, BE, Reece, GJ & Rodi, W. (1975) Progress in the development of a Reynolds-stress turbulence closure. *Journal of Fluid Mechanics Digital Archive*, 68, 537-566.

Launder, BE. & Spalding, DB, (1972) *Lectures in Mathematical Models of Turbulence*, Academic Press, London.

Launder, BE & Spalding, DB, (1974) The numerical computation of turbulent flows. *Computer Methods in Applied Mechanics and Engineering*, 3, 269-89.

Lee, FCC & Lockwood, FC, (1998) Modelling ash deposition in pulverized coal-fired applications. *Progress in Energy and Combustion Science*, 25, 117-132.

Lilley, DG, (1979) Flowfield modeling in practical combustors. *J. Energy*, 3(4), 193-210.

Liu, Y, Gupta, R, Sharma, A, Wall, T, Butcher, A, Miller, G, Gottlieb, P & French, D, (2005) Mineral matter-organic matter association characterisation by QEMSCAN and applications in coal utilisation. *Fuel*, 84, 1259-1267.

Lockwood, FC, Papadopoulos, C & ABBAS, AS, (1988) Prediction of a Corner-Fired Power Station Combustor. *Combustion Science and Technology*, 58, 5-23.

Lockwood, FC, Salooja, AP & Syed, SA, (1980) A prediction method for coal-fired furnaces. *Combustion and Flame*, 38, 1-15.

Ma, Z, Iman, F, Lu, P, Sears, R, Kong, L, Rokanuzzaman, AS, Mccollor, DP & Benson, SA, (2007) A comprehensive slagging and fouling prediction tool for coal-fired boilers and its validation/application. *Fuel Processing Technology*, 88, 1035-1043.

Magnussen, BF & Hjertager, BH (1977) On mathematical modeling of turbulent combustion with special emphasis on soot formation and combustion. *Symposium (International) on Combustion*, 16, 719-729.

Patankar, SV & Spalding, DB, (1973) A computer model for three-dimensional flow in furnaces. *Symposium (International) on Combustion*, 14, 605-614.

Patnakar, SV, (1980) *Numerical heat transfer and fluid flow*, Washington DC, Hemisphere Publishing Corp.

Pope, SB, (1985) PDF methods for turbulent reactive flows. *Progress in Energy and Combustion Science*, 11, 119-192.

Reid, WT, (1984) The relation of mineral composition to slagging, fouling and erosion during and after combustion. *Progress in Energy and Combustion Science*, 10, 159-169.

Robinson, GF, (1985) THREE-DIMENSIONAL ANALYTICAL MODEL OF A LARGE TANGENTIALLY-FIRED FURNACE. *Journal of the Institute of Energy*, 58, 116-150.

Rushdi, A., Gupta, R., Sharma, A. & Holcombe, D. (2005) Mechanistic prediction of ash deposition in a pilot-scale test facility. *Fuel*, 84, 1246-1258.

Sazhin, SS, Sazhina, EM, Faltsi-Saravelou, O & Wild, P, (1996) The P-1 model for thermal radiation transfer: advantages and limitations. *Fuel*, 75, 289-294.

Siegel, R & Howell, JR, (1992) *Thermal Radiation Heat Transfer*, Washington DC, Hemisphere Publishing Corporation.

Sivathanu, YR & Faeth, GM, (1990) Generalized state relationships for scalar properties in nonpremixed hydrocarbon/air flames. *Combustion and Flame*, 82, 211-230.

Spalding, DB, (1971) Mixing and chemical reaction in steady confined turbulent flames. *Symposium (International) on Combustion*, 13, 649-657.

Speziale, CG, (1987) On nonlinear K-l and K-ε models of turbulence. *Journal of Fluid Mechanics*, 178, 459-75.

Srinivasachar, S, Helble, JJ, & Boni, AA, (1990) Mineral behavior during coal combustion 1. Pyrite transformations. *Progress in Energy and Combustion Science*, 16, 281-292.

Srinivasachar, S, Senior, CL, Helble, JJ & Moore, JW, (1992) A fundamental approach to the prediction of coal ash deposit formation in combustion systems. *Symposium (International) on Combustion*, 24, 1179-1187.

Thiessen, G, Ball, CG & Grotts, PE, (1936) Coal Ash and Coal mineral Matter. *Industrial & Engineering Chemistry*, 28, 355-361.

Tillman, DA, (1991) *The combustion of solid fuels and wastes*, London, UK, Academic Press.

Versteeg, HK & Malalasekera, W, (2007) *An introduction to computational fluid dynamics The finitie volume method*, Pearson Education Limited.

Vuthaluru, HB, Vuthaluru, R, Yurismono, H & Parinussa, P, (2008) CFD based approach to control ash related problems in a large scale tangentially fired boiler. *6th International Conference on CFD in Oil & Gas, Metallurgical and Process Industries*. SINTEF/NTNU, Trondheim NORWAY.

Vuthaluru, R & Vuthaluru, HB, (2006) Modelling of a wall fired furnace for different operating conditions using FLUENT. *Fuel Processing Technology*, 87, 633-639.

Wall, TF, (1992) Mineral matter transformations and ash deposition in pulverised coal combustion. *Symposium (International) on Combustion*, 24, 1119-1126.

Walsh, PM, Sayre, AN, Loehden, DO, Monroe, LS, Beér, JM & Sarofim, AF, (1990) Deposition of bituminous coal ash on an isolated heat exchanger tube: Effects of coal properties on deposit growth. *Progress in Energy and Combustion Science*, 16, 327-345.

Wang, H & Harb, JN, (1997) Modeling of ash deposition in large-scale combustion facilities burning pulverized coal. *Progress in Energy and Combustion Science*, 23, 267-282.

Warnatz, J, Mass, U, & Dibble, RW, (1993, 2001) *Combustion - Physical and Chemical Fundamentals,Modelling and Simulations, Experiments, Pollutant Formation.*, Berlin, Springer - Verlag.

Wu, Z. (2005) Fundamental of Pulverised Coal Combustion. UK, London, UK, IEA *Clean Coal Centre*.

Wu, Z. (Oct. 2003) Understanding fluidised bed combustion. CCC/76, London, UK, IEA *Clean Coal Centre.*

Xu, M., Azevedo, JLT & Carvalho, MG, (2001) Modeling of a front wall fired utility boiler for different operating conditions. *Computer Methods in Applied Mechanics and Engineering*, 190, 3581-3590.

Xu, M., He, X., Azevedo, JLT & Carvalho, MG (2002) An advanced model to assess fouling and slagging in coal fired boilers. *International Journal of Energy Research*, 26, 1221-1236.

Yamashita, T., Asotani, T & Tachibana, K, (2008) Direct Observation of Ash Deposition in Pulverized Coal Fired Boiler Using CCD Camera and Model Development for Slagging Prediction. *Twenty - First Annual International Pittsburgh Coal Conference*.

Yan, L, Gupta, RP & Wall, TF, (2001) The implication of mineral coalescence behaviour on ash formation and ash deposition during pulverised coal combustion. *Fuel*, 80, 1333-1340.

Yan, L, Gupta, RP & Wall, TF, (2002) A mathematical model of ash formation during pulverized coal combustion. *Fuel*, 81, 337-344.

Yin, C, Caillat, S., Harion, JL, Baudoin, B. & Perez, E. (2002) Investigation of the flow, combustion, heat-transfer and emissions from a 609 MW utility tangentially fired pulverized-coal boiler. *Fuel*, 81, 997-1006.

Yin, C, Rosendahl, L & Condra, TJ, (2003) Further study of the gas temperature deviation in large-scale tangentially coal-fired boilers[small star, filled]. *Fuel*, 82, 1127-1137.

Zheng, C, Liu, Z, Duan, X & Mi, J, (2002) Numerical and experimental investigations on the performance of a 300 MW pulverized coal furnace. *Proceedings of the Combustion Institute*, 29, 811-818.